การจำลองมอนติคาร์โลเส้นใยนาโนและอนุภาคนาโนสำหรับพอลิเอทิลีน
ที่มีน้ำหนักโมเลกุลสองค่าผสมกัน

นายหาญชนะ เกตมาลา

MONTE CARLO SIMULATIONS OF BIDISPERSE

POLYETHYLENE NANOFIBERS AND

NANOPARTICLES

Harnchana Gatemala

A Thesis Submitted in Partial Fulfillment of the Requirements for the

Degree of Master of Science in Chemistry

Suranaree University of Technology

Academic Year 2010

MONTE CARLO SIMULATIONS OF BIDISPERSE

POLYETHYLENE NANOFIBERS AND NANOPARTICLES

Suranaree University of Technology has approved this thesis submitted in partial fulfillment of the requirements for a Master's Degree.

Thesis Examining Committee
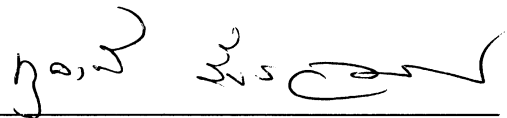
_____
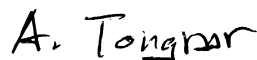(Asst. Prof. Dr. Kunwadee Rangsriwatananon)

Chairperson

_____
(Asst. Prof. Dr. Visit Vao-Soongnern)

Member (Thesis Advisor)

_____
(Prof. Dr. Kritsana Sagarik)

Member

_____
(Assoc. Prof. Dr. Anan Tongraar)

Member

_____
(Dr. Wut Dankittikul)

Acting Vice Rector for Academic Affairs

_____
(Assoc. Prof. Dr. Prapun Manyum)

Dean of Institute of Science

หาญชนะ เกตมาลา : การจำลองมอนติคาร์โลเส้นใยนาโนและอนุภาคนาโนสำหรับ
พอลิเอทิลีนที่มีน้ำหนักโมเลกุลสองค่าผสมกัน (MONTE CARLO SIMULATIONS
OF BIDISPERSE POLYETHYLENE NANOFIBERS AND NANOPARTICLES)
อาจารย์ที่ปรึกษา : ผู้ช่วยศาสตราจารย์ ดร.วิสิษฐ์ แววสูงเนิน, 133 หน้า.

ปัจจุบันนี้วัสดุนาโนของพอลิเมอร์ได้รับความสนใจเป็นอย่างมาก เพราะมีสมบัติที่น่าสนใจ
และสามารถประยุกต์ใช้ในหลายๆ ด้าน โมเลกุลขนาดใหญ่ที่ถูกจำกัดพื้นที่ จะแสดงพฤติกรรมที่
แปลกประหลาด และไม่สามารถคาดเดาได้ซึ่งแตกต่างจากวัสดุต้นแบบของมันเอง ได้มีการทดลอง
หลายอย่างเพื่อศึกษาพื้นผิว และพื้นผิวรอยต่อของพอลิเมอร์ แต่เนื่องจากเส้นใยนาโน และอนุภาค
นาโนมีขนาดเล็กมาก จึงเป็นสิ่งที่ท้าทายมากในการวิเคราะห์โดยการทดลอง ส่งผลให้ความรู้และ
ความเข้าใจในระดับโมเลกุลยังคงไม่สมบูรณ์ การจำลองแบบด้วยคอมพิวเตอร์จึงเป็นกุญแจสำคัญ
เพื่อแก้ไขข้อจำกัดนี้ ในวิทยานิพนธ์นี้จะใช้การจำลองมอนติคาร์โลเส้นใยนาโนและอนุภาคนาโน
สำหรับพอลิเอทิลีนที่มีน้ำหนักโมเลกุลสองค่าผสมกัน เพื่อจำลองแบบโครงสร้างของหน่วยเอทิลีน
บนผลึกของเพชร แต่ละบีดแทนการเชื่อมกันของหน่วยของเอทิลีน แรงกระทำระยะใกล้สามารถ
คำนวณโดยใช้ rotational isomeric state model และแรงกระทำระยะไกลคำนวณโดยใช้ฟังก์ชัน
ศักย์ของ Lennard-Jones (LJ) ซึ่งมีค่าตัวแปร σ และ ε/k_B เท่ากับ 4.2 อังสตรอม และ 205
เคลวิน ตามลำดับ หลังจากนั้นได้ศึกษาสมบัติของระบบเส้นใยนาโน และอนุภาคนาโนหลอมเหลว
ที่อุณหภูมิ 509 เคลวิน ของพอลิเอทิลีนที่มีค่าน้ำหนักโมเลกุลสองค่าผสมกัน (B50 ผสมกับ B40
B30 และ B20) ซึ่งร้อยละโดยน้ำหนักของ B50 มีค่าเท่ากับ 25, 50 และ 75 ตามลำดับ ผลการจำลอง
พบว่า ความหนาแน่นของเส้นใยนาโนมีค่าน้อยกว่าอนุภาคนาโนในทุกระบบที่ได้ศึกษา
และความหนาแน่นจะมีค่าลดลงเมื่อความยาวของสายโซ่ของพอลิเอทิลีนที่นำมาผสมสั้นลง
ที่บริเวณพื้นผิวพบพอลิเอทิลีนสายสั้นมากกว่าสายยาว และ พอลิเอทิลีนที่มีสายโซ่สั้นกว่าจะมี
ปริมาณมากกว่าสายโซ่ยาว ส่วนบีดตรงปลายจะพบมากกว่าบีดตรงกลาง การจัดเรียงตัวของโมเลกุล
พอลิเอทิลีนที่มีสายโซ่ยาวจะมีการเปลี่ยนแปลงมากกว่าสายโซ่สั้น โมเลกุลพอลิเอทิลีนที่มีสายโซ่
ยาวและสั้น มีการจัดเรียงตัวของโมเลกุลให้ตั้งฉากกับพื้นผิวของเส้นใยนาโนและอนุภาคนาโน
โดยให้แกนเอกตั้งฉากกับพื้นผิว ซึ่งสังเกตได้อย่างชัดเจนเมื่อความยาวของสายโซ่เพิ่มขึ้น
ขนาดของโมเลกุลของพอลิเอทิลีนจะมีขนาดเล็กและแบนลงเมื่อเข้าใกล้พื้นผิว สมบัติของ
พอลิเอททิลีนที่มีสายโซ่ยาวมีลักษณะคล้ายกับระบบที่มีการกระจายน้ำหนักโมเลกุลแบบเดี่ยว
และเหมือนกันทั้งระบบเส้นใยนาโน และอนุภาคนาโน แต่สมบัติของพอลิเอทิลีนที่มีสายโซ่สั้นกว่า
มีการเปลี่ยนแปลงไป ส่วนการเปลี่ยนอัตราส่วนโดยน้ำหนักของพอลิเอทิลีนทั้งสายโซ่ยาว และสั้น
จะไม่มีผลต่อสมบัติต่างๆ มากนัก

สุดท้ายได้ศึกษาการตกผลึกของพอลิเอทิลีนที่มีค่าน้ำหนักโมเลกุลสองค่าผสมกัน (B20 และ B20 ร้อยละ 50 โดยน้ำหนัก) ที่อุณหภูมิ 298 เคลวิน ผลการศึกษาพบว่า ความหนาแน่นของเส้นใยนาโน และอนุภาคนาโน มีลักษณะคล้ายกันกับระบบเส้นใยนาโน และอนุภาคนาโนหลอมเหลว สำหรับเส้นใยนาโนพอลิเอทิลีนสายโซ่สั้นจะถูกผลักดันให้ไปอยู่ตรงกลางเส้นใย ในขณะที่อนุภาคนาโนจะพบมากที่บริเวณพื้นผิว ในระบบอนุภาคนาโนการตกผลึกจะเกิดได้ง่ายกว่าระบบเส้นใยนาโน และเกิดจากด้านนอกเข้าไปด้านใน พอลิเอทิลีนสายโซ่สั้นจะตกผลึกได้เร็วกว่าสายโซ่ที่ยาว ซึ่งสามารถสังเกตได้อย่างชัดเจนในระบบอนุภาคนาโน และโมเลกุลของพอลิเอทิลีนในเส้นใยนาโนจะมีการจัดเรียงตัวเป็นระเบียบมากกว่าอนุภาคนาโน

สาขาวิชาเคมี   ลายมือชื่อนักศึกษา _____

ปีการศึกษา 2553   ลายมือชื่ออาจารย์ที่ปรึกษา _____

HARNCHANA GATEMALA: MONTE CARLO SIMULATIONS

OF BIDISPERSE POLYETHYLENE NANOFIBERS AND

NANOPARTICLES. THESIS ADVISOR : ASST. PROF. VISIT

VAO-SOONGNERN, Ph.D. 133 PP.

NANOFIBER/ NANOPARTICLE/ MONTE CARLO SIMULATION ON 2NND

LATTICE/ BIDISPERSE PE

Polymeric nanostructured materials have gained considerable attention recently owing to their unique properties that can be used in diverse applications. Confined macromolecules at nanometer scale exhibit a fascinating and unexpected dynamic behavior and provide many unique properties. Various experimental techniques have been applied to polymer surfaces and interfaces. Individual polymeric nanofibers as well as nanoparticles are challenging to characterize experimentally due to their small size. So, the knowledge at the molecular level is not completely understood. Computer simulation is a key to solve this limitation. In this thesis, Monte Carlo (MC) simulation of bidisperse polyethylene (PE) nanofibers and nanoparticles has been performed on the second nearest neighbor diamond (2nnd) lattice. An atomistic chain is mapped onto a coarse-grained model which each bead represents series of linked vector connecting the CH_2CH_2 was constructed. Both short-range interactions based on the rotational isomeric state model and long-range interactions from a discretized form of the Lennard-Jones (LJ) potential energy function are included. LJ parameters σ and ε/k_B of 4.2 Å and 205 K, respectively, are estimated for the coarse-grained model. Then, the static and dynamic properties of

bidisperse PE melts (B40, B30 and B20 mixed with B50) which the B50 composition is 25, 50 and 75% wt respectively, were studied at 509 K. The results show that the overall density profiles of bidisperse PE nanofibers are smaller than those of nanoparticles and decrease with decreasing the chain length of mixed chain. At the surface, the shorter chain is more abundant than longer one and end beads are more enrich middle beads. The longer chains are more anisotropic arrangement than the shorter ones. PE chains and largest principal axis tend to orient perpendicular to the surface which is predominant with increasing the chain length. Molecular sizes are decrease with decreasing chain length toward the surface. The longer chain behaviors are similar to monodisperse system and it processes similar properties in the same particle shape system but shorter chain properties are affected due to the present of longer chain and highly difference with decreasing chain length. These properties are not affected by the composition difference.

Finally, the bidisperse PE crystallizations were studied. The density profiles both of nanofiber and nanoparticle are similar to those of melt bidisperse nanofiber and nanoparticle system. For nannofiber, the shorter chains are forced into center of fiber. But in nanoparticle, it enriches near the surface. The crystallization process is easier than in nanoparticle system and occurs from the surface to inner region. The shorter chain is more easily crystallizing than longer chain and can be clearly observed in nanofiber system. The chain ordering in nanofiber is higher than that in nanoparticle.

School of Chemistry   Student's Signature   *Horrchana Gratemala*

Academic year 2010   Advisor's Signature   _____

ACKNOWLEDGEMENTS

Harnchana Gatemala

CONTENTS

CONTENTS (Continued)

CONTENTS (Continued)

LIST OF TABLES

LIST OF FIGURES

LIST OF FIGURES (Continued)

LIST OF FIGURES (Continued)

LIST OF FIGURES (Continued)

LIST OF FIGURES (Continued)

LIST OF FIGURES (Continued)

LIST OF FIGURES (Continued)

LIST OF FIGURES (Continued)

LIST OF FIGURES (Continued)

LIST OF FIGURES (Continued)

LIST OF FIGURES (Continued)

LIST OF ABBREVIATIONS

K	Kelvin
Å	angstroms
et al.	et alia (and other)
ε	depth of the potential well
σ	zero point of Lennard-Jones potential
PE	polyethylene
LJ	the Lennard-Jones potential
k_B, k	Boltzmann constant ($\sim 1.38 \times 10^{-23}$ J K^{-1})
B	bead number
i.e.	id est (that is)
nm	nanometer
T_g	glass transition temperature
IUPAC	International Union of Pure and Applied Chemistry
CPU	central processing unit
E	potential energy
E_σ, E_ω	the first-, second-order short-range interaction energies
f	Mayer f-function
g (g^+, g^-)	gauche (gauche plus, gauche minus)
t	trans

LIST OF ABBREVIATIONS (Continued)

MC	Monte Carlo
MD	Molecular Dynamics
rand	random number
RIS	rotational isomeric state
SNND, 2nnd	second nearest neighbor diamond
u	statistical weight
U	statistical weight matrix
Z	partition function
θ	(1) bond angle, (2) angle between chords
Φ	torsion angle
T_m	melting temperature
MCS	Monte Carlo Step
°C	degree Celcius
D	dimension
N	particle number
R_g	radius of gyration
$\langle\rangle$	ensemble average
S	chord order parameter
L	principal axis

LIST OF ABBREVIATIONS (Continued)

As	asphericity
Ac	acylindricity
ψ	angle between the main axes of two chains
S_G	global orientation correlation function
LDPE	low density polyethylene
HDPE	high density polyethylene
HMW	high molecular weight
UHMW	ultra high molecular weight
etc.	et cetera (and other things)
J/m^2	joule per square meter

CHAPTER I

INTRODUCTION

The prefix "nano" can be traced to the Greek word nanos, meaning the dwarf. It is used presently to indicate one billionth. A nanometer (nm) is one billionth of a meter, roughly ten times the size of an individual atom. A common comparison places on nanometer at approximately 100 times smaller than the diameter of a single human hair. Nanoscience involves the study of materials at the nanoscale. From this point on, terminology becomes less clear, as there are not internationally standardized definitions of nano-related term (Evans *et al*., 1999).

Nanotechnology, shortened to "nanotech", is the study of the controlling of matter on an atomic and molecular scale. Generally, nanotechnology deals with structures and size in range 1 to 100 nm in at least one dimension, and involves developing materials or devices within that size. Figure 1.1 gives a partial list of zero-dimensional nanostructures with their typical ranges of dimension (Dong Lu, 2003). Nanotechnology is very diverse, ranging from extensions of conventional device physics to completely new approaches based upon molecular self-assembly, from developing new materials with dimensions on the nanoscale to investigating whether we can directly control matter on the atomic scale (Wikipedia, 2011(a)). Today, nanotechnology is still at the beginning, and only rudimentary nanostructures can be created with some control.

Nanostructures and nanomaterials possess a large fraction of surface atoms per volume. The ratio of surface atoms to interior atoms changes quickly if divides a macroscopic object into smaller parts. For example, for a cube of 1 cm^3, the percentage of surface atoms would be only 10^{-5}%. When the cube is divided into smaller cubes with an edge of 10 nm, the percentage of surface atoms would increase to 10%. In a cube of 1 nm^3, every atom would be a surface atom. Figure 1.2 shows the percentage of surface atoms changes with a palladium cluster diameter (Nützenadel *et al.*, 2000). Such a dramatic increase in the ratio of surface atoms to interior atoms in nanostructures and nanomaterials might illustrate why changes in the size range of nanometers are expected to lead to great changes in the physical and chemical properties of the materials. Nanostructures and nanomaterials can be classified by their dimensions within nanoscale. A "nanoparticle" can be considered as a zero-dimensional nano-element, which is the simplest form of the nanostructure. It follows that a "nanotube or nanorod" is a one-dimensional nano-element form which slightly more complex nanostructure can be constructed of. Following this thought, a "nanoplatelet or nanodisk" is a two-dimensional element which along with its one-dimensional counterpart, are useful in the construction of nanodevices.
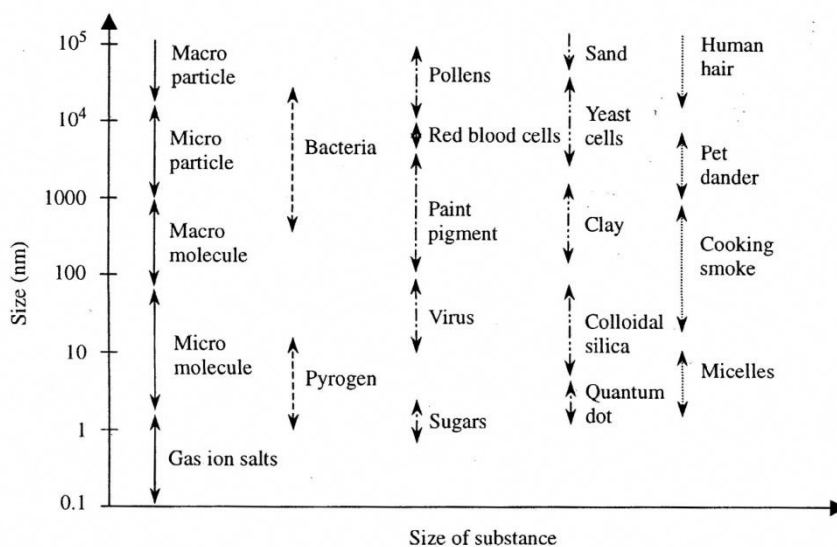
Figure 1.1 schematic representation of the examples of zero-dimensional nanostructures or nanomaterials with their typical ranges of dimension (Dong Lu, 2003).

The science of atoms and simplest molecules, on one end, and the science of matter from microstructures to larger scales, on the other, are generally established. The remaining size-related challenge is at nanometer scale (roughly between 1 to 100 molecular diameters) where the fundamental properties of materials are determined and can be engineered. A revolution has been occurring in science and technology, based on the developed ability to measure, manipulate and organize matter on this scale. Recently discovered organized structures of matter (such as carbon nano-tubes, molecular motors, DNA-based assemblies, quantum dots, and molecular switches) and new phenomena (such as giant magnetoresistance, coulomb blockade and those caused by size confinement) are scientific breakthrough that merely hints at possible future developments (Roco, 2001).
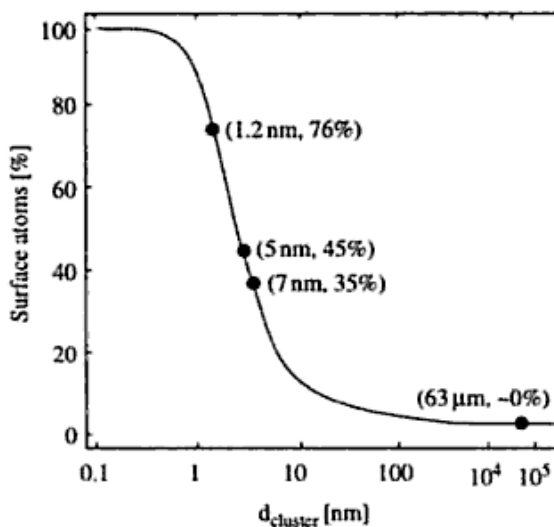
Figure 1.2 The percentage of surface atoms changes with the palladium cluster diameter (Nützenadel *et al*., 2000).

More and more, small structures with dimensions in nanometer regime play an important role within molecular biology, chemistry, materials science and solid-state physics. Of particular interest in biology there is, for example, the replication of proteins, the functionality of special molecular mechanism like hemoglobin or even such seemingly simple structures like the flagella of certain bacteria. Chemistry, on the other hand, deal with the synthesis (and therefore also with an improvement) of these structures with which nature solves so many problem. For example, the design of catalyst is a considerable commercial factor within the chemical industry. Specific modifications of properties of well-known materials using small particles and the development of fabrication processes of nanoparticles are topic of modern materials science. Self-cleaning surfaces as well as pigments are typical example for applications of nanostructures where, interestingly, the latter already led to some success within the cosmetic industry.

Recently, nanostructural materials have gained considerable attention owing to their unique properties and intriguing applications in many areas. One of these materials which the scientist was very interested is polymeric nanostructure materials. Polymers are a large class of materials consisting of many small molecules (called monomers) that can be linked together to form long chains, thus they are known as macromolecules. A typical polymer may include tens of thousands of monomers. Because of their large size, polymers are classified as macromolecules. Now, these polymeric materials can be created very fine particles of wide range composition and size. Therefore these materials have small diameter and large surface area of such polymeric nanostructure offer a new class of materials that can be used in diverse applications including filters, composites, fuel cells, catalyst supports, drug delivery devices, and tissue scaffolds. Confined macromolecules at nanometer scale exhibit a fascinating and unexpected dynamic behavior, which has attached much attention in recent years. These polymeric nanostructures provide many unique properties due to the size reduction to the point where critical length scales of physical phenomena become comparable to or larger than the size of the structure. Applications of such particles take the advantage of a high ratio of surface area to volume and the confinement effect, which leads to nanostructures with properties that differ from conventional materials. An example of the dependence of the physical properties on size is the liquid-glass transition temperature (T_g) with the film thickness. Generally, these indicate a reduction of T_g upon confinement, *i.e.* when film thickness becomes comparable to the size of polymer (or radius of gyration, R_g).

Americans consume approximately 60 billion pounds of plastics each year. There are two main types of plastics. The first is thermoplastics which soften on

heating and harden on cooling. The second is thermosets, on which heating, flow and cross-link to form rigid material which does not soften on future heating. Thermoplastics are more commercial usage than thermosets. Among the most important and versatile of the hundreds of commercial plastics is polyethylene (PE). PE is a thermoplastic polymer which consisting of long chains of the ethylene monomer (IUPAC name ethene). The ethene molecule (known almost universally by its common name ethylene) C_2H_4 is $CH_2=CH_2$. Two CH_2 groups are connected by a double bond. The recommended scientific name PE is systematically derived from the scientific name of the monomer. It is the most widely used plastic, with an annual production of approximately 80 million metric tons (Piringer and Baner, 2008). PE is used in a wide variety of applications because, based on its structure, it can be produced in many different forms. The first type of commercial PE is called low density PE (LDPE) or branched PE which is characterized by a large degree of branching, forcing the molecules to be packed rather loosely forming a low density material. LDPE is soft and pliable and has applications ranging from plastic bags, containers, textiles, and electrical insulation, to coatings for packaging materials. Another form of PE differing from LDPE is high density PE (HDPE) or linear PE. It differs from LDPE only in structure. This form demonstrates little or no branching, enabling the molecules to be tightly packed. HDPE is much more rigid than LDPE and is used in applications when the rigidity is needed. Major uses of HDPE are plastic tubing, bottles, and bottle caps. Other forms of this material include high and ultra-high molecular weight PE. HMW and UHMW are known. These are used in applications where extremely tough and resilient materials are needed.

● = C

○ = H
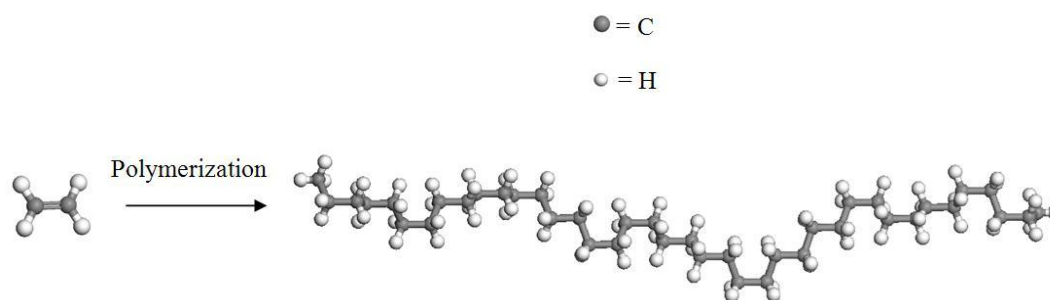
Polymerization

Figure 1.3 Schematic representation of the polymerization of PE.

Polymeric nanofibers can be processed by a number of techniques such as Drawing, Template synthesis, Phase separation, Self-essembly and Electrospinning. A comparison of the various issues relating to the processing methods and some of the polymers that can be converted into nanofiber can be found in Table 1.1 and 1.2.

As well as nanofiber, nanoparticle can be synthesized by several ways, for example, gas phase synthesis and sol-gel processing which is the major efforting in nanoparticle. Nanoparticles with diameters ranging from 1 to 10 nm with consistent crystal structure, surface derivatization, and a high degree of monodispersity have been processed by both gas-phase and sol-gel techniques. Typical size variances are about 20%. However, for measurable enhancement of the quantum effect, this must be reduced to less than 5% (Murray *et al*., 1993).

Table 1.1 Comparison of processing techniques for obtaining nanofibers.

Process	Technological advances	Can the process be scaled?	Repeatabi-lity	Convenient to process?	Control on fiber dimensions
Drawing	Laboratory	√	√	√	X
Template synthesis	Laboratory	X	√	√	√
Phase separation	Laboratory	X	√	√	X
Self-essembly	Laboratory	X	√	X	X
Electrospinning	Laboratory (with potential for industrial processing	√	√	√	√

Table 1.2 Advantages and disadvantages of various processing techniques to synthesis nanofiber.

Process	Advantages	Disadvantages
Drawing	Minimum equipment requirement.	Discontinuous process.
Template synthesis	Fibers of different diameters can be easily archieved by using different templates.	
Phase separation	Minimum equipment requirement. Process can directly fabricate a nanofiber matrix. Batch-to-batch consistency is archieved easily. Mechanical properties of the matrix can be trailored by adjusting polymer concentration.	Limited to specific polymers.
Self-essembly	Good for obtaining smaller nanofibers.	Complex process.
Electrospinning	Cost effective. Long, continuous nanofiber can be produced.	Jet instability.
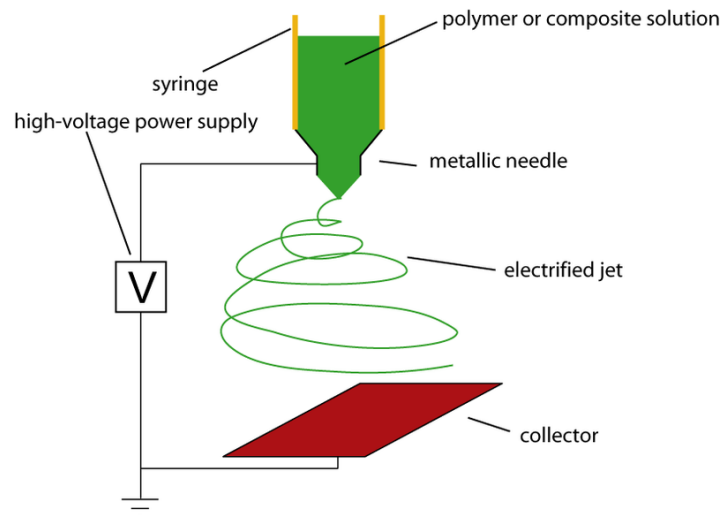
Figure 1.4 Schematic representation of nanofiber formation by Electrospinning process (Wikimedia Commons, 2009).

Initial development of new crystalline materials based on nanoparticles was generated by evaporation and condensation (nucleation and growth) in a subatmospheric inert-gas environment (Gleiter, 1989; Siegel, 1991; Siegel, 1994). Various aerosol processing techniques have been reported to improve the production yield of nanoparticles. (Uyeda, 1991; Friedlander, 1998) These include synthesis by combustion flame (Zachariah, 1994; Brezinsky, 1996; Axelbaum, 1997; Pratsinis, 1997); plasma (Rao and Heberlein, 1997); laser ablation (Becker and Nichols, 1997); chemical vapor condensation (Kear, 1997); spray pyrolysis (Messing, 1994); electrospray (de la Mora, 1994); and plasma spray (Berndt, 1997).

Sol-gel process is a wet chemical synthesis approach that can be used to generate nanoparticles by three steps. Firstly, gelation process is performed, and then the precipitation process and follows by hydrothermal treatment or drying process (Kung and Ko, 1996).
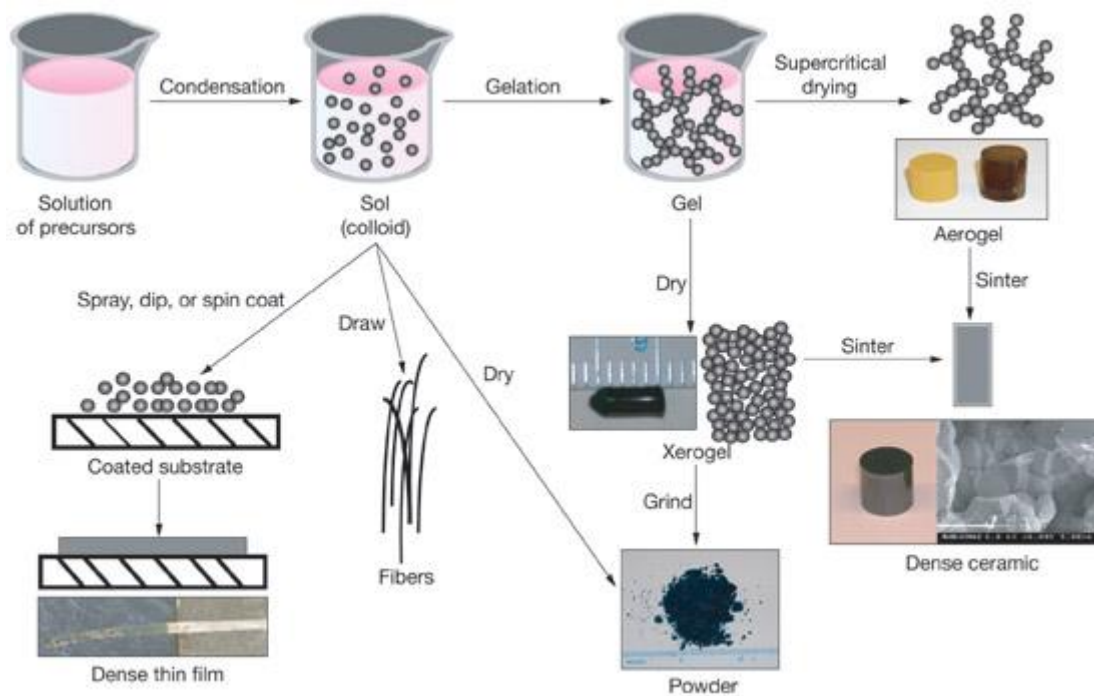
Figure 1.5 schematic representations of the sol-gel process and their products (Lawrence Livermore National Laboratory, 2005).

Various experimental techniques have been applied to polymer surfaces and interfaces. But individual polymeric nanofibers as well as polymeric nanoparticles are challenging to characterize experimentally due to their too small size. This is due in large part to the requirement that single nanostructured materials be isolated and manipulated without introducing defects prior to physical or mechanical analysis. Although considerable experimental investigations have been made but the knowledge at the molecular level is not completely understood. The key to beneficially exploiting these interesting materials and technology is a detailed understanding of the connection of polymeric nanostructure technology to atomic and molecular origins of the process. Computer simulation is one of the methods for investigating the properties of these systems. While real polymeric nanofiber and

nanoparticle may present difficulties in experimental studies in the laboratory, their models are easily created and studied in computer simulations. So, a few decades ago many of scientists used computer simulation to solve the problem which is the limitation of experiment. The simulations use a variety of approaches, for examples to represent the system in discretized (lattice) (Madden, 1987; Theodorou, 1988; Olaj *et al*., 1995; Doruker and Mattice, 1998; Muller and MacDowell, 2000) or continuous (Mansfield and Theodorou, 1990; Mansfield and Theodorou, 1991; Harris, 1992; Kumar *et al*., 1994; Misra *et al*., 1995) space, adoption of coarse-grained (Kumar *et al*., 1994; Doruker and Mattice, 1998; Muller and MacDowell, 2000) or atomistically detailed (Mansfield and Theodorou, 1990; Mansfield and Theodorou, 1991; Harris, 1992; Misra *et al*., 1995) models, and focus on either static (Madden, 1987; Theodorou, 1988; Mansfield and Theodorou, 1990; Kumar *et al*., 1994; Misra *et al*., 1995; Olaj *et al*., 1995; Doruker and Mattice, 1998; Muller and MacDowell, 2000) or dynamic (Mansfield and Theodorou, 1991; Harris, 1992; Doruker and Mattice, 1998) aspects of the surface. In Molecular Dynamic (MD) simulation, the equations of motion for the system of molecules are solved to obtain time-dependent dynamic properties of the system. The MD simulation is very high efficiency for studying the atomistic details of nanometer-scale PE particles with up to 120,000 atoms (Rapold and Mattice, 1995; Rapold and Mattice, 1996; Cho and Mattice, 1997; Doruker and Mattice, 1997; Baschnagel *et al*., 2000; Xu and Mattice, 2001). This simulation method creates homogeneous nanoparticles that are in good agreement with 2-D diffraction observations on experimentally generated polymer nanoparticles. Due to the system size limitation of MD simulations, only local properties and

energetic of free surfaces have been considered in the studies so far. However it is impractical to repeat because of time-consuming in MD simulation.

Several earlier studies in 1980's looked at the interfacial structure of polymer malts using lattice Monte Carlo (MC) (Madden, 1987; ten Brinke *et al.*, 1988; Mansfield and Theodorou, 1989), off-lattice MC (Kumar, 1988; Yethiraj and Hall, 1989), and the lattice fluid model (Theodorou, 1989(a & b)) which these technique are coarse-grained model based on the Sanchez-Lacombe theory (SanchezI, 1976). Recently, interest in the development of simulation methods for bridging between atomistic and coarse-grained models of polymers provides an opportunity for simulation of larger models of real systems (Baschnagel *et al.*, 2000). One type of implementation of these methods involves mapping Rotational Isomeric State (RIS) models onto high coordination lattice (Rapold and Mattice, 1995; Rapold and Mattice, 1996; Cho and Mattice, 1997) with subsequent reverse mapping of the equilibrated model to an atomistic description in continuum space (Doruker and Mattice, 1997).

If confined polymer in nanoscale can crystallize. The crystallization of polymers in the confined geometry has received much attention since the control of anisotropic molecular orientations inside the ordered block copolymer may be potentially significant for novel technological applications (Evans, *et al.*, 1999). On the other hand, from a theoretical point of view, the crystallization of one component may affect the original phase-separated structures above the melting temperature (T_m), and the crystallization process may also be changed in the confined geometry (Hamley, 1988; Chen *et al.*, 2001). However, the rapid development of the modeling method and dramatic increase of the computational speed, computer simulation has become a powerful and promising tool for investigating the molecular process of

polymer crystallization in the confined geometry. The properties of freestanding thin films have been investigated by various simulation techniques such as MD simulation, MC simulation, *etc*. Reducing the temperature of the amorphous freestanding thin, for example film will spontaneously change the initial structure to one that contains highly ordered domains. But the time scale required for development and propagation of the crystals from the melt is not conveniently accessible to simulation with atomistically detailed models. Therefore, this type of film is less studied by simulation than the amorphous films. An excellent example of the application of MD methods to this difficult system is a robust simulation of a freestanding film of a united atom model of PE.

Research objectives

In this research, the MC simulation on 2nnd lattice will be employed to study the effects of chain length and composition on the on the structural and dynamic properties of bidisperse PE nanofibers and nanoparticles which compose of short PE chain. Moreover, this technique will be applied to study the crystallization of bidisperse PE nanofibers and nanoparticles.

Scope and limitations

Second-nearest neighbor diamond (2nnd) lattice based MC approach was applied throughout this study to investigate the effect of mixed molecular weight (short- and long-chain bi-mixtures) on structures, dynamics and crystallization of PE nanofiber and nanoparticle.

Effect of molecular weight bidispersity on structural and dynamic properties of PE nanofibers

The systems used in this section is composed of the mixture of short and long chains : each systems contain B50+B40, B50+B30 and B50+B20 (the numbers after B are the bead numbers for each PE chain which each bead was contained CH_2-CH_2 unit) which the composition of B50 in each system is varied at 75, 50 and 25% by weight respectively. The simulations are performed at 509 K for all simulation with 0.18% of bead occupancy. The system is equilibrated at least 10 million Monte Carlo steps (MCS). Then the latest conformation is run for an additional 10 million MCS to obtain data for subsequent analysis.

Effect of molecular weight bidispersity on structural and dynamic properties of PE nanoparticles

The latest conformation structure of nanofibers in each system is extended in the *y* axis dimension and run at least 10 million MCS to equilibrate the structure. Data analysis is performed after another 10 million MCS of this equilibrated structure. These nanoparticles are analyzed for the effect of bidispersity on structural and dynamic properties in similar way to those of nanofibers.

Crystallization Study

The systems represent the mixture of B20+B15 with 0.22% of bead occupancy. The composition of B20 is fixed at 50% by weight. The simulation method is similar to bidisperse systems. When the nanofibers and nanoparticles are obtained, the temperature is instantaneously dropped from 509 K to 298 K, and the

simulation is continued at 298 K. 30 million MCS is needed to observe the crystallization.

Data Analysis

For all of systems, the structural, conformational, and structural formation from crystallization is investigated in terms of :

Density profile

- Radial density profile of nanofiber and nanoparticle.

- Radial density profile of middle beads and end beads of nanofiber and nanoparticle.

Orientation

- Chords orientation of nanofiber and nanoparticle.

- Orientation of the largest and smallest principal moment to fiber axis after equilibration.

Chain properties

- Changing in R_g component as a function of radial displacement of the center of mass of nanofiber and nanoparticle.

- Changing in chain shape as a function of radial displacement of the center of mass of nanofiber and nanoparticle.

- Principal moment of chains as a function of radial displacement of the center of mass of nanofiber and nanoparticle.

CHAPTER II

LITTERATURE REVIEW

Macromolecules differ from small molecules in enormous number of conformations that they populate at ordinary temperature. Computer simulations are a useful tool for understanding the equilibrium and dynamic properties of surfaces at the molecular level of these macromolecules. A number of different model and theorical devices has been created since the early days of polymer science for the treatment of macromolecules to average the conformation-dependent physical properties.

2.1 Simulation of amorphous polymer

Molecular shape and the way molecules are arranged in a solid are important factors in determining the properties of polymers. The molecular structure, conformation and orientation of the polymers can have a major effect on the macroscopic properties of the material. In 1985, D.N. Theoderou and U.W. Suter (Theodorou and Suter, 1985) was the pioneer worker who studied the amorphous polymer by using computational technique. They used a modified Markov process, based on Rotational Isomeric State (RIS) theory and incorporating long-range interactions to generate an initial structure. Then this structure was relaxed by potential energy minimization, using analytical derivatives. A model was developed for the detailed atomistic modeling of well-relaxed amorphous glassy polymers.

Atactic polypropylene at -40°C was used for an example as shown in figure 2.1.

This model system was a cube with the periodic boundaries. The results show that the cohesive energy density and the Hilderbrand solubility parameter agree with the experimental results. The conformation of the single chains in the relaxed model system closely resembles that of perturbed chains. Pair distribution functions and bond direction correlation functions show that the predominant structural features are intramolecular and long-range orientational order is completely absent. In addition, in 1989 D. Brown *et al.* (Brown and Clarke, 1991) used MD simulation to study the properties of a linear polymer model resembling PE over a wide range of temperatures. Polymer samples were generated by using a modified self-avoiding random walk performed within the confines of the periodic boundary conditions, followed by dynamical relaxation at constant pressure. The results show that phenomena such as elasticity, yield, and plastic flow are all accessible to dynamic atomistic modeling. The short time scale broadens the temperature range and reduces the magnitude of the changes observed as the material transforms from a viscoelastic fluid to an elastic solid.

In 2003, K.V. Workum *et al.* (Van Workum and de Pablo, 2003) used both of MC and MD simulations to investigate the properties of amorphous polymeric nanostructures. A continuum mechanics model was applied to determine an apparent modulus for such structures from results of virtual deformation simulations. The effect of size on the apparent modulus of ultra-small structures was explored and the results show that for a given system at a specified temperature, the modulus of a small structure can be significantly smaller than that of the bulk material.
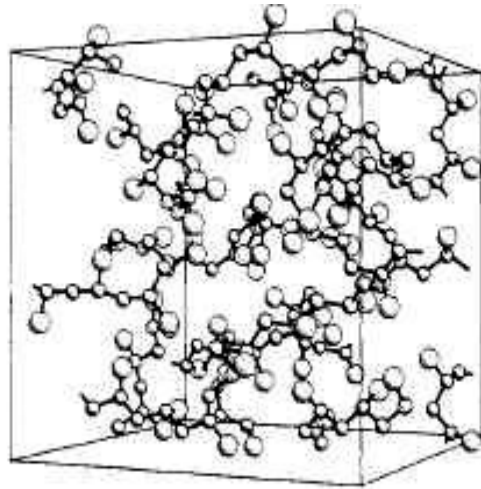
Figure 2.1 "Relaxed" model structure in detailed mechanical equilibrium. The small spheres denote skeletal carbon atoms, the large spheres indicate methyl groups, and hydrogen atoms have been omitted for clarity (Theodorou and Suter, 1985).

2.2 Molecular simulation of monodisperse and bidisperse PE thin film

Polymer films of various materials have been developed for many purposes. For example, bags and wrapping material was used for storage or to provide protection from the environment. PE film is a resinous material with thermoplastic properties which can be synthesized by inducing oxidative polymerization of ethylene gas. The degree of pressure used in its manufacturing varies according to the density and melting point of the virgin polymer resin being used. The process which the most common to produce the sheets of PE film is blown film extrusion, in which the polymer resin is melted to its flow point and then extruded through a die to produce a tube of plastic. While the PE is still supple, the tube is closed off at one end and then

blown to inflate and stretch the film into the desired length and thickness. By this process the thickness of PE film can be as thin as 0.0004 inch (10.16 microns).

The simulations are useful tool to analyze polymer thin films that present free surfaces to vacuum. In 1990, Mansfield and Theodorou (Mansfield and Theodorou, 1990) reported a detailed atomistic simulation of the surface of a thin ($\approx$6.2 nm) film of atactic polypropylene which was a confinement of polymeric systems. They used the potential gradient method to generate the films and use orthorhombic box to pack the chains. A steep potential was employed at the faces of the cell normal to the longest direction to confine the chains within the box. The results show that except for the region slightly thinner than 1 nm near the free surfaces as shown in figure 2.2(a), the bond orientations and density exhibited bulk properties. Backbone bonds near the surface had a tendency to orient parallel to the plane of the surface as shown in figure 2.2(b), and the distribution of rotational isomeric states near the surface deviated from the bulk values which the experiments to measure properties of these films become very difficult.

VARIATION OF POLYMER SEGMENT DENSITY

— BULK VALUE ●——● TOTAL △——△ C ■——■ CH₃ ◇——◇ H

(a)

BOND ORIENTATION CHARACTERISTICS

$$S_B = (1/2)[3\langle\cos^2(\theta)\rangle - 1]$$

□——□ C-C ●——● C-H △——△ C-CH₃

(b)
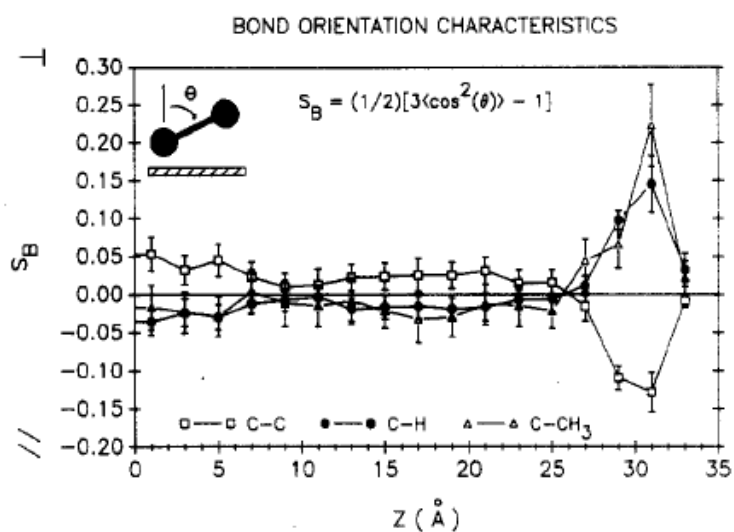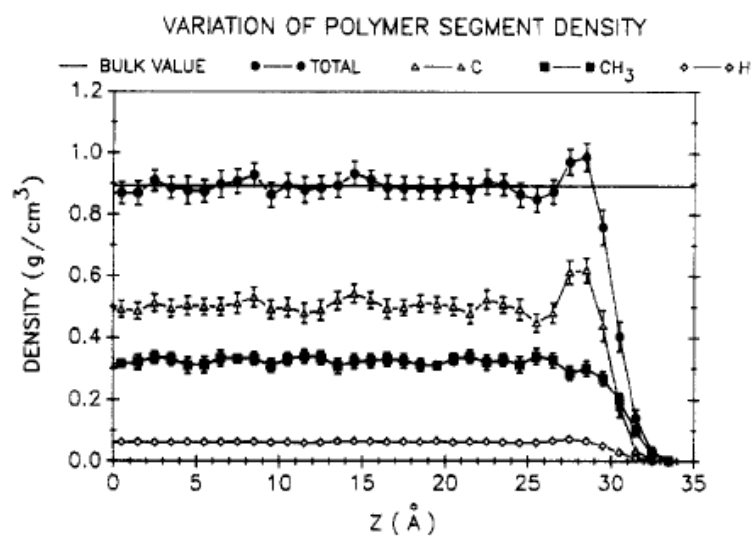
Figure 2.2 (a) The local mass density distribution at a glassy polymer vacuum interface. (b) Local order parameter for C-C, C-H, and C-CH₃ bonds as a function of distance from the film midplane (Mansfield and Theodorou, 1990).

In 1995, Misra *et al.* (Misra *et al.*, 1995) prepared free-standing cis-1,4-poly-butadiene thin films from equilibrated bulk amorphous cells by extending the *z* dimension of the periodic box normal to the proposed plane of the film. This

dimension was extended far enough (10 nm) so that the single parent chain did not experience any interactions with its images in that direction. With a subsequent relaxation, this extension technique gave films with "pseudo-2D" periodicity along the film plane. Films with thickness of 2.5 nm were obtained. The density and orientation function conformed to values expected for a bulk isotropic structure near the mid-plane of the film. The density was found to drop from a value of bulk density to zero over a distance slightly smaller than 1 nm, and the backbone bonds had preferential orientation in the surface region. The calculated contribution of the internal energy to the surface energy was within 17% of the experimental value. This atomistic simulation technique for preparation of a freestanding thin film was subsequently applied to PE (He *et al*., 1997), random copolymers (Natarajan *et al*., 1998), and polybenzoxazine (Kim and Mattice, 1998).

MD simulations of thin films formed by single chains of one hundred monomers were performed with amorphous PE (Misra *et al*., 1995). But the thickness of the films which are produced by MD simulations is quite small (less than 40 Å between the two free surfaces). So the films consist mainly of two interface regions with the density in the center of the film approaching the bulk polymer density at the specific temperature. It is still possible to analyze the local interfacial properties, such as the distribution of torsional angles and the orientation of bonds. The estimated surface energy which compare with bulk simulations was close to experimental results. However, it is impossible to fully atomistically simulate larger films with a thicker cross section and/or for a longer time, to analyze the global equilibrium properties and/or the dynamics of chains.

P. Doruker and W.L. Mattice (Doruker and Mattice, 1998) used MC simulation on high coordination (2nnd) lattice by including short- and long-range interactions to study the monodisperse PE films which contain up to 108 chains of C99 and have thicknesses of more than 100 Å. In these films, the density profiles are hyperbolic, with end beads being more abundant than the middle beads at the interface. There are orientational preferences at the interface on the scale of individual bonds and whole chains. The center of mass distribution of the chains exhibits oscillatory behavior. A comparison of films with different thicknesses, which contain different number of chains, does not indicate any significant differences in local and global equilibrium properties as shown in figure 2.3(a). At lower temperatures, the interfaces get sharper and the orientational preferences are more pronounced as shown in figure 2.3(b). Surface energies close to experimental values are calculated directly from the on-lattice energetics. It is also possible to reverse map equilibrated snapshots from the lattice back to the atomistic model and minimize their energy. The energetics of the resulting film snapshots in continuous space seem to be in agreement with the experimental data on PE.
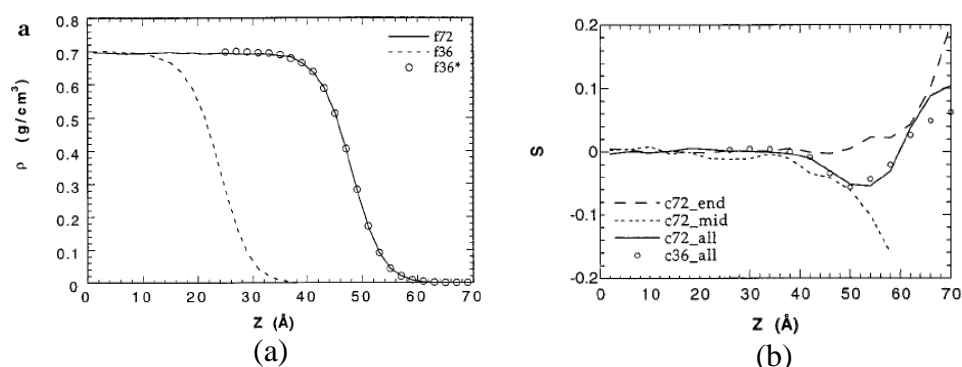
Figure 2.3 (a) Density profiles of two PE films at 509 K as a function of the distance from the center of mass in the Z direction. (b) Orientation of the coarse-grained 2nnd bonds with the Z-axis (Doruker and Mattice, 1998).

In general, polymers in the real system contain various chain lengths which affect the properties of the materials. P. Doruker *et al.* (Doruker, 2002) used an on-lattice MC technique to study the effect of bidispersity (number of carbon per each chain are 50, 100 and 316 atoms) on the properties of free-standing thin film. It was found that the global and local properties at the surface, such as an orientation of bonds and chains, were enhanced in film compose of longer chains. Films that contain two different chain lengths were found that the longer chains possess similar properties in the monodisperse and mixed films as shown in figure 2.4.
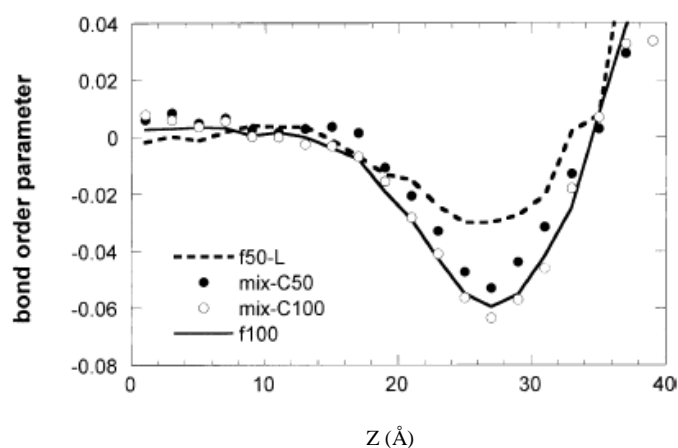
Figure 2.4 Comparison of the orientation of C50 and C100 bonds in the mixed film f100/50 with the orientation in the monodisperse film. The *z* position (*x* axis) is defined as the middle point of each coarse-grained bond (Doruker, 2002).

2.3 Molecular simulation of monodisperse PE nanofiber

Individual polymeric nanofibers are challenging to characterize experimentally because of their small size. This is due in large part to the requirement that a single nanofiber be isolated and manipulated without introducing defects prior

to physical or mechanical analysis. Atomistic computer simulations can be helpful in determining and predicting the properties of individual nanofibers, especially as a function of length scales that are comparable to molecular dimensions. S. Curgul *et al.* (Curgul *et al*., 2007) used MD simulation to investigate the effect of nanofiber size to size-dependent properties of PE nanofibers with the chain lengths between 50 to 300 carbon atoms. These nanofiber diameters are in the range 1.9 to 23.0 nm. The results show that the mass density at the center of all fibers is constant and comparable to that of the bulk polymer. The surface layer thickness ranges from 0.78 to 1.39 nm for all fibers and increases slightly with fiber size. The calculated interfacial excess energy is 0.022 ± 0.002 J/m^2 for all of the simulated nanofibers. The chains at the surface are more confined compared to the chains at the center of the nanofiber; the latter acquire unperturbed dimensions in sufficiently large nanofibers. Consistent with experiments and simulations of amorphous polymer films of nanoscale thickness, the glass transition temperature of these amorphous nanofibers decreases with decreasing fiber diameter, and is independent of molecular weight over the range considered.

In 2000, V. Vao-soongnern *et al.* (Vao-soongnern *et al*., 2000) reported the structural and dynamic properties of monodisperse PE nanofiber using MC simulation on 2nnd lattice which incorporates the rotational isomeric state (RIS) theory that gives the molecular detail depending on the level of coarse-graining and long-range interaction. It was found that, for nanofiber, the density profiles were hyperbolic tangent with end beads being more abundant than middle beads at the surface as shown in figure 2.5(a). There were orientational preferences at the surface on the scale of individual bonds and the whole chains as shown in figure 2.5(b). Even if

there is different thickness of fibers, it was not observed any significant differences in the local and global equilibrium properties.

(a)

(b)
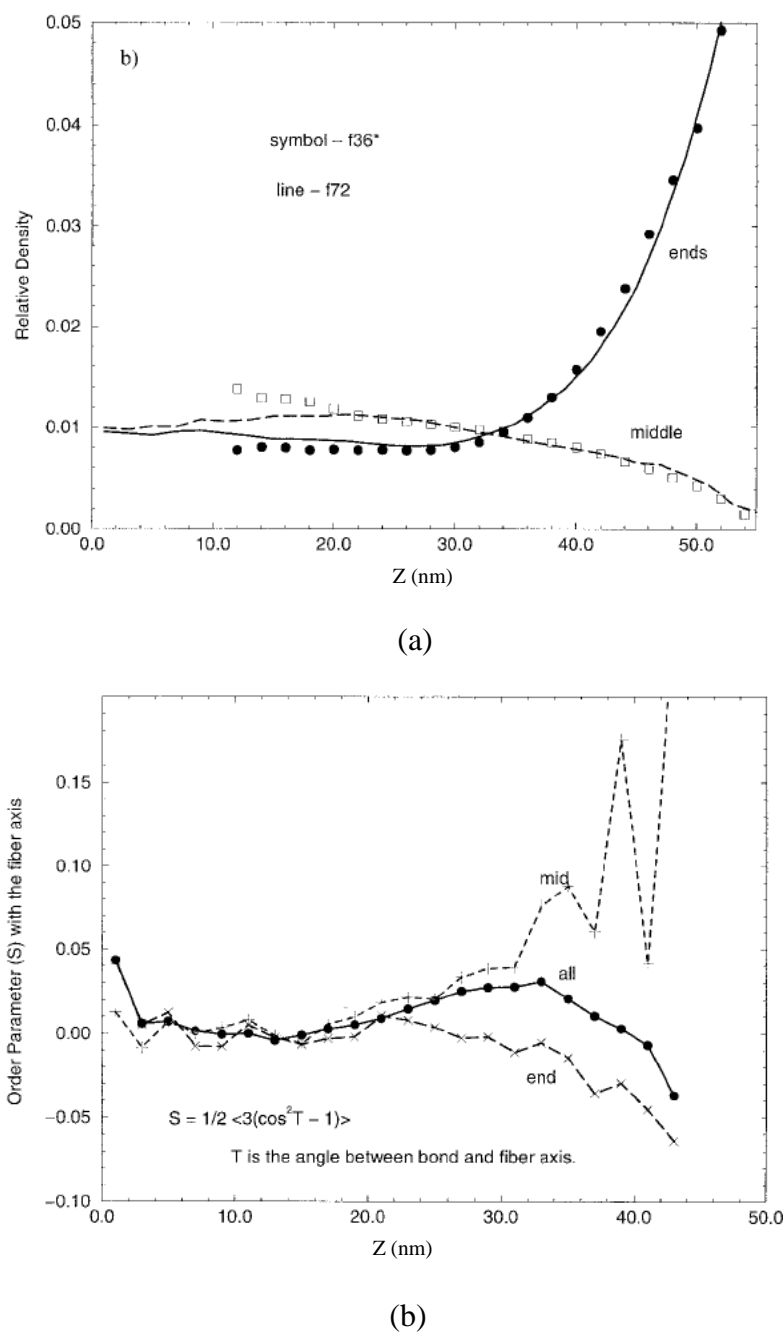
Figure 2.5 (a) Normalized radial density profiles for mid/end beads for f36 and f72 of C99 at 509 K. (b) The orientation of chords (mid-, end- and all) (Vao-soongnern *et al*., 2000).

2.4 Molecular simulation of monodisperse PE nanoparticle

Nowadays, an experimental technique was developed for creating very fine polymer particles of arbitrary composition and size (Barnes *et al*., 1999).These particles in the nanometer size range provide many unique properties due to the size reduction to the point where critical length scales of physical phenomena become comparable to or larger than the size of the structure. The experiments to measure properties of these particles were very difficult. Fortunately, this is the regime where it is possible to use molecular simulation to perform the analysis of the desired physical properties. In their pioneering works, Fukui *et al*. (Fukui *et al*., (1999a&b); Fukui *et al*., 2000; Fukui *et al*., 2001) have performed the large-scale MD simulation to study the atomistic details of nanometer-scale PE particles. Although those MD works gave insights into the properties of nanoparticles, more detailed knowledge at the molecular level is needed. As well as nanofibers the MD technique was limited by the system size. More efficient method to study the larger systems was a coarse-grained MC simulation on a high coordination lattice was developed to explore the behavior of large polymeric systems.

In 2001, V. Vao-soongnern *et al.* (Vao-soongnern *et al*., 2001) reported the structural and dynamic properties of monodisperse PE nanoparticle as shown in figure 2.6 using the same technique which was applied for nanofiber. For polymer nanoparticle system, it was found that the results were similar to that of nanofiber systems. The density profiles were also hyperbolic which show in figure 2.7(a), with end beads being more abundant than middle beads at the surface. There were orientational preferences at the surface on the scale of individual bonds and whole

chains. While the different size of droplets did not show any significant differences in the local and global equilibrium properties as shown in figure 2.7(b).
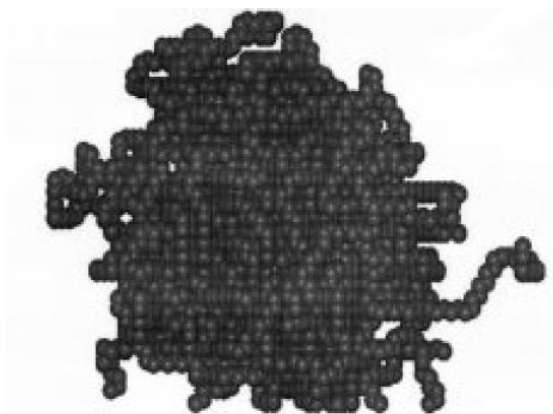
Figure 2.6 Illustration of the smaller amorphous PE nanoparticle composed of 36 coarse-grained chains of $C_{100}H_{204}$ from the 2nnd lattice simulation. Only the backbone carbon atoms are shown (Vao-soongnern *et al*., 2001).
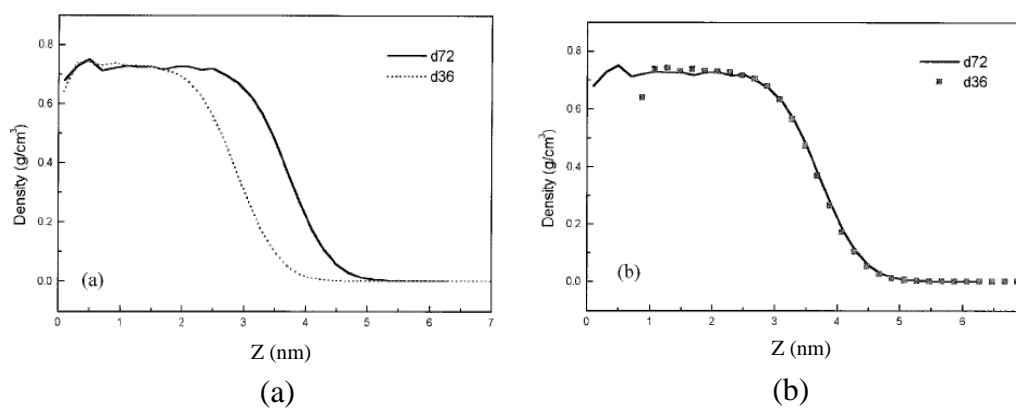
Figure 2.7 (a) Radial density profiles as a function of distance from the center of mass of the nanoparticle. (The bulk density is ~0.7 g.cm^{-3}). In (b) the data for d36 are moved to the right by 0.10 nm to show the superimposition on the d72 curve (Vao-soongnern *et al*., 2001).

2.5 Molecular simulation of monodisperse and bidisperse of crystallization of PE nanostructure

M. Ito *et al*. (Ito *et al*., 1998) used the MD to quench the temperature of PE free standing film from 500 to 300 K. The results show that the crystallization begins from both surfaces into the interior of the film which show in figure 2.8. The ordered chains are oriented with their long axis in the plane of the surface, but different direction on the two sides of the thin film. Unfortunately, it is impractical to repeat this time-consuming MD simulation many times. In 2001, Xu *et al*. (Xu and Mattice, 2002) reported the study of crystallization and annealing of free standing film of $C_{40}H_{82}$ by MC method on high-coordination (2nnd) lattice. The coarse-grained chain, represented by 20 beads, can be reverse-mapped into the fully atomic description. When the melt is instantaneously quenched from 473 to 298 K, the crystallization begins from the surface into the interior of the film which corresponds to the simulation from MD method of M. Ito *et al*. work. In addition, annealing process with temperature higher than the melting point of PE finds that the thin film with a grain boundary between two differently oriented crystalline domains can transform into a configuration with only a single crystalline domain and no grain boundary. In contrast, shorter chain properties were affected due to the presence of longer chains, displaying increased surface anisotropy in the mixture. In addition, G. Xu *et al*. (Xu and Mattice, 2002) used the same technique to study the effect of bidispersity on co-crystallization of a mixture of shorter chains (number of carbon per each chain are 30 and 40 atoms) PE in thin film. It was found that at high temperature, 420 K, (above T_m of two pure components) two kinds of chains had a trend to separate in the surface region which shorter chains were enriched on the free surface because of the larger

amount of chain ends. At low temperature, 298 K, (below T_m of two pure components) the film indicated two behaviors which depended on the prior history of the mixture. If the quench took place from a homogeneous mixture, the chain crystallized together with almost the same density profile except for a large fluctuation in the bulk region of thin film. For the equilibrated thin film at 402 K, the shorter chains remained enrich on the surface, and the segregation of the shorter chain was enhanced.

(a)   (b)
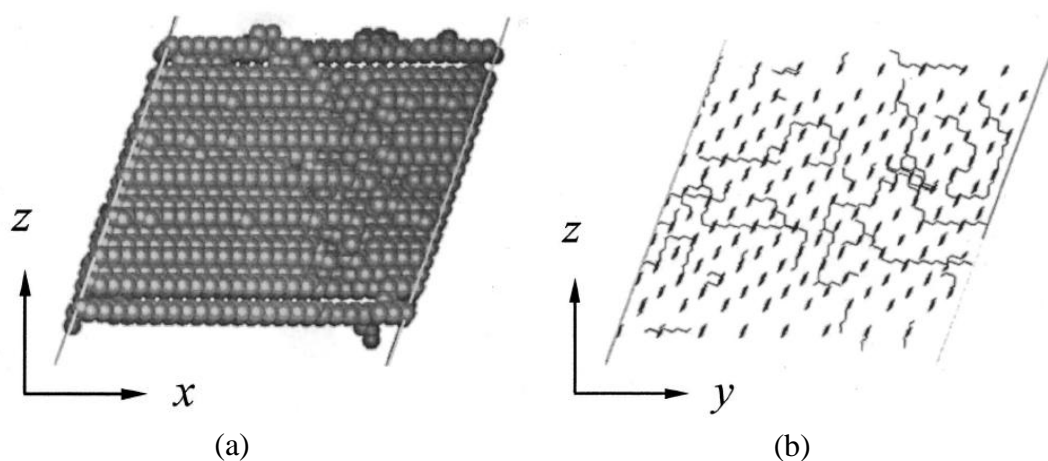
Figure 2.8 Snapshot of the internal structure of the final conformation of an atypical thin film at 298 K, represented by (a) all carbon atoms, viewed along the y axis, and (b) all C-C bonds, viewed perpendicular to the x axis (along the long axis of the ordered chains) (Xu and Mattice, 2002).

In this research, the MC simulation on 2nnd lattice will be employed to study the effects of chain length and composition on the properties of bidisperse PE nanofibers and nanoparticles which compose of short PE chain. Moreover, this technique will be applied to study the crystallization of bidisperse PE nanofibers and nanoparticles.

CHAPTER III

RESEARCH METHOLOGY

3.1 Monte Carlo (MC) simulation

The Monte Carlo method is a stochastic strategy that relied on probabilities. It is the simulation technique that gathers simplest in a random way. As the name of "Monte Carlo" implies, the MC simulation uses random numbers for making decision during the simulation. In terms of molecular mechanics, the MC provides another way to explore a conformational space. MC simulation can find a conformational state in a stochastic way by generating random numbers. With a given potential like Equation 3.1, the simulation involves a successive energy evaluation to make a decision for acceptance of a move attempt which is chosen randomly.

$$V_{totla} = \underbrace{V\left(r\right)_{bond} + V\left(\theta\right)_{angle} + V\left(\phi\right)_{torsion} + V\left(\chi\right)_{out-of-plane}}_{V_{bonded}} + \underbrace{V\left(r\right)_{vwd} + V\left(r\right)_{elec}}_{V_{non-bonded}} \qquad (3.1)$$

To simulate polymer systems, transition between different states or configurations are achieved by : (a) generating a random trial configuration; (b) evaluating an "acceptance criterion" by calculating the change in energy as equation 3.1 and other properties in the trial configuration; (c) comparing the acceptance criterion to the random number and either accepting or rejecting the trial configuration. It is

important to rely that not all states will make a significant contribution to the configurational properties of the systems. To accurately determine the properties of the system in the finite time available for simulation, it is important to sample those states that make the most significant contributions this is achieved by generating a Markov chain.

A Markov chain is sequence of trials in which outcome of successive trials depends only on the immediate predecessor. In a Markov chain, a new state will only be accepted if it is more "favorable" than the existing state. In the context of simulation using an ensemble, this is usually means that the new trial state is lower in energy.

A MC simulation samples from a 3N-dimentional space represented by the position of particles. It is not necessary to know particle momenta to calculate thermodynamics properties because the momenta contribute exclusively to the ideal gas term. Deviation from ideal behavior is caused by the interaction between particles which can be calculated from potential energy function (Equation 3.1). The potential energy depends only on the positions of atoms and not their momenta. In effect, a MC simulation calculates excess thermodynamics properties that result in deviations from ideal gas behavior. The appropriate ideal gas term can be simply added at the conclusion of the simulation to obtain the total thermodynamics property.

The average of any thermodynamics property $\langle A(r^N) \rangle$ can be obtained by evaluating the following multidimensional integral over the 3N degrees of freedom on the N particles in system.

$$\langle A(r^N) \rangle = \int A(r^N) \rho(r^N) dr^N \qquad (3.2)$$

Where $\rho\left(r^{N}\right)$ is the probability of the obtaining configuration r^{N} which depends on

the potential energy V_{total} of the configuration.

$$\rho\left(r^{N}\right) = \frac{\exp\left[-\beta E\left(r^{N}\right)\right]}{\int \exp\left[-\beta E\left(r^{N}\right)\right] dr^{N}}$$ (3.3)

These integral cannot be evaluated analytically and conventional methods of are also

not feasible. For example to apply either Simpson's rule or the trapezium rule to

evaluate a 3N-dimentional integral would require m^{3N} function evaluations, where m

is the number of points required to determine the integral in each dimension. The MC

simulation is generating a large number of trial configurations r^{N} and replacing the

integral by summation over a finite number of configurations. If the configurations

are chosen randomly, equation 3.1 becomes:

$$\left\langle A\left(r^{N}\right)\right\rangle = \frac{\sum_{i=1}^{N_{trial}} A_{i}\left(r^{N}\right)\exp\left[-\beta E_{i}\left(r^{N}\right)\right]}{\sum_{i=1}^{N_{trial}} \exp\left[-\beta E_{i}\left(r^{N}\right)\right]}$$ (3.4)

In practice, this simple approach is not feasible because random sampling

yields many configurations which have very small Boltzmann factor. Such

configurations make very little contribution to the average. Therefore, a prohibitively

large number of configurations are required to obtain the correct number. The

limitations of random sampling can be avoided by generating configurations that

make a large configuration to the right hand side of the equation 3.4. This is the

philosophy behind Metropolis sampling (Metropolis *et al*., 1953). Metropolis

sampling biases the generation of configurations towards those that make the most

significant contribution to the integral. In generate states with a probability of

$\exp\left[-\beta E\left(r^N\right)\right]$ and count each of them equally. In contrast, simple MC integration generates states with equal probability assigning them a weight of $\exp\left[-\beta E\left(r^N\right)\right]$. Metropolis sampling generates a Markov chain which satisfies the condition in following criteria.

$$\Delta E = V\left(r\right)_{new} - V\left(r\right)_{old} \leq 0 \qquad \text{accepted}$$

$$\Delta E = V\left(r\right)_{new} - V\left(r\right)_{old} > 0 \text{ and } \exp\left(-\Delta E / kT\right) \geq rand\left(0,1\right) \text{ accepted} \qquad (3.5)$$

$$\Delta E = V\left(r\right)_{new} - V\left(r\right)_{old} > 0 \text{ and } \exp\left(-\Delta E / kT\right) < rand\left(0,1\right) \quad \text{rejected}$$

If the new state is in a lower energy state, the new state replaces the previous state. If the new state is in a higher energy state, the decision is based on the energy difference between two states. For the decision procedure, MC simulation allows a system to move to higher energy state. The probability to overcome the higher energy barrier depends on the energy difference between the new attempt and the current conformation. By doing so, MC simulation explores the conformational space to calculate the ensemble averaged properties. Much effort has drawn attention to increasing the computational efficiency of MC simulation. One of the efforts is to run the simulation on a lattice, which reduces the floating number calculation. Another way to gain speed in the MC simulation is to use an efficient move algorithm that allows the faster relaxation or equilibration. Many beads can move at a single move attempt. The computational time of the lattice simulation based on MC method is proportional to the power of 1 to 2 depending on the quality of the potential energy function.

3.2 Monte Carlo simulation on a high coordination lattice

There is considerable interest in the application of MC algorithm (Baschnagel and Binder, 1995) to determine the properties of large molecules such as polymers. In principle, the approach used for small flexible molecules could be extended to polymers. However, the practice of changing randomly the torsional angle is likely to lead to a high rejection rate. Even a relatively small change in the torsional angle in the middle of large flexible molecule is likely to result in a large translational displacement of the terminal atoms. Consequently, there is a high probability of molecular overlap resulting in the rejection of the move. Another limitation of the small flexible molecule approach is determining Euler angles or using quaternion ions for each atom of a large molecule requires considerable computational effort.

One representative MC simulation is the bond fluctuation model (Deutsch and Binder, 1991; Paul *et al.*, 1991; Baschnagel *et al.*, 1998), which is a more efficient method compared to simple cubic lattice model in that it allows a better flexibility for the bond length and bond angle; it would be more appropriate to say step length and angle between two successive steps. Another way to give a more flexibility to span a conformational space is to use a high coordination lattice like diamond lattice (Rapold and Mattice, 1995). In a lattice based MC simulation, the computational cost can be largely reduced by using large-scale moves. As shown in figure 3.1, there are several elementary moves such as kink jump, crank shaft rotation, and end rotation known as the standard Verdier-Stockmayer type move (Verdier and Stockmayer, 1962). In addition to the basic moves, the reptative move (Fried and Binder, 1991), the end-bridging move, and the concerted rotation move (Pant and Theodorou 1995) can be

useful for the faster relaxation and can deal with a more delicate situation like a polydisperse system, as illustrated in figure 3.2.

(a) kink jump   (b) crank shaft rotation   (c) end rotation
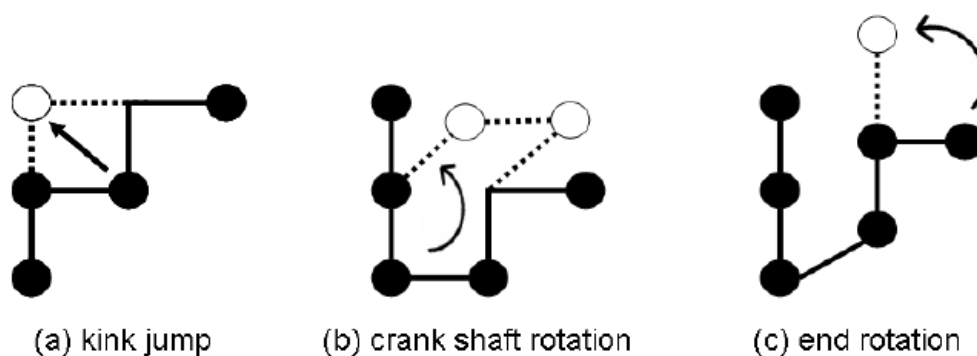
Figure 3.1 Basic elementary moves based on the standard Verdier-Stockmayer type model.

A coarse graining model in a lattice has the computational efficiency that comes from two reasons. The first one is the reduction of the evaluation of energy terms, which is generally proportional to the square of the number of particles because many energetic terms are two-body potentials. The second reason is that the positions of particles during simulation can be stored as integers, which reduces the number of instructions done by a central processing unit (CPU) and memory usage compared to the real number operation in off-lattice simulation. As a result of the efficiency, the method enables running a simulation in a large scale, which is required for polymer simulation. As often is the case, the pros come with the cons. Due to the coarse graining, the detailed chemical information such as the chemical nature of the coarse-grained particle (bead) and the nature of bond between the two beads disappears. The drawback would not be an important issue when a polymer chain is expressed by a collective set of simple beads. In the bulk state of polyolefin, the simplification works

well with only the topological consideration. However, many variables are coupled with each other to make the understanding of a polymer surface difficult. The decoupling of the effect of the variables or the ruling-out of an effect of a variable using a computer simulation requires a detailed description of a polymer chain embodied in the simulation as well as its applicability to the large-scale system.

3.3 Coarse graining into Rotational Isomeric State model

Often the energy state of a molecule can be described by a sum of energetic contributions of internal coordinates and non-bonded interactions, as in Equation 3.1. Among them, the bond stretching and angle bending terms are so strong, because of large force constants, that they do not vary much with time, staying at the most probable bond length and bond angle. Since computational efficiency is indispensable for a polymer simulation, these two terms are neglected in most cases. Accordingly, a property of a polymer chain cannot be only dependent on the remaining energy terms, torsional energy and non-bonded energy.
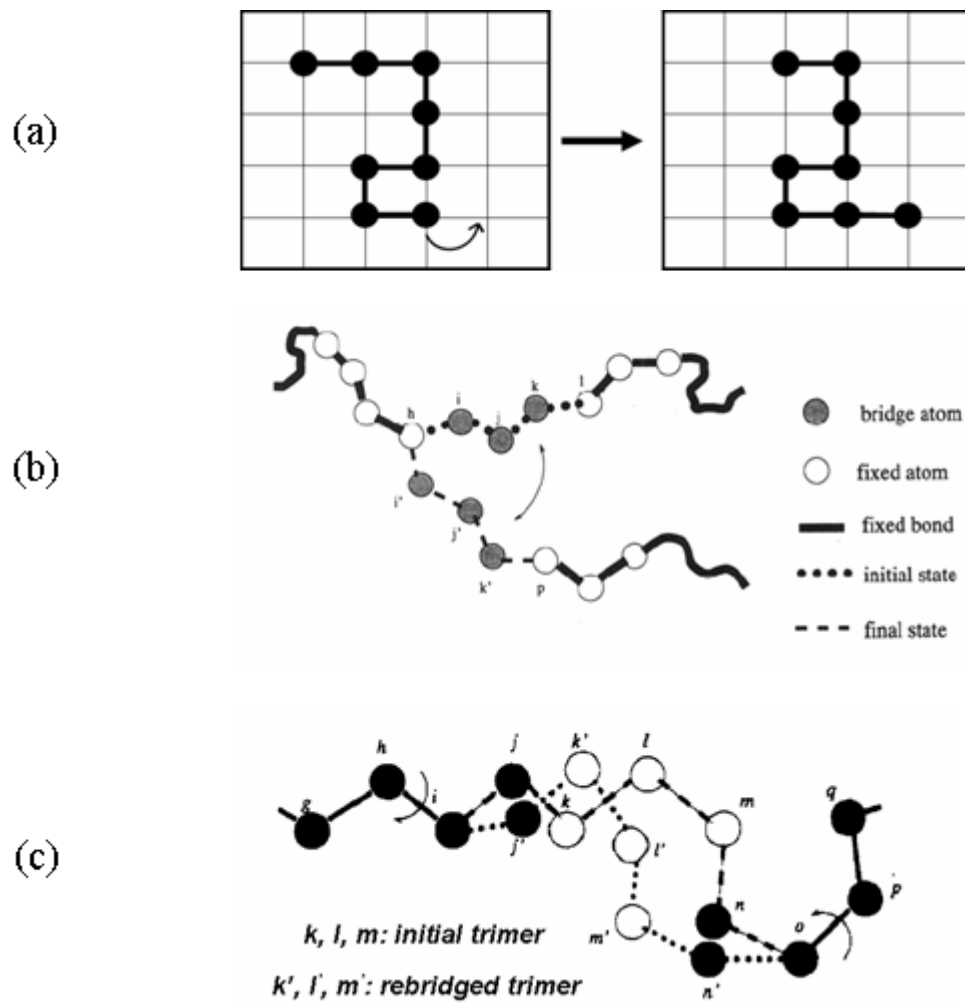
Figure 3.2 Collective moves (a) reptative move (b) end-bridge move (c) concerted rotation.

Furthermore, if a polymer chain is not perturbed by the existence of others, the importance of the long range interaction is diminished. In that case, the partition function of a single chain can be expressed by only torsional partition function or conformational partition function as follows.

$$Z = \int_{\theta_1} ... \int_{\phi_n} \exp\left(\frac{-E_{\phi_1...\phi_n}}{kT}\right) d\phi_1...d\phi_n \qquad (3.6)$$

Then, the average of a property, <A>, can be written as,

$$\langle A \rangle = Z^{-1} \int_{\phi_1} \ldots \int_{\phi_n} \exp\left[\frac{-E_{\phi_1\ldots\theta_n}}{kT}\right] A\left(\phi_1\ldots\phi_n\right) d\phi_1\ldots d\phi_n \tag{3.7}$$

The continuous torsional states can be grouped to have several discrete states. This assumption is reasonable because discrete torsional states are separated by an activation barrier. The torsional states are called "rotational isomeric state (RIS)". With the discrete torsional states, the conformational partition function of Equation 3.6 can be rewritten as the summation over the discrete conformationals space.

$$Z = \sum_{\phi_1} \ldots \sum_{\phi_n} \exp\left(\frac{-E_{\phi_1\ldots\phi_n}}{kT}\right) \tag{3.8}$$

The RIS model (Mattice and Suter, 1994) is a coarse grained model, which only considers the discrete rotational isomeric states with other internal coordinates frozen. Schematically, the mapping from a realistic chain to a RIS chain is illustrated in figure 3.3. For a PE chain, which is the model polymer chain in this study, Abe *et al.* (Abe *et al.*, 1966) presented a RIS model with three torsional states of $\phi_{CCCC} = 180°$ (*trans*; *t*), 60° (*gauche plus*; g^+), and -60° (*gauche minus*; g^-) at the fixed bond length $l_{CC} = 1.54$ Å and the fixed bond angle $\theta_{CCC} = 112°$. Based on the model, a linear PE chain can be mapped onto the tetrahedral lattice very successfully except for the very small bond angle mismatch. In this mapping, each occupied lattice site of the tetrahedral lattice represents a single -CH$_2$- group of the PE chain. The bond between two neighboring occupied lattice sites can be one of three rotational states; *trans* (*t*), *gauche*$^+$ (g^+), or *gauche*$^-$ (g^-)
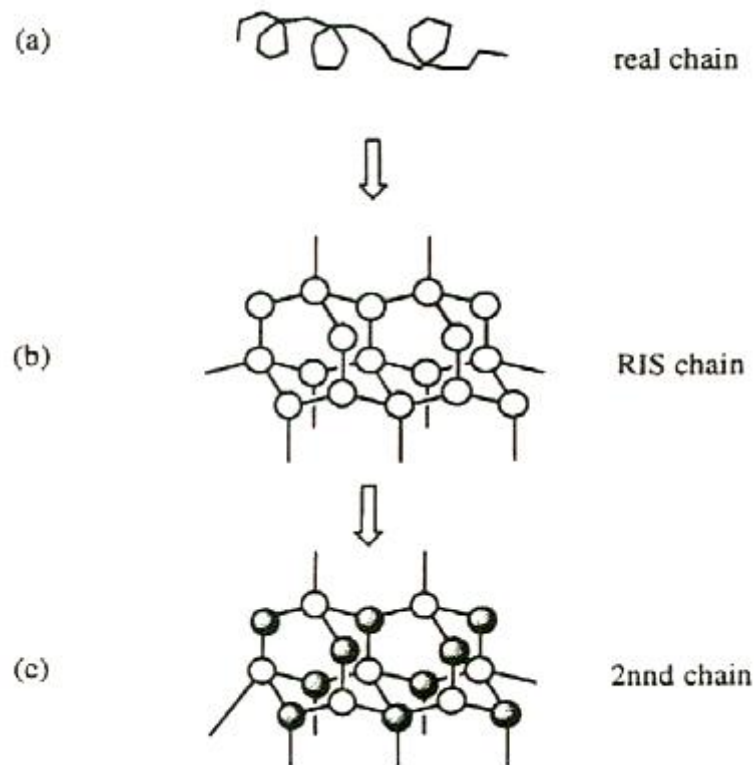
Figure 3.3 Example of the mapping of a real chain into lattice by coarse graining. The degree of coarse graining increases from (a) to (c). (a) continuous space, (b) space available with a single bond length, tetrahedral bond angle, and $\phi = 180°$, $\pm60°$, (c) rejection of alternate sites from (b).

3.4 Further coarse graining

A further coarse-grained lattice from the RIS model for PE chain can be obtained by discarding every second site from the tetrahedral lattice. This process corresponds to the coarse graining from figure 3.3(a) to figure 3.3(c). The coarse graining generates a slanted cubic cell whose length is 2.5 Å in a, b, and c directions, and the angles between any two unit vectors are 60°. The modification produces a coordination number of 12 (or $10i^2 + 2$ sites in shell i), which is higher than that of the

tetrahedral lattice. The high coordination number provides a flexibility to define a rotational state in the lattice. The new lattice is identical to the closest packing of uniform hard spheres. The high coordination lattice is named as the "second nearest neighbor diamond (2nnd) lattice". Each occupied site in this model represents an ethylene ($-CH_2-CH_2-$) group. Figure 3.4 shows the structure of the 2nnd lattice and the twelve coordination sites around a central bead. This coarse-grained lattice provides a better computational efficiency due to the reductions in the number of particles and in the number of conformational states, which facilitates its application to the fairly large polymeric systems. More detailed information about the 2nnd lattice is found elsewhere (Balijepalli and Rutledge, 1998).
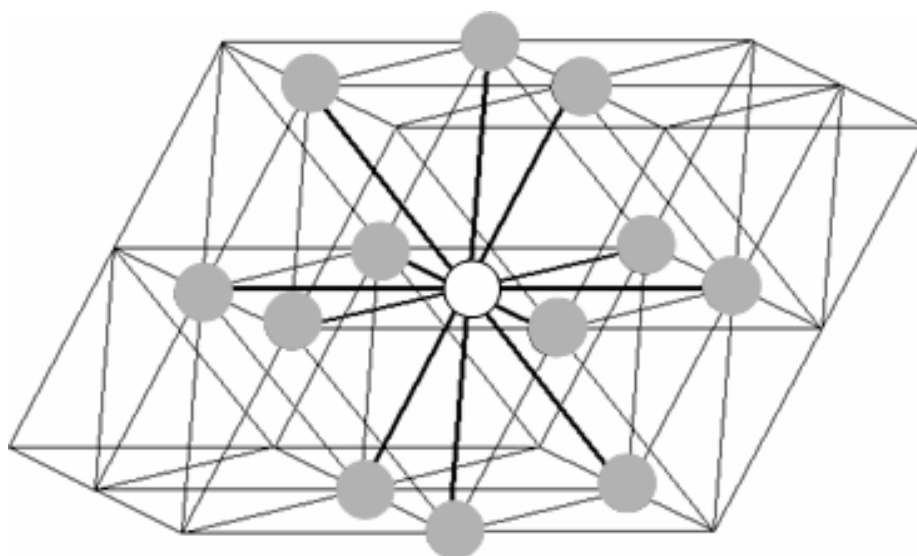
Figure 3.4 The 2nnd lattice. The gray spheres represent the possible twelve coordination lattice sites around a central bead (open circle).

3.5 Conventional RIS formalism

In the RIS scheme for n-alkane homologs, the first approximation is to handle the rotable bonds independently. On the assumption that a rotational state of a bond is not affected by other bonds and defined solely by the first order interaction, the conformational energy of a chain will be

$$E\{\phi\} = \sum_i E_i(\phi_i) = \sum_i E_{\xi;i} \tag{3.9}$$

where ξ denotes the rotational state of bond i. The statistical weights $u_{\xi;i}$ can be defined by the Boltzman probability, which means the relative population of the ξ state in the ith bond.

$$u_{\xi;i} = \exp\left(-E_{\xi;i} / RT\right) \tag{3.10}$$

Then, the conformational partition function of a chain Z as a whole is given by

$$Z = \prod_i \sum_\xi u_{\xi;i} \tag{3.11}$$

If the rotor has three rotational states as shown in figure 3.5 (a), which is a proper choice for the n-alkane homologs, the Z is given by $(1+2\sigma)^{n-2}$ for a linear alkane or PE chain with n carbon, where 1 and σ correspond to the statistical weights of trans and gauche states, respectively.

The first approximation, independent bonds approximation, is invalid in real situation because of the second order interaction known as pentane effect. The interdependence of bonds destroys the degeneracy of the energy state of the *gauchegauche* (*gg*) conformation and splits into g^+g^+ and g^+g^- or g^-g^- and g^+g^-. As a result, the total energy of a chain with the interdependent bonds given by

$$E\{\phi\} = \sum_i E_i(\phi_{i-1}, \phi_i) = \sum_i E_{\xi\eta;i} \tag{3.12}$$

where $\xi_{\eta;i}$ means the $(i\text{-}1)^{th}$ bond is in ξ state and i^{th} bond is in η state. The statistical weights corresponding to $E_{\xi\eta;i}$ can be written as a matrix form as

$$U_i = \left[u_{\xi\eta}\right]_i \tag{3.13}$$

The conventional RIS model for PE of Abe *et al.* (Abe *et al.*, 1966) is defined by the statistical weight for two successive rotable internal bonds,

$$U_i = \begin{bmatrix} 1 & \sigma & \sigma \\ 1 & \sigma & \sigma\omega \\ 1 & \sigma\omega & \sigma \end{bmatrix} \tag{3.14}$$

where σ and ω are the first- and the second-order interaction parameters and the rows are indexed by the states of $(i\text{-}1)^{th}$ bond and the columns are indexed by the states of ith bond. The orders of indexing are t, g^+, and g^-. Then, the total conformational partition function will be

$$Z = \prod_i U_i \tag{3.15}$$

In a MC simulation using a RIS scheme, a move attempt can change the rotational states of the chain which is affected by the move. The change enters the Metropolis evaluation (Metropolis *et al.*, 1953) to decide to accept or reject the move attempt. This decision can be simply done by obtaining bond probabilities from the statistical weights.

3.6 RIS formalism for 2nnd chain

The two successive bonds are contracted into one virtual bond between two neighboring beads in the 2nnd lattice. The formalism of the RIS model of the virtual bonds for the coarse-grained chain should be modified. A virtual rotor in the 2nnd

frame, as shown in figure 3.6, contains four successive rotors corresponding to n-heptane in the original RIS frame. The detailed description of n-heptane at the same place, which requires a 9×9 statistical weight matrix, is given by

$$U = \begin{bmatrix} 1 & \sigma & \sigma & \sigma & \sigma & \sigma^2 & \sigma^2 & \sigma^2\omega & \sigma^2\omega \\ 1 & \sigma & \sigma & \sigma & \sigma\omega & \sigma^2 & \sigma^2\omega & \sigma^2\omega & \sigma^2\omega^2 \\ 1 & \sigma & \sigma & \sigma\omega & \sigma & \sigma^2\omega & \sigma^2 & \sigma^2\omega^2 & \sigma^2\omega \\ 1 & \sigma & \sigma & \sigma & \sigma & \sigma^2 & \sigma^2 & \sigma^2\omega & \sigma^2\omega \\ 1 & \sigma & \sigma & \sigma & \sigma & \sigma^2 & \sigma^2 & \sigma^2\omega & \sigma^2\omega \\ 1 & \sigma & \sigma & \sigma & \sigma\omega & \sigma^2 & \sigma^2\omega & \sigma^2\omega & \sigma^2\omega^2 \\ 1 & \sigma & \sigma & \sigma\omega & \sigma & \sigma^2\omega & \sigma^2 & \sigma^2\omega^2 & \sigma^2\omega \\ 1 & \sigma & \sigma & \sigma\omega & \sigma & \sigma^2\omega & \sigma^2 & \sigma^2\omega^2 & \sigma^2\omega \\ 1 & \sigma & \sigma & \sigma & \sigma\omega & \sigma^2 & \sigma^2\omega & \sigma^2\omega & \sigma^2\omega^2 \end{bmatrix} \qquad (3.16)$$

(a)

$g+$ $g-$

t

E

$\implies$ $U_i = (1, \sigma, \sigma)$

(b)

i-1

$g+g-$ $g-g+$

$g+g+$ $g-g-$

$tg+$ $tg-$ $g+t$ $g-t$

tt

E

$\implies$ $U_i = \begin{pmatrix} 1 & \sigma & \sigma \\ 1 & \sigma & \sigma\omega \\ 1 & \sigma\omega & \sigma \end{pmatrix}$
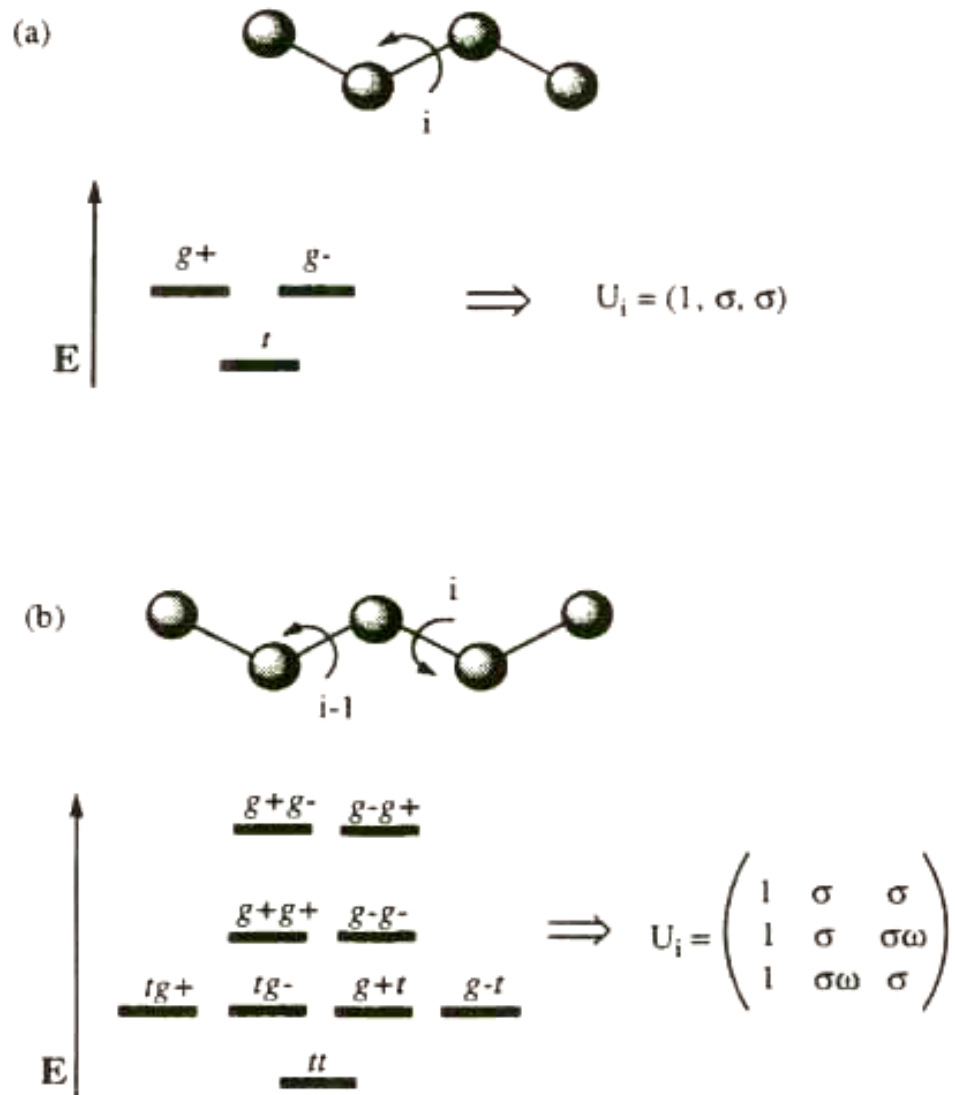
Figure 3.5 The rotational states of a linear chain and corresponding statistical weights (a) independent bond (b) interdependent bond.
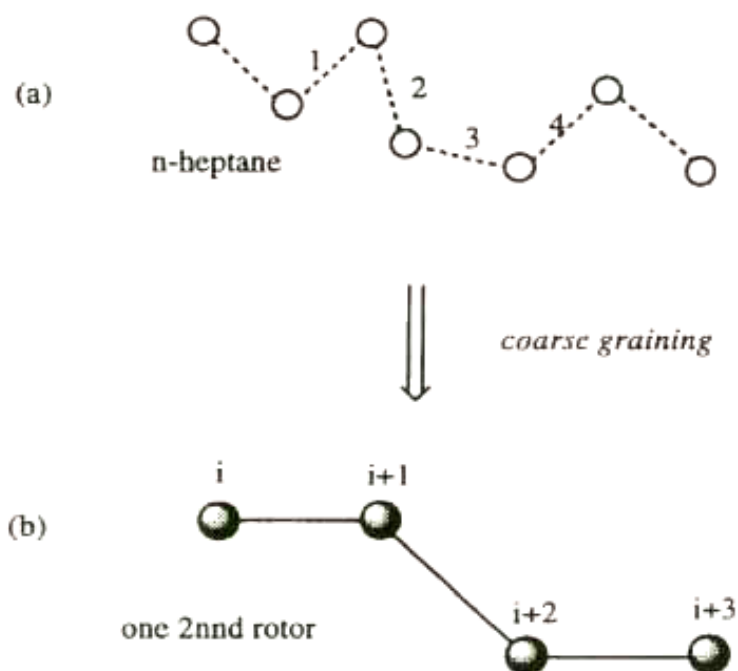
Figure 3.6 The coarse graining of n-heptane with 4 rotors to a single rotor in 2nnd lattice: (a) n-heptane   (b) 2nnd chain equivalent to n-heptane.

The row represents 1 and 2 rotors and the column represents 3 and 4 rotors in figure 3.6 (a). The order of the rotational states of the rows and columns are *tt, tg$^+$, tg$^-$, g$^+$t, g$^-$t, g$^+$g$^+$, g$^-$g$^-$, g$^+$g$^-$, g$^-$g$^+$*. By the nature of the coarse graining, several details of conformational information are missing in such a way that some torsional states are no longer distinguishable in the coarse-grained chain. Then, Equation 3.16 can be modified into a simpler form with the modified statistical weights, *a*, *b*, and *c*, which are obtained from the geometric mean $a = \sigma\omega^{1/8}$, $b = \sigma\omega^{1/4}$, $c = \sigma^2\omega^{1/2}$

$$U = \begin{bmatrix} 1 & \sigma & \sigma & \sigma & \sigma & \sigma^2 & \sigma^2 & \sigma^2\omega & \sigma^2\omega \\ 1 & a & a & a & a & b\sigma & b\sigma & b\sigma\omega & b\sigma\omega \\ 1 & a & a & a & a & b\sigma & b\sigma & b\sigma\omega & b\sigma\omega \\ 1 & a & a & a & a & b\sigma & b\sigma & b\sigma\omega & b\sigma\omega \\ 1 & a & a & a & a & b\sigma & b\sigma & b\sigma\omega & b\sigma\omega \\ 1 & b & b & b & b & c & c & cb\omega & cb\omega \\ 1 & b & b & b & b & c & c & cb\omega & cb\omega \\ 1 & b & b & b & b & c & c & cb\omega & cb\omega \\ 1 & b & b & b & b & c & c & cb\omega & cb\omega \end{bmatrix} \tag{3.17}$$

Equation 3.17 can be reduced further because of the symmetry of the torsional potential energy (Rapold and Mattice, 1996)

$$U_{2nnd} = \begin{bmatrix} 1 & 4\sigma & 2\sigma\sigma & 2\sigma\sigma\omega \\ 1 & 4a & 2\sigma b & 2\sigma\omega b \\ 1 & 4b & 2c & 2c\omega \\ 1 & 4b & 2c & 2c\omega \end{bmatrix} \tag{3.18}$$

Here, the rows define the lengths of the vectors connecting beads i and $i+2$ in figure 3.6 (b) and the columns define the lengths of the vectors connecting bead $i+1$ and $i+3$. This reduction means that the rotational isomeric states in 2nnd lattice can be categorized into four groups based on the vectors, which are specified by the distances between these two beads. The distances of 5.00 Å, 4.33 Å, 3.53 Å, and 2.50 Å as shown in table 1.1 which correspond to the local conformations of A: tt, B: (tg^+, tg^-, g^+t, g^-t), C: (g^+g^+, g^-g^-), and D: (g^+g^-, g^-g^+), respectively. Equation 3.18 can be condensed further to a 3×3 matrix with the modified indexing, A, B, and (C+D).

$$U_{2nnd} = \begin{bmatrix} 1 & 4\sigma & 2\sigma^2(1+\omega) \\ 1 & 4a & 2b\sigma(1+\omega) \\ 1 & 4b & 2c(1+\omega) \end{bmatrix} \tag{3.19}$$

Table 3.1 Length of vectors connecting beads i and i +2 for coarse-grained PE model.

Category	Length in nm	Detailed conformation
A	0.500	tt
B	0.433	tg^+, tg^-, g^+t, g^-t
C	0.353	g^+g^+, g^-g^-
D	0.250	g^+g^-, g^-g^+

3.7 Long-range interactions

The incorporation of the rotational isomeric state model is not enough to describe the energetics of the melt system because the RIS model is a single chain model in the unperturbed state, ϕ state. The model only accounts for the short-range intermolecular interaction up to next nearest neighbor bonds on the 2nnd lattice. For the remaining long-range intramolecular and intermolecular interaction, the Lennard-Jones (LJ) pair potential, $u(r)$, seems to be a reasonable choice since there are only dispersive interactions in a PE melt. Including the long-range interaction, the total energy which will be used in Metropolis evaluation will be

$$E_{total} = E_{RIS} + E_{LJ} \qquad (3.20)$$

The lattice representation of the continuous LJ potential at the ith shell, u_i, is obtained from an averaged Mayer f-function which is used for the description of the second

virial coefficient of a non-ideal gas. The interaction parameter at the ith shell is defined through following equation.

$$epp\left(-\frac{u_i}{k_B T}\right) - 1 \equiv \bar{f}_i \tag{3.21}$$

The average Mayer f-function at the ith shell, f_i, is obtained by integrating $u(r)$ over the cells in the ith shell.

$$\bar{f}_i = \frac{\int_{cell} f dr}{\int_{cell} dr} \tag{3.22}$$

$$f = \exp\left(-\frac{u(r)}{k_B T}\right) - 1 \tag{3.23}$$

The set of the interaction parameters for 2nnd beads is derived from the LJ potential for an ethylene molecule ($CH_2=CH_2$). Table 3.2 shows the interaction parameters (1st, 2nd and 3rd shell) of coarse-grained C_2H_4 units at various temperatures (Xu and Mattice, 2002). And Table 3.3 gives a set of interaction parameters obtained by the averaging method at 509 K. The details about the long-range interaction are given by Cho *et al*. (Cho and Mattice, 1997).
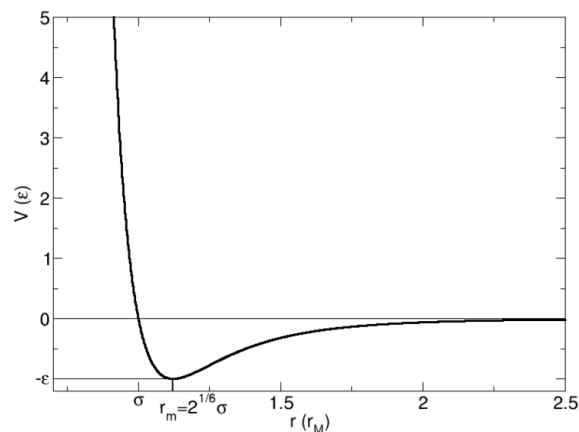
Figure 3.7 The LJ potential energy as a function of distance (Wikipedia, 2011(b)).

Table 3.2 Long-range interaction (kJ/mol) of coarse-grained C_2H_4 units at various temperatures.

T (K)	1st shell	2nd shell	3rd shell
473	15.048	0.620	0.625
460	14.659	0.580	0.626
440	14.056	0.517	0.627
420	13.448	0.453	0.629
400	12.835	0.388	0.630
395	12.681	0.371	0.631
390	12.527	0.355	0.631
380	12.198	0.322	0.632
350	11.281	0.220	0.635
298	9.625	0.038	0.642

Table 3.3 Non-bonded energy parameters for coarse-grained PE model on 2nnd lattice simulation at 509 K.

2nnd parameter	value
ε/k_b	185
σ (nm)	0.44
u_1 (kJ/mol)	16.214
u_2 (kJ/mol)	0.731
u_3 (kJ/mol)	-0.623

The single bead move is always employed in this study with the restriction that a chain cannot pass through itself, as in a self-avoiding random walk. A randomly chosen bead can move to a vacant site in the first shell when the attempt does not change the bond length to its two bonded neighbors. Local bead moves on the 2nnd lattice are accepted according to the Metropolis Monte Carlo algorithm which the probability of bead moving within a chain is given by

$$P_{move} = \ min[1, P_{LR}/P_{new}/P_{old}] \tag{3.21}$$

where, $P_{LR} = \exp(-\Delta E_{LR}/RT)$ is the probability from the change in the long-range interaction energy (ΔE_{LR}), and P_{new}/P_{old} is the ratio of the probabilities for the new and old local conformations according to the short-range interaction. After mapping the chains on this coarse-grained lattice, Dynamic MC simulations will be performed. In this simulation, one Monte Carlo step (MCS) is defined as a series of single bead move, in which all the beads in the system are randomly attempted once on average. A moving on lattice corresponds to displacement of two or three backbone atoms on the real PE chain. Even though the relaxation or equilibration of a system is quite slow with the single bead move, the move provides the reliable dynamic properties at the time scale of MCS. One MCS is defined as the simulation length when every bead in the system has attempted one move, on average.

3.8 Applications of the method

Due to the computational efficiency that comes from the lattice characteristic and the chemical details that comes from the RIS characteristic, this MC simulation method on the high coordination lattice has proven to be quite successful to visit many polymeric questions which show a large scale chain behavior. These include the

successful mapping of polyoxyethylene and polythiaethylene onto the 2nnd lattice (Doruker *et al*., 1996), the restoring of PE chains to the fully atomistic chains (Doruker and Mattice, 1997), the simulation of the dynamics of PE in the bulk state, the simulation of PE thin film (Doruker and Mattice, 1998; Doruker and Mattice, 1998), the simulation of PE nanofibers (Vao-soongnern *et al*., 2000), and the bulk simulation on polydisperse PE melt (Ozisik *et al*., 2000).

3.9 System constructions

3.9.1 Bulk system

A random configuration of the PE chains is generated by mapping beads on 2nnd lattice with an application of periodic boundary conditions in all three directions. For an initial step, only self-avoiding random walks with excluded volume condition is employed and the next step, intramolecular and intermolecular interactions are introduced. Then the initial structure is relaxed by minimizing the potential energy of the system by Dynamics MC technique.

3.9.2 Nano thinfilm, nanofiber and nanoparticle formation

Thin film can be obtained by extending the x axis of the periodic box of the bulk system about 3-4 times. This new box size is large enough to ensure that there is no interaction between the parent chains and their images. Then the system is equilibrated and employed as an initial structure of fiber. The nanofiber can be obtained by extending the y axis of the latest conformation of thin film about 3-4 times to prevent any interaction between the parent chains and their images with other chains. Then the system is carried out in the same way as the thin film system.

Eventually the equilibrated nanofiber will be obtained. Finally, polymer nanoparticle can be obtained in a similar way to nanofiber by extending the z axis of the latest conformation of the fiber about 3-4 times. After equilibration step, nanoparticle is obtained. All structural generation can be described by the following scheme:

Bulk   nano-thicked thin film   nanfiber
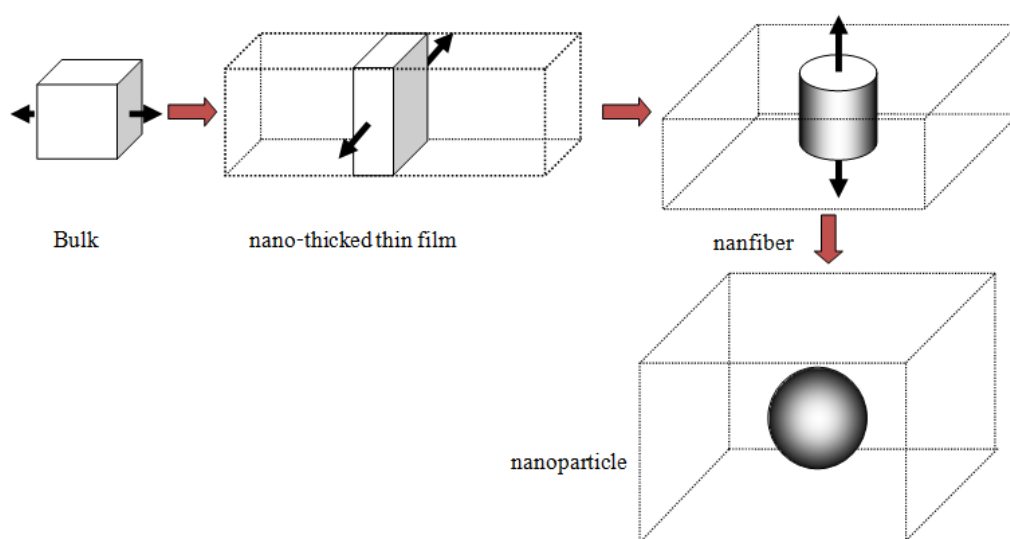
nanoparticle

Figure 3.8 The method to generate a new cohesive polymer structure from bulk (3D) → nano-thicked thin film (2D) → nanofiber (1D) → nanoparticle(0D).

3.9.3 Bidisperse system generation

For the bidisperse systems, the total number of chains in each system geometry is initially constructed with only the longer chains. Afterward, the long chains from the latest conformation of the equilibrated systems are cut down to shorter ones according to the length of short chains needed in the simulation. Then the system is equilibrated at least 10 million MCS and is employed as new initial

structures. The latest conformation of nanofiber and nanoparticle will be run for an additional 10 million MCS to obtain data for subsequent analysis.

3.9.4 Crystallization study

When the latest conformation of bidisperse nanofibers and nanoparticles are obtained, the temperature is instantaneously dropped from 509 K to 298 K, and the simulation is continued at 298 K. At least 30 million MCS is needed to observe the crystallization.

3.10 System

The systems of monodisperse PE nanofibers and nanoparticles are shown in table 3.4 which the number behind B are the number of beads (one bead represent the CH_2-CH_2 unit). All systems were the same number of beads. These systems were used to compare the effect of bidispers on the properties of PE nanofibers and nanoparticles.

Table 3.4 Number of chains in monodisperse PE nanofiber and nanoparticle systems.

System	Number of chains
B50	56
B40	70
B30	94
B20	140

The effect of bidisperse was used to investigate the behavior of each chain which can be classified into 2 objectives. The fist one is the effect of chain length on the properties of nanofiber and nanoparticle. The B50 chain will be mixed with mixed chain (B40, B30 and B20 respectively) in each composition (75, 50 and 25% respectively). The second one is the effect of composition on the properties of nanofiber and nanoparticle. The composition of B50 was varied (75, 50 and 25% respectively). In each system (B50+B40, B50+B30 and B50+B20 respectively), the chain number of each chain in each system is shown in Table 3.5.

Table 3.5 The number of chains in bidisperse PE nanofibers and nanoparticles (B50+B40, B50+B30, and B50+B20) systems.

% of B50	N_{B50}	N_{B40}	N_{B30}	N_{B20}
75	42	18	24	36
50	28	36	48	71
25	14	53	71	106

The systems of bidisperse PE nanofibers and nanoparticles which used to study the crystallization are shown in table 3.6. The system is only composed of 50**%** by weight of B20 and B15.

Table 3.6 Bidisperse PE nanofibers and nanoparticles (B20+B15) system.

% of B20	N_{B20}	N_{B15}
50	78	104

CHAPTER IV

RESULTS AND DISCUSSION

4.1 Effect of chain length on monodisperse PE nanofiber and nanoparticle systems

4.1.1 Density profile

Radial density profile

Figure 4.1 illustrates the definition of the radial density profile for the fiber. Firstly, we find the principal moments of the fiber structure by diagonalzing the radius of gyration tensor. The principal axis always lies parallel to the x' axis in 2nnd coordinates. Next we divide the fiber into cylindrical bins, starting from center of fiber, with the thickness of 0.2 nm. The number of beads that fall into each bin are counted and normalized by its shell volume. With this technique, the radial density profile can be obtained. The density profiles of all systems were investigated. Figure 4.1 shows the density profile of all systems in each chain length. The results show that the bulk densities of all system drop at the simulated temperature which increase with increasing the chain l ength in the range of 0.6-0.7 g/cm^3. But the density of longer chain system was quickly dropped to the surface than that of shorter ones. At starting point of density decreasing, it is found that the shorter chain is decreased nearer the principal axis than longer one. These points are around 20 Å while the highly decrease are around 30 Å. In addition, the diameter and the interfacial thickness of shorter chain system was larger than the longer chain system, when interfacial

thickness is defined as the distance over which the density of the fiber decreases from 90% to 10% of its bulk value. Because the shorter chain component has more number of end beads, they need more room to move than the longer chains. So, it has more excluded volume than the long chain. This effect of excluded volume results in decreasing of density at bulk region.

For nanoparticle system, the results similar to those of nanofiber systems but the total densities are slightly higher. The diameters of nanoparticle are bigger than that of nanofiber with the same number of beads (for example of B20 nanofiber and nanoparticle is 50 and 55 Å respectively) as shown in figure 4.2 (*f* and *p* means nanofiber and nanoparticle respectively). This behavior should be related to the stronger confinement effect in nanoparticle which is more dominant than nanofiber. Therefore, the chains in nanoparticle should pack denser and its density is more increased.
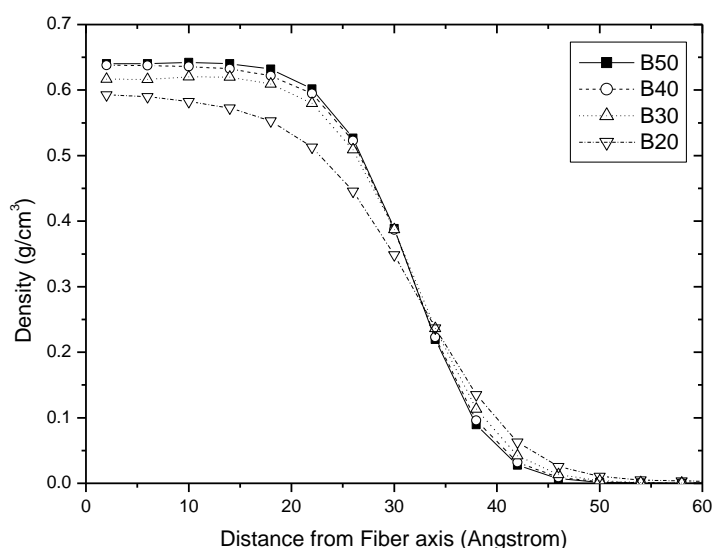
Figure 4.1 Radial density profiles of monodisperse B50, B40, B30 and B20 PE nanofibers at 509 K.
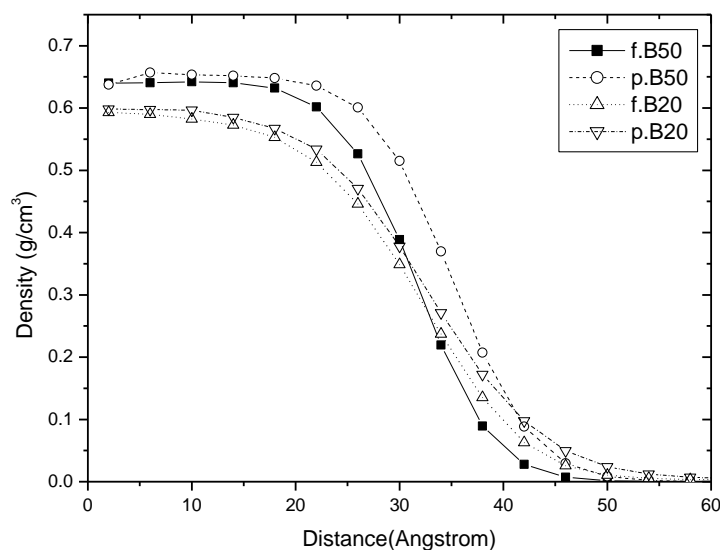
Figure 4.2 Comparison of density profile between monodisperse B50 and B20 PE nanofiber and nanoparticle at 509 K.

Beads distribution and segregation of chain ends

Figure 4.3(a) gives the example density profile of the end (the first or the last carbon atom of the chain) and middle carbon atoms across the fiber of B50 nanofiber. The results show that the end beads are abundant near the surface of nanofiber while the middle beads prefer at the center. The profiles are in qualitative agreement with those observed in thin film and free surface of polymer melts form of V.Vao-soognern *et al.* work (Vao-soongnern *et al.*, 2000) which long chain PE was used to form nanofiber. In figure 4.3(b), the bead density profiles are normalized by the total bead density in that bin, so that the segregation at the surface can be observed clearly. The behavior of the end beads distribution is determined mainly by entropic effects, contrary to the enrichment of centers of mass in the interface layer which is dependent on the energetic situation. For other system, the end bead density of the shorter chain system was higher than that of longer chain system. This behavior of the

short chain system is determined by larger number of end beads than long chain system. For all results are not shown here.
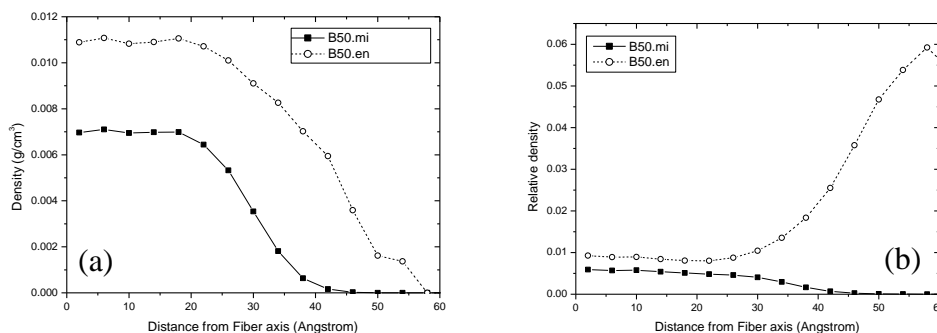
Figure 4.3 (a) Radial density profiles for mid/end beads of monodisperse PE B50 at 509 K. (b) result after normalization by the bulk density.

4.1.2 Orientation

Bond orientation

Local orientational tendencies of chords (from carbon atom *i* to carbon atom *i + 2*) across the fiber are examined in figure 4.4. The definition of chord order parameter is

$$S = \frac{1}{2}\left\langle 3\left(\cos^2 \theta\right) - 1 \right\rangle \tag{4.1}$$

where θ is the angle formed between a 2nnd bond and the fiber axis. $\left\langle \ \right\rangle$ is indicative of an ensemble average within the cylindrical bin. The *S* value -0.5, 0.0 or 1.0 means perfectly perpendicular, random, and parallel orientation with respect to the fiber axis respectively.

Figure 4.4 shows order parameter of B30 nanoparticle chords which plotted as a function of a distance from the center of particle. The line label "all"

represents the orientation of all   coarse-grained 2nnd bonds. The results show that

the bond orientation in the bulk region is random orientation. Toward the surface, the

middle bonds seem to prefer parallel orientation, whereas the end beads tend to stick

out to the vacuum by normal orientation to the surface. These two opposite effects are

averaged in the orientation of all bonds. The change of bond orientation is starting in

the same region which the density is decreased. All results are in good accordance

with previous simulations of   V. Vao-soognern *et al.* work (Vao-soongnern *et al*.,

2000) which the longer chain PE was used for nanofiber and nanoparticle formation.

The orientation of middle bond and end bond are similar for all systems of nanofibers

and nanoparticles. Most bond orientations of nanofibers are perpendicular while they

are relatively random in nanoparticle which shows in figure 4.5.
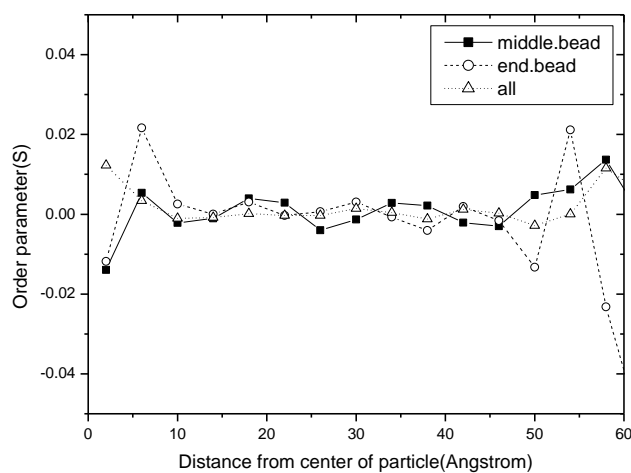
Figure 4.4 The orientation of chords (mid-, end- and all) of monodisperse B30 PE
nanoparticle.
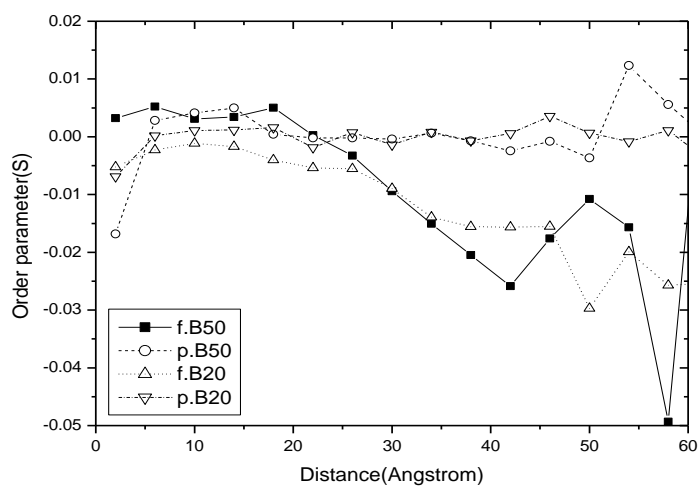
Figure 4.5 Comparison of the orientation of chords (all) between monodisperse PE nanofibers and nanoparticles.
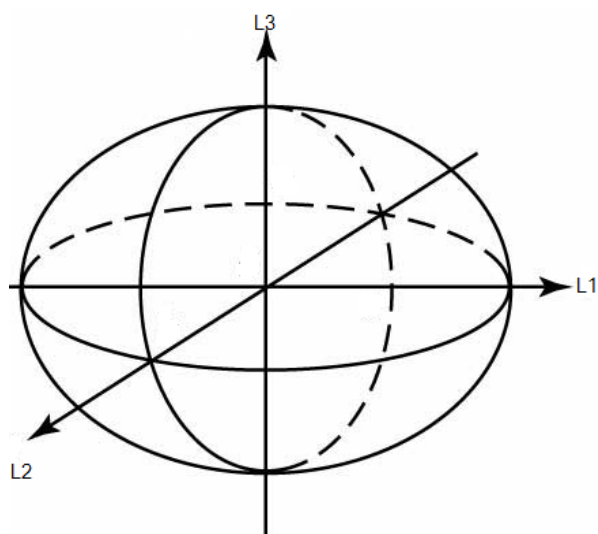
Figure 4.6 The ellipsoid was defined of the principal components *L3 < L2 < L1* for PE molecule.
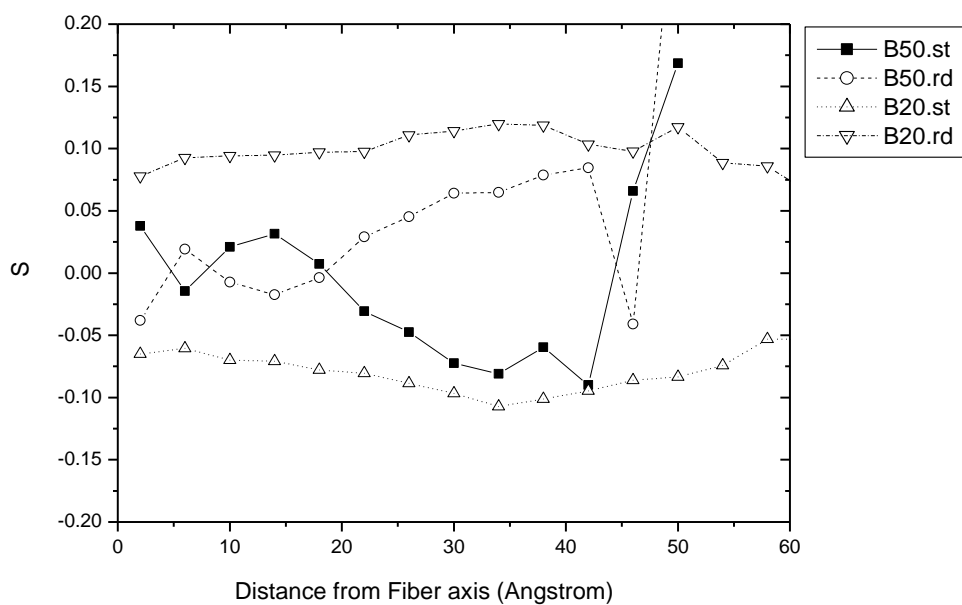
Figure 4.7 The orientation of the largest and smallest principal moment to fiber axis after equilibration of monodisperse B50 and B20 PE nanofibers.
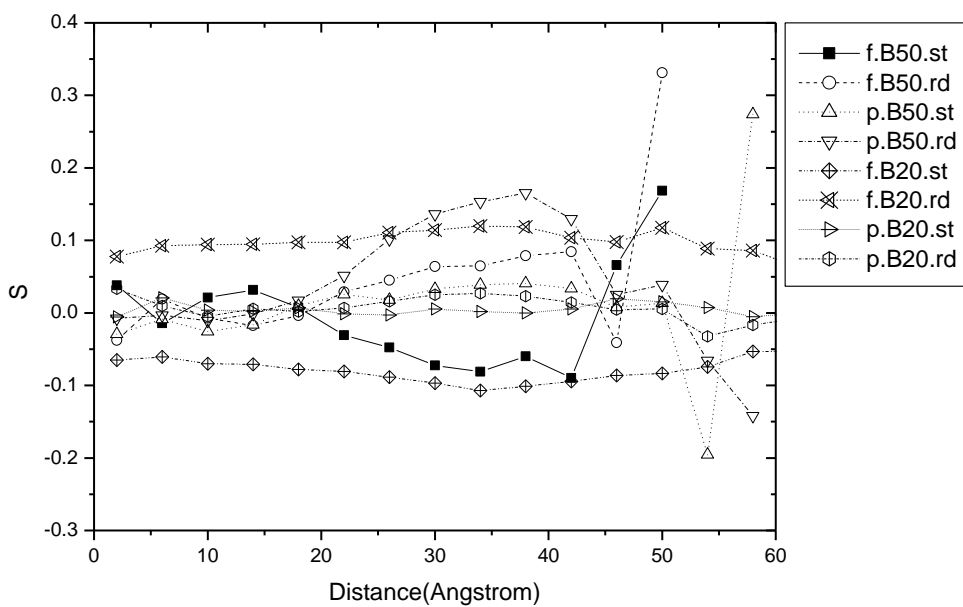
Figure 4.8 Comparison of the orientation of the largest and smallest principal moment to center of particle between monodisperse PE nanofibers and nanoparticles.

Particle orientation

To define the shape and orientation of the chains more clearly, it is appropriate to approximate a coil by an equivalent ellipsoid, which is defined by the principal components $L3 < L2 < L1$ of the radius of gyration tensor for individual configurations taken along the principal axes system as shown in figure 4.6.

Figure 4.7 shows the orientations of the largest and smallest eigenvectors of the whole chains (*L1* and *L3*, respectively) of B50 and B20 nanofibers. All first (largest) axes tend to orient parallel to the fiber axis and all third (smallest) axes perpendicular to the fiber axis. In the case of longer chain system, *L1* and *L3* are random at the bulk region and then they are perpendicular and parallel to the fiber axis toward the surface respectively. But shorter chain system, *L1* is perpendicular and *L3* is parallel at the bulk region and they are slightly changing toward the surface. These changes are occurred after bulk region. These results can be described that at the surface, it is more confined than bulk region. So, L1 is adjusting to perpendicular orientation. In addition, the longer chain is bigger size than shorter one. In limitation of space, the longer chains would adjust their molecular orientation to perpendicular direction which is more confined than shorter chains.

In opposite, for nanoparticle, they are in perpendicular direction. Both of *L1* and *L3* are parallel to the center of particle (incline to the center of particle) which shown in figure 4.8. The longer chain is more perpendicular than the shorter one. These changes are occurred after bulk region. The results can be described similar to nanofiber systems because the chains in nanoparticle are more confined than those in nanofiber. The longer chains have to adjust their molecular orientation perpendicular to the surface than shorter chains.

4.1.3 Chain properties

In this section, we will look at the global equilibrium properties of the chains. Firstly, the spatial distribution of chain center of mass, shown in figure 4.9, characterizes structure at the level of the entire chain. The center of mass profiles of the chains are expressed as the number of chains per volume of bin ($\mathring{A}^3$). The profiles of nanofiber system are shown in figure 4.9(a). It is found that distance which has the highest center of mass densities of nanofibers are not significant different in all systems. But the density of shorter chain is higher than the longer chain because the number of chain of is larger than longer chain with the same number of overall beads. As well as nanofiber system, nanoparticle is similar result. The comparison between nanofiber and nanoparticle is shown in figure 4.9(b). The result shows that the distance which has the highest center of mass densities of nanoparticle is closer to the surface than nanofiber whereas their distribution of nanoparticle is broader than nanofiber. The increase in the density close to the center seems to accompany the similar increase in the middle bead distribution. Moreover, the middle bead distribution of nanofiber is closer to the center than nanoparticle in the same system.

The root mean square radius of gyration $\left\langle R_g^2 \right\rangle^{1/2}$ is referred to the size of molecule. The change in the R_g components as a function of radial displacement of the center of mass from fiber axis is shown in figure 4.10. The size of long chain is larger than the short chain due to the larger number of beads. The change in the R_g components of long chain is higher than that of short chain because of the entropic effect of end beads. The longer chain has more number of middle beads which are less entropy than the shorter chain. So, the longer chains are highly packed and they are higher change than shorter one. The R_g in X component becomes smaller as chains

approach the surface region from the bulk side. In accord with *X* component, the *Y-Z* component increases, while the total R_g remains relatively decrease. These results are simply a manifestation of the flattening of chains into pancake like objects as their centers of mass are forced to lie near an impenetrable surface which corresponding to V.Vao-soognern *et al.* work(Vao-soongnern *et al.*, 2000). For nanoparticle systems, the changes in R_g components are similar to nanofiber. But the R_g in all components are decrease because confinement effect which shows in figure 4.11.   As well as other properties, these changes are occurred after bulk region.
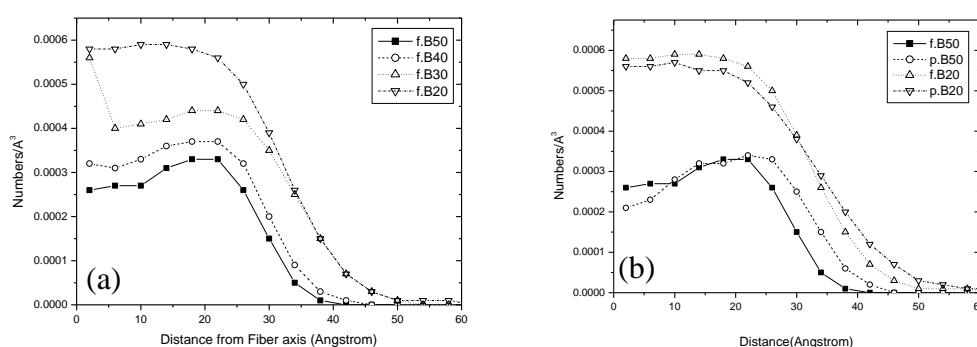
Figure 4.9 The center of mass distribution as a function of radial displacement (a) mono disperse nanofiber (b) comparison between monodisperse PE nanofiber and nanoparticle (B50 and B20).
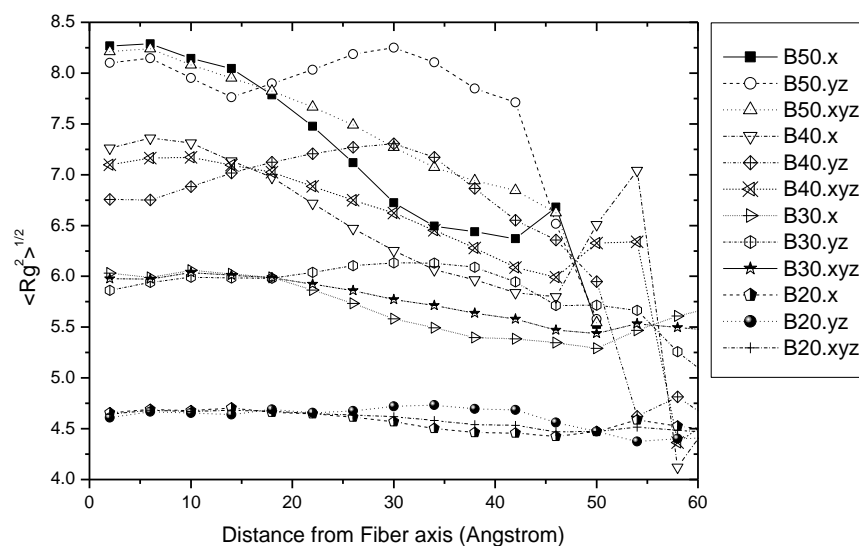
Figure 4.10 The change in the R_g components as a function of radial displacement of the center of mass from fiber axis of monodisperse PE nanofibers.
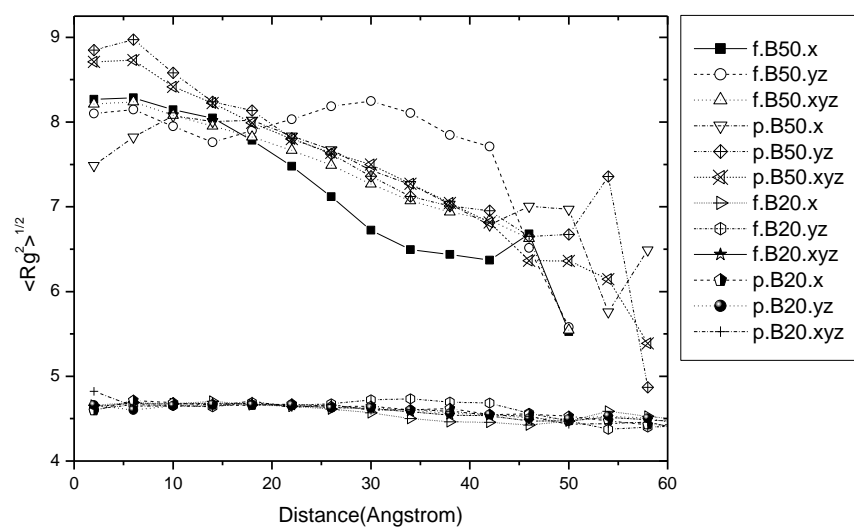
Figure 4.11 Comparison of the change in the R_g components as a function of radial displacement of the center of mass between monodisperse PE nanofibers and nanoparticles.

The chain shapes can be investigated by the acylindricity and the aspericity values, which are defined as $Ac = L_2^2 - L_3^2$ and $As = L_1^2 - \frac{1}{2}\left(L_2^2 - L_3^2\right)$, respectively. These values were divided by the squared radius of gyration to determine the extent of deviation from cylindrical and spherical shape in the range of 0 to 1. From figure 4.12, it is observed that chain shape changes as a function of the radial displacement from the center. The aspericity decreases toward the surface whereas the acylindricity is slightly increased, most of which is occurring close to the vacuum side. The change in aspericity and acylindricity of long chain is higher degree than short chain which can be described by the same reason of the change in R_g. For nanoparticle systems, the results are similar to those of the nanofiber systems as shown in figure 4.13.
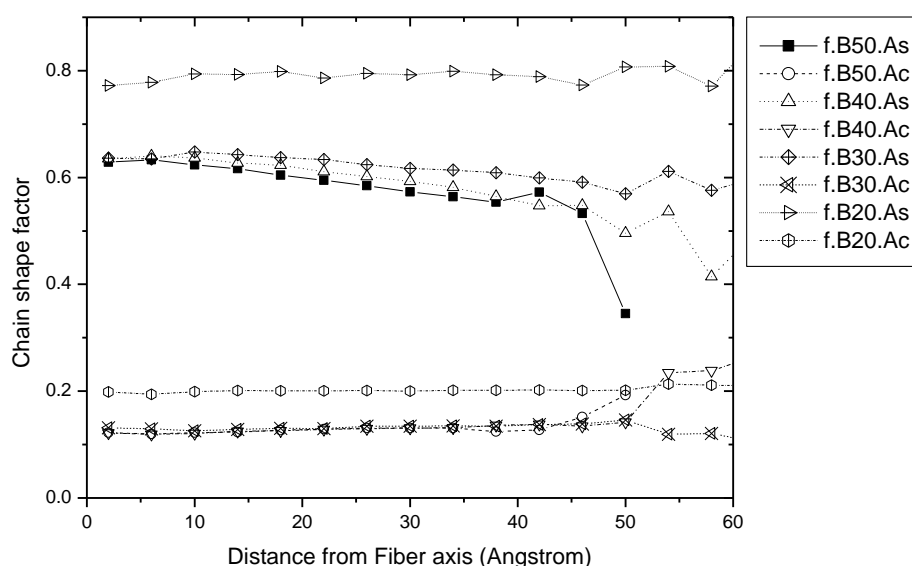
Figure 4.12 The change in chain shape (aspericity and acylindricity) as a function of radial displacement of the center of mass from fiber axis of monodisperse PE nanofibers.

Figure 4.14 and 4.15 show the comparison of the three eigenvalues (principal moments) of the chains normalized by their square radius of gyration as a function of radial displacement of the center of mass. There are slightly changing in the eigenvalues at the interface region of all system. The second and third principle moment are decrease while the first principle moment is decrease, most of which is occurring close to the vacuum side. The long chain is higher degree of change than short chain in both systems because the same reason as change in chain shapes property.
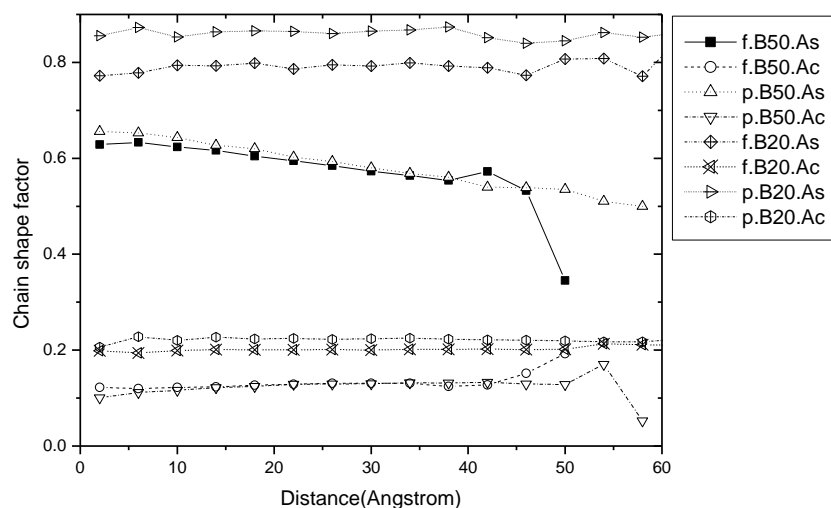
Figure 4.13 Comparison of the change in chain shape (asphericity and acylindricity) as a function of radial displacement of the center of particle of monodisperse PE nanoparticles.
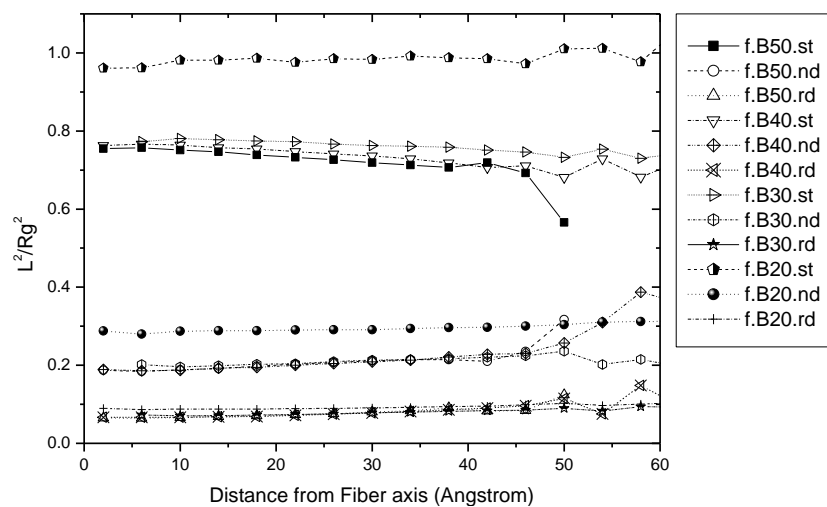
Figure 4.14 The principal moment of chains (normalized by R_g^2) as a function of radial displacement of the center of mass from fiber axis of monodisperse PE nanofibers.
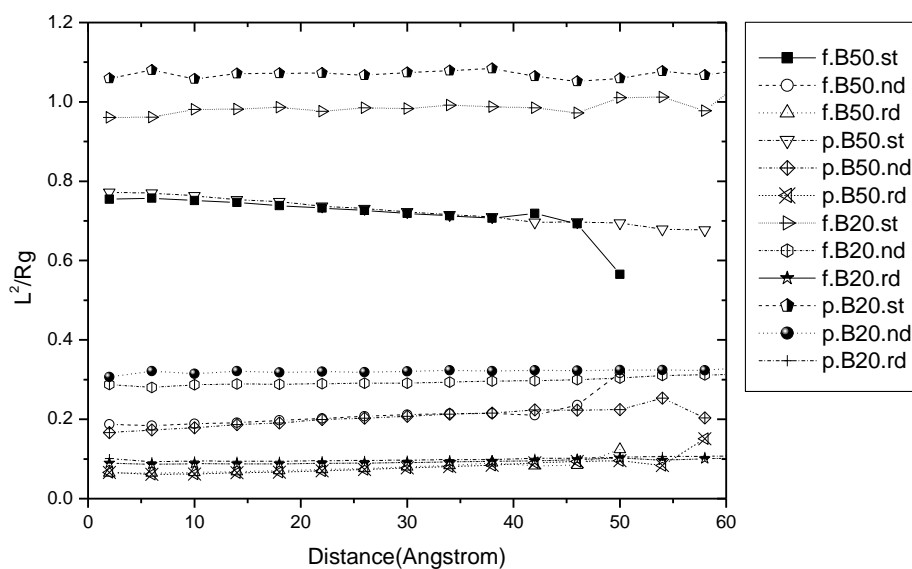
Figure 4.15 Comparison of the principal moment of chains (normalized by R_g^2) as a function of radial displacement of monodisperse PE nanofiber and nanoparticle.

4.2 Effect of chain length on bidisperse PE nanofiber and nanoparticle systems

The results of effect of chain length on bidisperse PE nanofibers and nanoparticles are similar in all compositions. So, all results are not shown here. Only results of 50% B0 are shown.

4.2.1 Density profile

Radial density profile

The radial density profiles of bidisperse systems are similar to monodisperse systems. The total densities of all short and long chain systems and the diameters are close to monodisperse systems. But the tendency is decrease when the shorter chain was mixed. This behavior can be described by excluded volume of chain end. The overall densities are then decreased for short chain system. Figure 4.16 shows the density profiles of bidisperse system (B50+B40 while composition of B50 = 50%). The results show that the shorter chains are also more predominant at the interface compared to the bulk region. For the mixed system, there is a small difference in overall density. The shorter chains disperse near the surface than longer ones as shown in figure 4.17.

In nanoparticle system, the characteristics of density profiles of shorter and longer chain are similar to those of nanofiber system but the total densities are slightly higher. The diameters of nanoparticles are smaller than those of nanofibers with the same system as shown in figure 4.18. This behavior can be described by the same reason of monodisperse system.
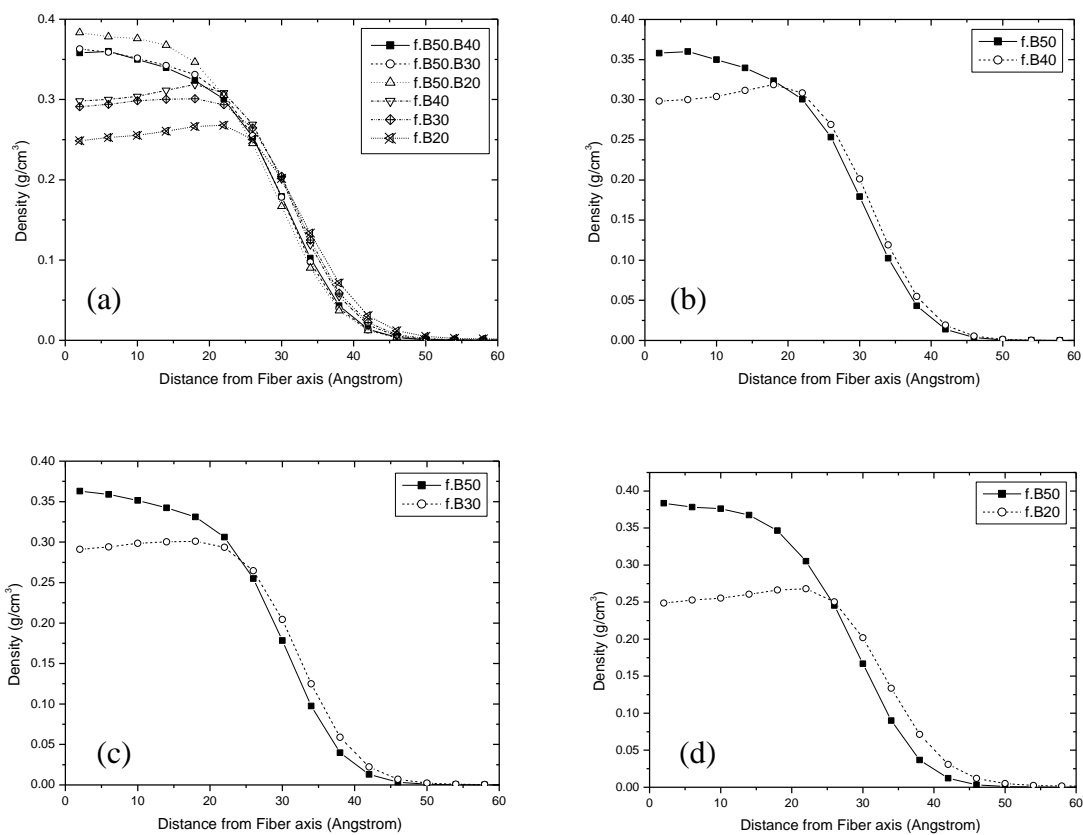
Figure 4.16 The density profile of bidisperse PE nanofibers which B50 composition is 50% (a) total density of short and long chain, (b) B50+B40, (c) B50+B30 and (d) B50+B20.
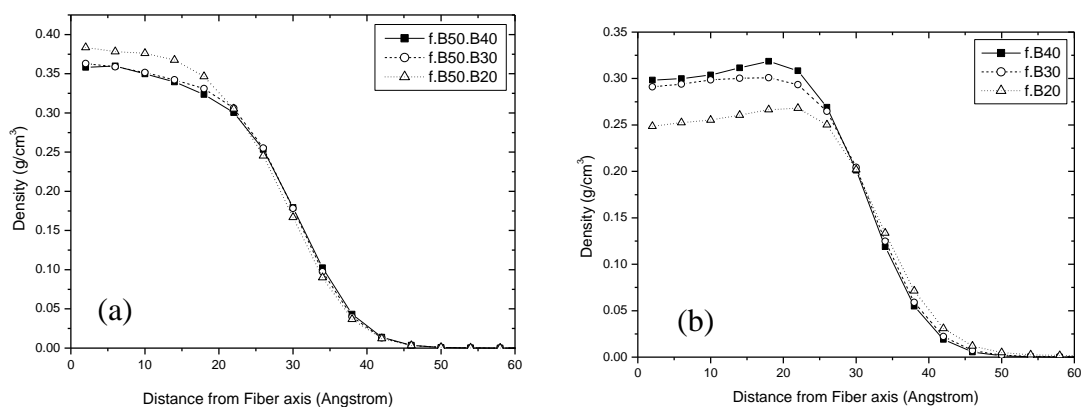
Figure 4.17 The density profile of bidisperse PE nanofibers which B50 composition is 50% (a) B50 and (b) B40, B30, B20.
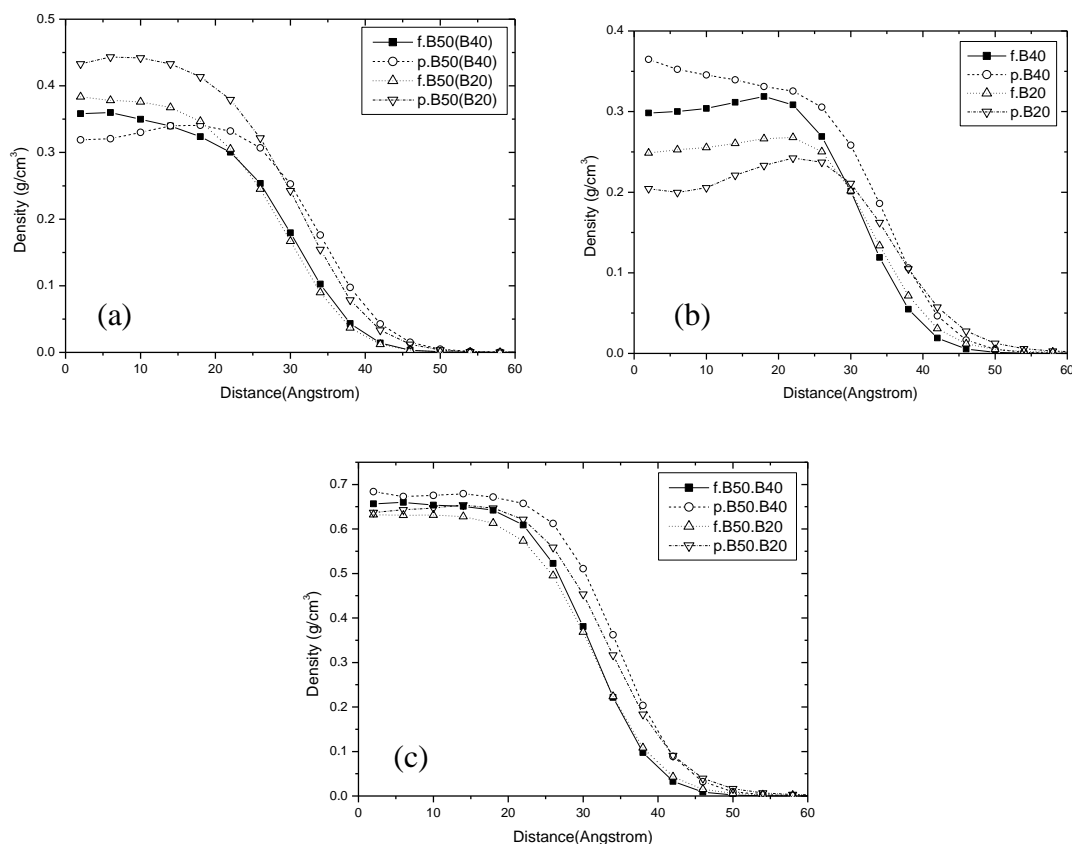
Figure 4.18 Comparison of density profile of bidisperse PE between nanofibers and nanoparticle which B50 composition is 50% (a) B50 and (b) B40, B30, B20 and (c) total density.

Beads distribution and segregation of chain ends

The distributions of middle bead and end bead of short and long chains both of nanoparticle and nanofiber are similar result to the monodisperse systems. Compared between the shorter chain and the longer one, the results show that the densities of end beads of the shorter chain are higher than that of longer ones. In addition, the bead densities are increasing with decreasing chain length of mixed system. These results can be described by greater number of short chain end beads. Figure 4.19 shows a comparison of bead distributions between nanoparticle and nanofiber. Both of beads distributions of longer chain (B50) in nanofiber and

nanoparticle system are not different but the distribution in the mixed system is quite different. The bead distributions of mixed chains of nanofiber are higher than those of nanoparticle with the same number of beads. Therefore nanofiber has lower surface area per volume than nanoparticle, the distribution of end beads near the surface of nanofiber is higher than that seen in nanoparticle. These behavior is similar to P. Doruker work (Doruker, 2002) which studied the bidisperse system of longer chains PE thin films.

4.2.2 Orientation

Bond orientation

The orientation of end bonds and middle bonds of nanofibers and nanoparticles are similar to those of monodisperse systems. The all bonds orientations of longer chain and mixed chains are not significant difference when the shape of particle is changed. Figure 4.20 shows the example of all chain orientation of nanofibers and nanoparticles. The orientation change of all bonds for both of longer chain and mixed chains is not significant difference for the particle with the same shape. As well as other properties, these changes are observed after the bulk region.

Particle orientation

The largest and smallest eigenvectors of the whole chains of bidisperse nanofibers and nanoparticles systems have the same behavior with the monodisperse systems. Furthermore, mixing of shorter chains does not affect to the longer chain behavior. The tendency of changing in orientation of mixed chains is higher magnitude when the chain length different increases as shown in figure 4.21. These effects of chain length can be described by the same reason of monodisperse.
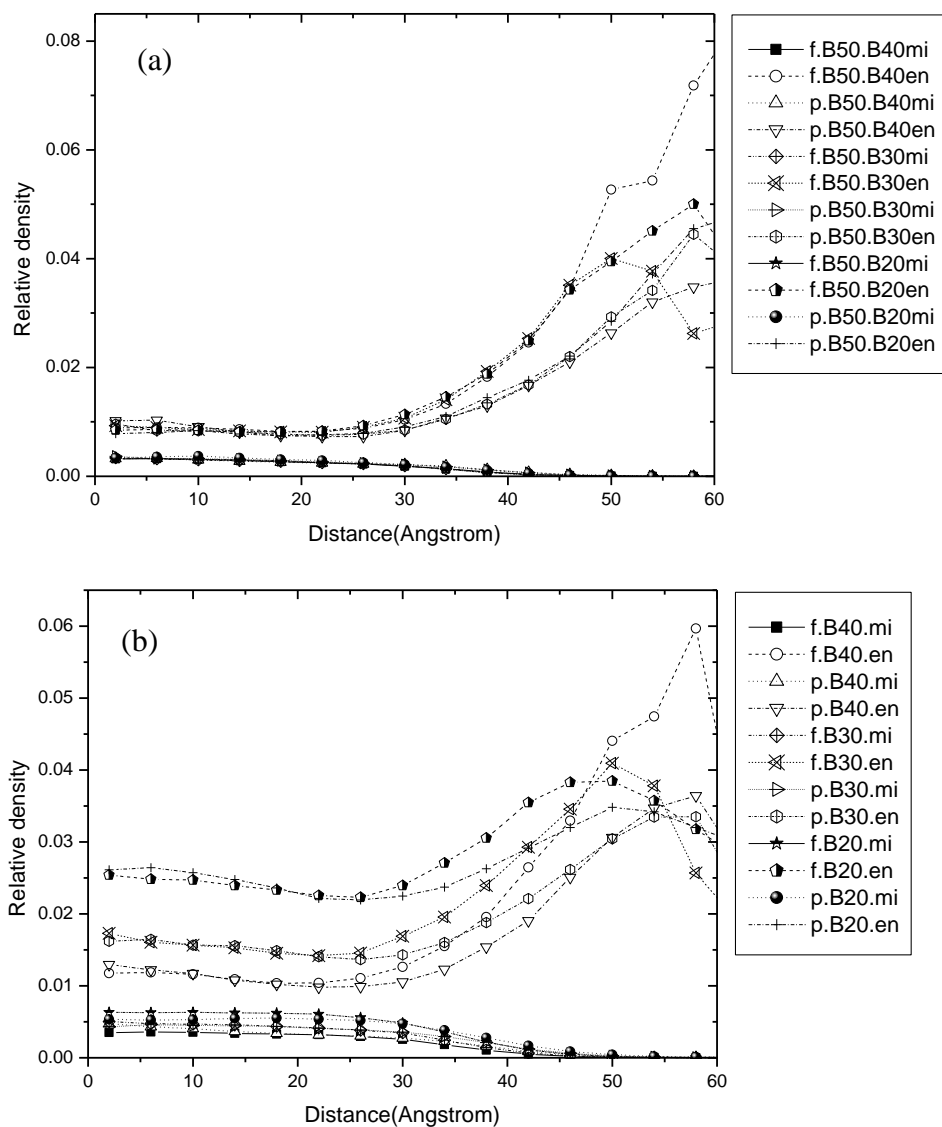
Figure 4.19 The relative density of middle bead and end bead of bidisperse PE nanofibers and nanoparticle which B50 composition is 50% (a) B50 and (b) B40, B30, B20.
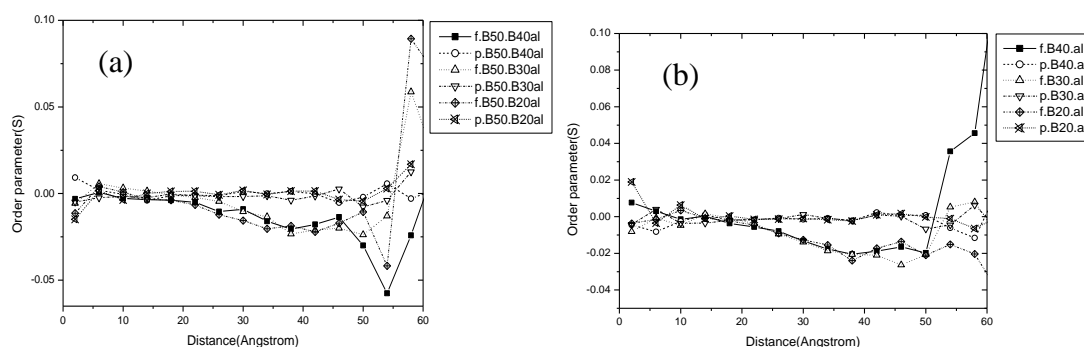
Figure 4.20 Comparison of the orientation of chords (all) of bidisperse PE nanofibers and nanoparticles which B50 composition is 50% (a) B50 and (b) B40, B30, B20.
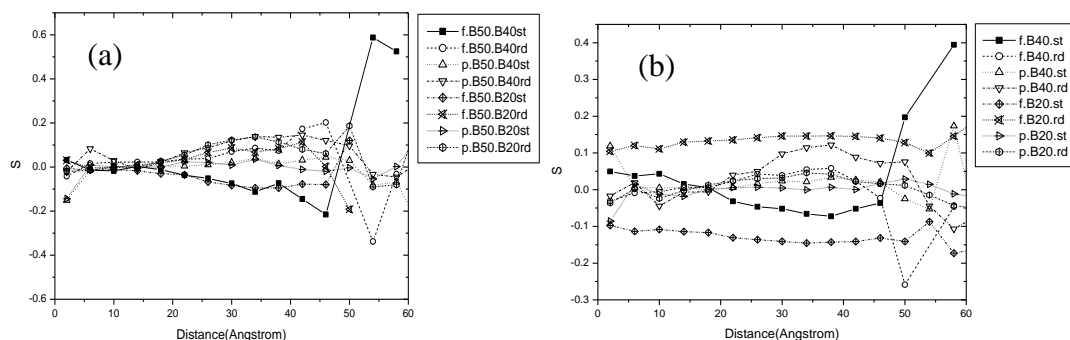
Figure 4.21 Comparison of the orientation of the largest and smallest principal moment to axis after equilibration between bidisperse PE nanofibers and nanoparticles which B50 composition is 50% (a) B50 and (b) B40 and B20.

4.2.3 Chain properties

The profiles of center of mass distribution of nanofiber system are shown in figure 4.22(a). It is found that for long chain, the highest densities of center of mass are not significant different in all systems. For mixed system; however, the highest density increases with decreasing chain length. This behavior is related to higher number of chains for shorter chain system. For nanoparticle, the results are similar to nanofiber systems. A comparison between longer chain and mixed system is shown in

figure 4.22(b) and 4.22(c) respectively, for nanofiber and nanoparticle. The distance which has the highest center of mass densities of nanoparticle is closer to the surface than nanofiber whereas their distribution of nanoparticle is broader than nanofiber.
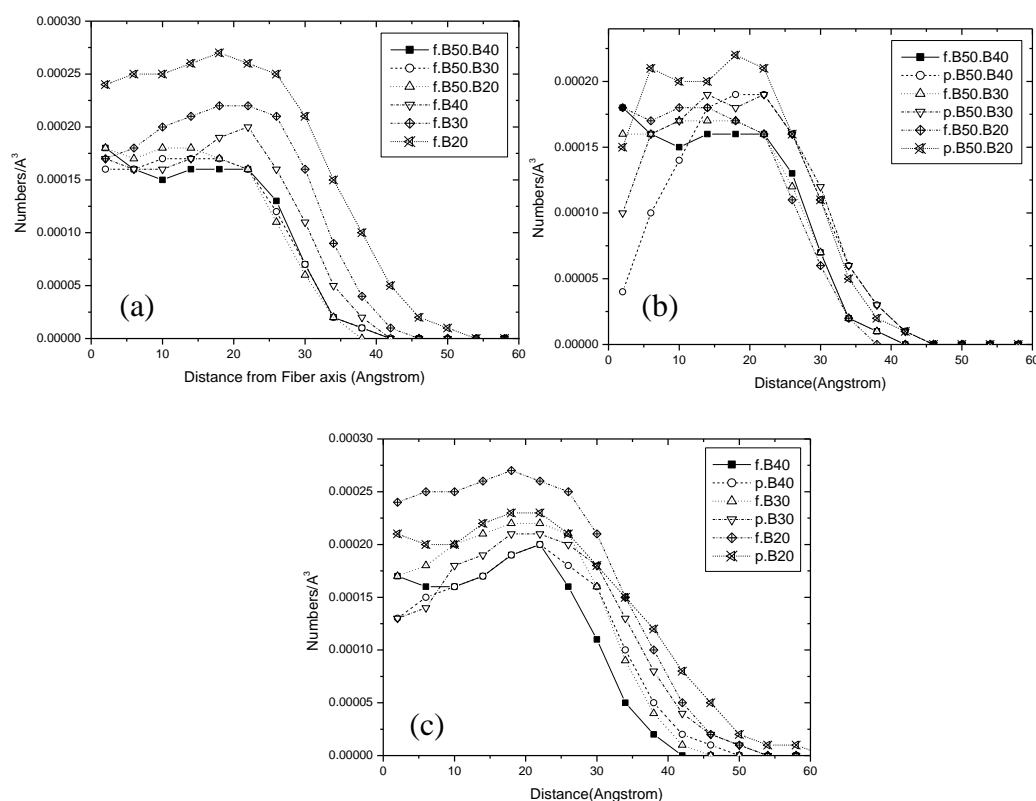
Figure 4.22 The center of mass distribution as a function of radial displacement bidisperse PE systems which B50 composition is 50% (a) nanofiber (b) the long chain(B50) nanofiber and nanoparticle (c) the mixed chain nanofiber and nanoparticle.

The change in the R_g components as a function of radial displacement from center of mass both of bidisperse nanofiber and nanoparticle in X, *Y-Z* and *X-Y-Z* component is the same result of monodisperse systems. Mixing of the shorter chain does not affect the longer chain behavior. Comparing the change in R_g components of

mixed system, the change in overall R_g and its component is depended on their chain length that increase with increasing chain length as shown in figure 4.23. The results can be described by the same reason of monodisperse system.
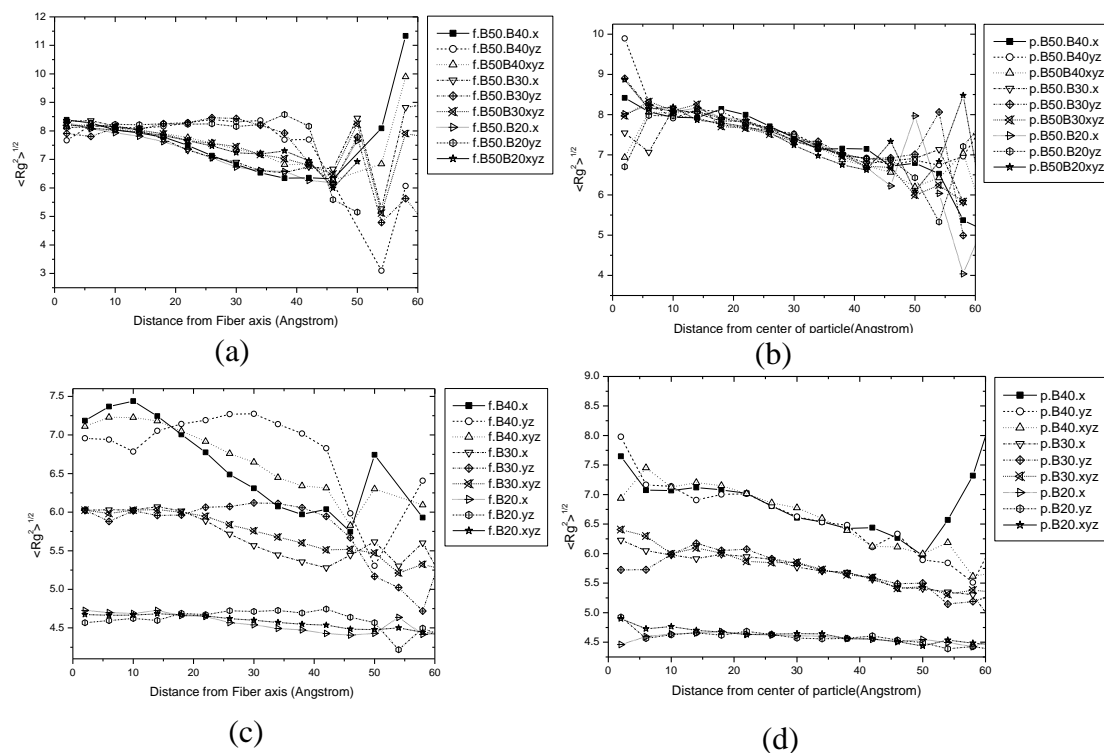
Figure 4.23 Comparison of the changing in the R_g components to center of mass after equilibration between bidisperse PE nanofibers and nanoparticles which B50 composition is 50% (a) B50 nanofiber (b) B50 nanoparticle (c) B40, B30 and B20 nanofiber and (c) B40, B30 and B20 nanoparticle.

(a) (b)
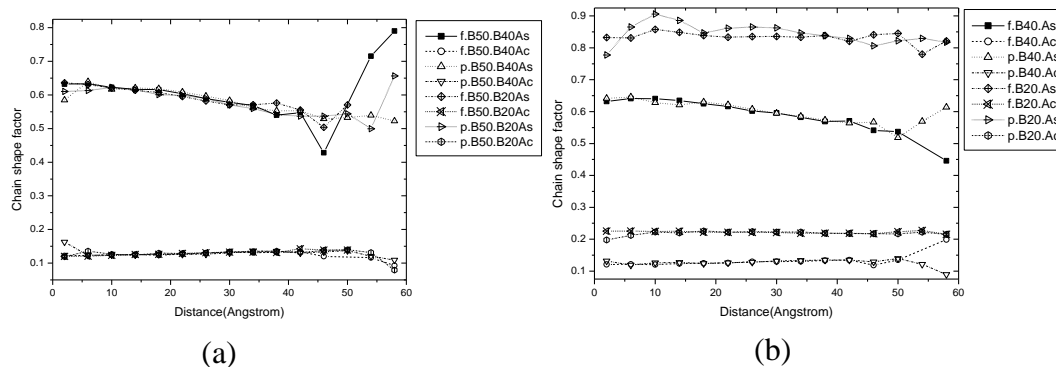
Figure 4.24 Comparison of the changing in shape (asphericity and acylindricity) as a function of radial displacement of the center of mass of bidisperse PE systems which B50 composition is 50% (a) B50 nanofiber and nanoparticle (b) B40 and B20 nanofiber and nanoparticle.

As well as the change in the R_g components, the chain shape properties of bidisperse systems are similar to those of monodisperse systems. The long chain (B50) is not affected by mixing of shorter chain. For mixed chain, the change in asphericity and acylindricity of longer chain is higher than that of short ones and can be described by the same reason of monodisperse system. These results do not different both nanofibers and nanoparticles as shown in figure 4.24.

Figure 4.25 shows the comparison of the three eigenvalues (principal moments) of the chains normalized by their square radius of gyration as a function of radial displacement from the center of mass of nanofiber and nanoparticle. The results are similar to those of monodisperse system. There is slightly changing in the eigenvalues at the surface region both longer chain (B50) and mixed chains in all systems. This property is not affected by mixing of shorter chain. The change in these eigenvalues for longer chain is higher magnitude than that of shorter chain in both

systems. For the mixed system, this change is decreasing with decreasing chain length. This can be explained in a similar way to the change in R_g component.

It is found that there is a slightly changing in the eigenvalues in the interface region both long chain (B50) and mixed chains in all systems, most of which is occurring close to the vacuum side. This behavior of long chain is not affected by mixing of short chain as shown in figure 4.25(a). The change in these eigenvalues for longer chain is higher magnitude than that of short chain for both systems. For mixed chains, the changes are decrease with decreasing chain length and can be explained in a similar way to the change in R_g component.

(a) (b)

Figure 4.25 Comparison of the principal moment of chains (normalized by R_g^2) as a function of radial displacement of the center of mass of bidisperse PE systems which B50 composition is 50%   (a) B50 nanofiber and nanoparticle (b) B40 and B20 nanofiber and nanoparticle.

4.3 Effect of composition on bidisperse PE nanofiber and nanoparticle systems

The results of of composition on bidisperse PE nanofibers and nanoparticles are not different when chain length of mixed chain was varied. So, all results are not shown here. Only results of B0+B30 are shown.

4.3.1 Density profile

Radial density profile

The density profile of bidisperse PE nanofiber was shown in figure 2.26. The results show that the mixed chain predominates near the surface of fiber which can be clearly observed in high composition. The results of nanoparticle systems are similar to those of nanofiber systems. Comparing the profile between both systems, it is found that the density of nanoparticle is higher than that of nanofiber in all compositions as shown in figure 4.27. In all composition, the total density profile of nanofiber is not difference and less than nanoparticle as shown in figure 4.28. These behaviors can be described in the same reason of monodisperse system.

Beads distribution and segregation of chain ends

Figure 4.29(a) and 4.29(b) shows the relative density profiles of middle bead and end bead of bidisperse PE nanofiber and comparison between nanofiber and naoparticle respectively. The results show that the mixing of shorter chains does not affect to longer chain and mixed chains behavior different composition of shorter chain.
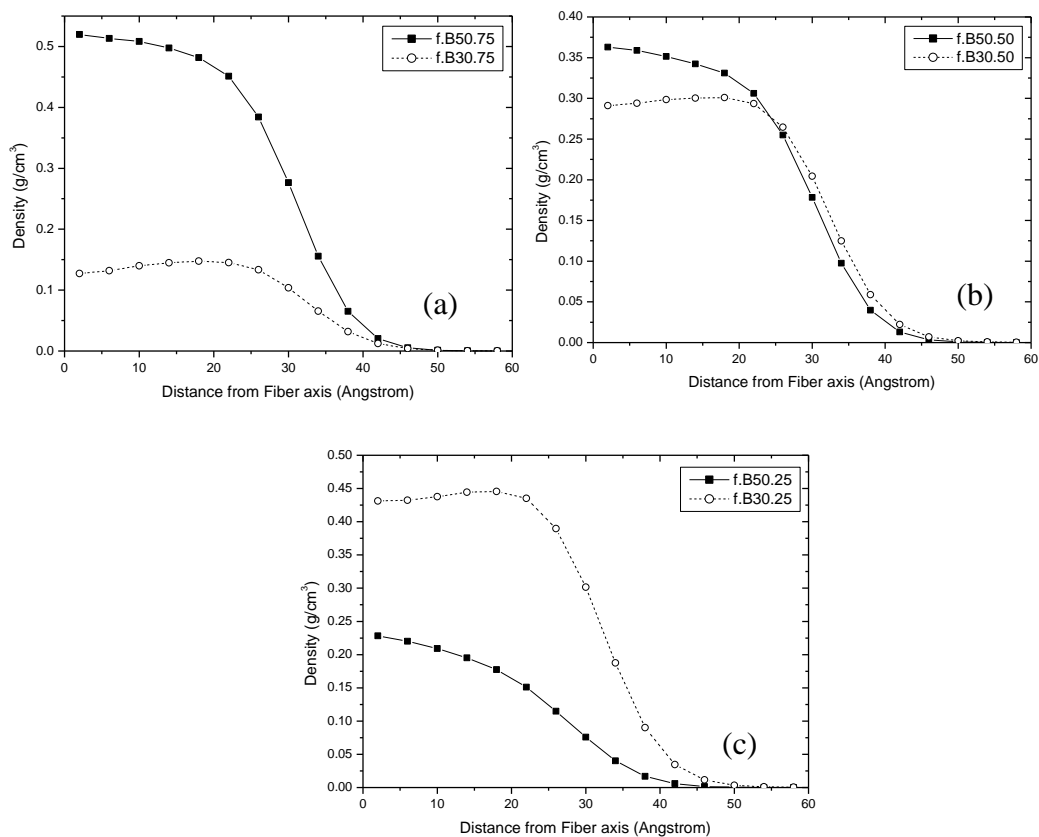
Figure 4.26 Density profiles of bidisperse PE nanofiber in the system of B50+B30 which the composition of B50 is (a) 75% (b) 50% and (c) 25%.
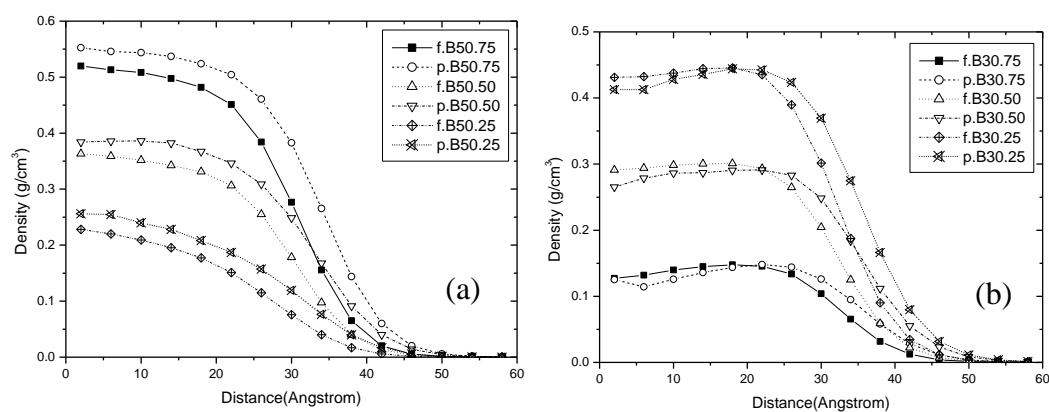
Figure 4.27 Comparison the density profile of B50+B30 between bidisperse PE nanofiber and nanoparticle system (a) long chain (B50) and (b) mixed chain.
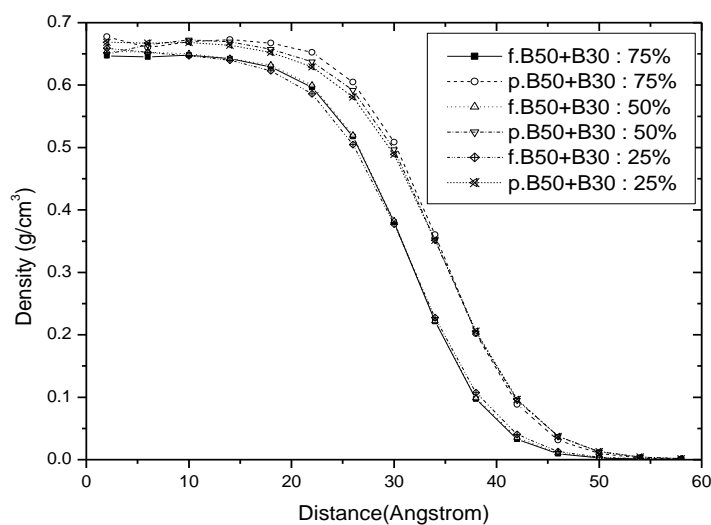
Figure 4.28 Effect of composition on total density profile of bidisperse PE naofiber and nanoparticle in B50+B30 system.
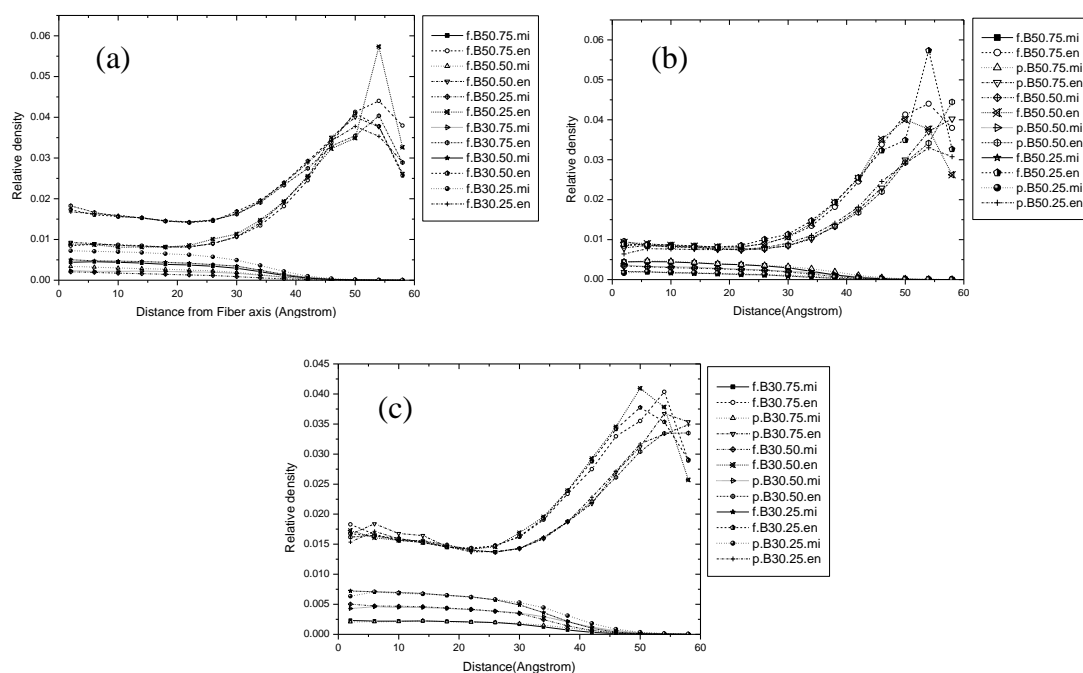
Figure 4.29 The relative density of middle bead and end bead of bidisperse PE in B50+B30 system (a) nanofiber (b) comparison between B50 nanofiber and nanoparticle and (c) comparison between B30 nanofiber and nanoparticle.

4.3.2 Orientation

Bond orientation

As well as the bead distribution properties, the orientation of chord (all bond) of nanofiber and nanoparticle with the same chain length system was not affected by the different composition as shown in figure 4.30.

Particle orientation

Figure 4.31 shows the orientation of largest and smallest principal moment. They are found that the effect of composition does not affect to this property in all systems.
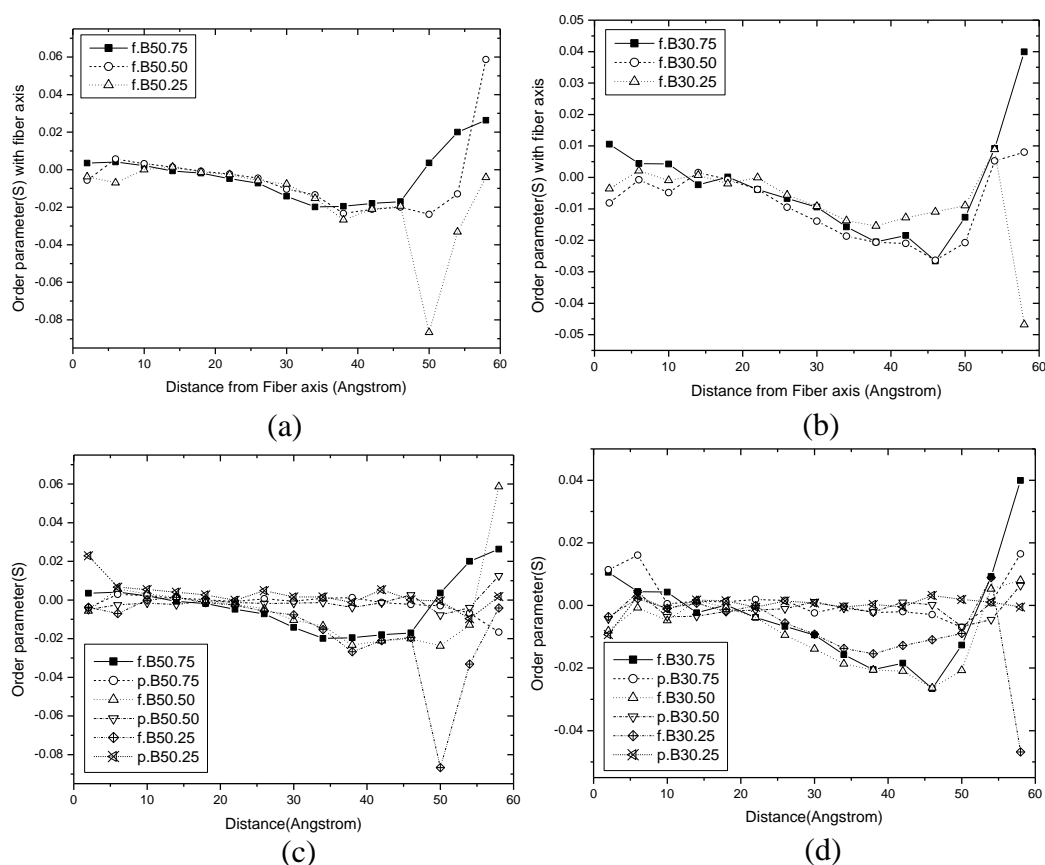
Figure 4.30 The orientation of chord (all) in B50+B30 system (a) B50 PE nanofiber, (b) B30 PE nanofiber, (c) B50 PE nanofiber and nanoparticle and (d) B30 PE nanofiber and nanoparticle.
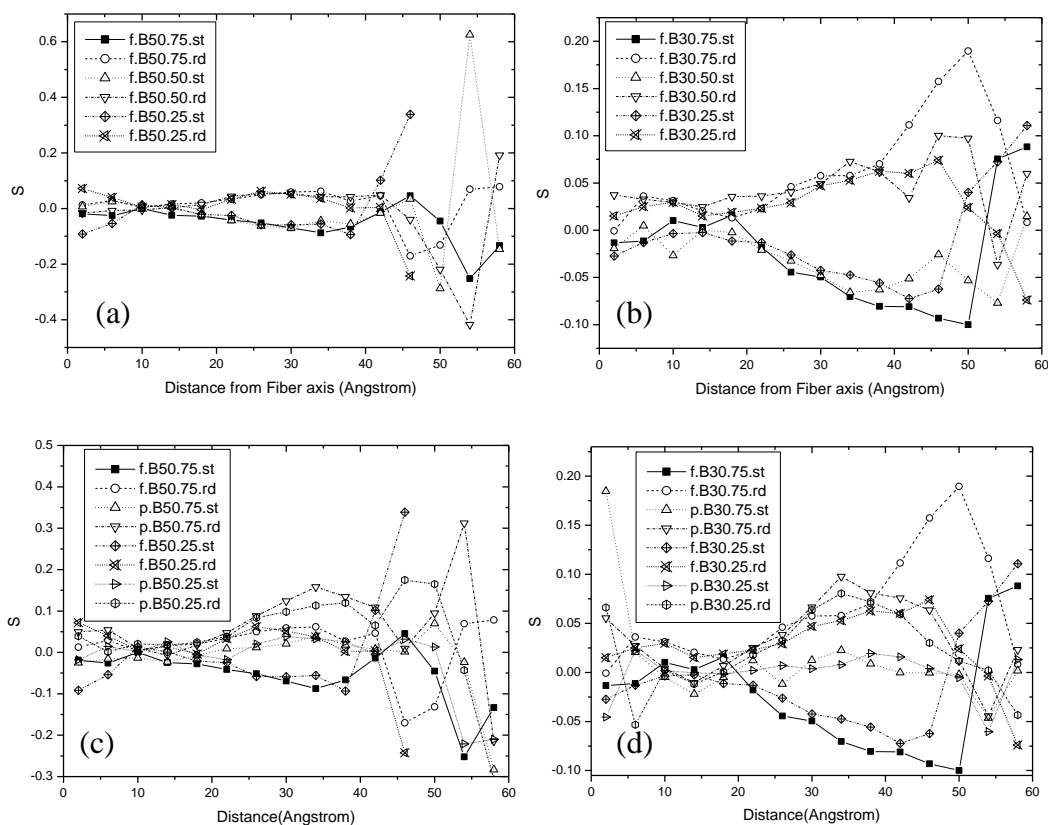
Figure 4.31 The orientation of largest and smallest principal moment in the system of B50+B30 (a) B50 PE nanofiber, (b) B30 PE nanofiber, (c) B50 PE nanofiber and nanoparticle and (d) B30 PE nanofiber and nanoparticle.
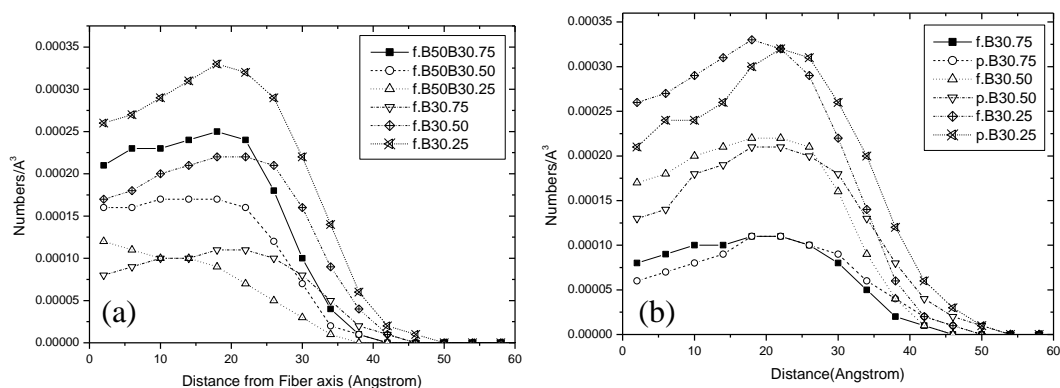
Figure 4.32 The center of mass distribution as a function of radial displacement in B50+B30 system (a) PE nanofiber (b) PE nanofiber and nanoparticle.

4.3.2 Chain properties

The center of mass distribution as a function of radial displacement is shown in figure 4.32. The results show that the maximum values of the center of mass number per volume depends on the amount of each chain in the system. Moreover, the distance from center of mass which is the maximum values does not different in the same chain length system.

The change in the R_g components as a function of radial displacement of the center of mass both bidisperse nanofiber and nanoparticle in X, *Y-Z* and *X-Y-Z* component are shown in figure 4.33. Varying of the B50 component does not affect to the long chain and mixed chain behavior.

Changing in shape (asphericity and acylindricity) and the principal moment of chains (normalized by R_g^2) as a function of radial displacement of the center of mass is shown in figure 4.34 and 4.35 respectively. The results are similar to other properties. Varying of the B50 component does not affect to the long chain and mixed chain behavior.
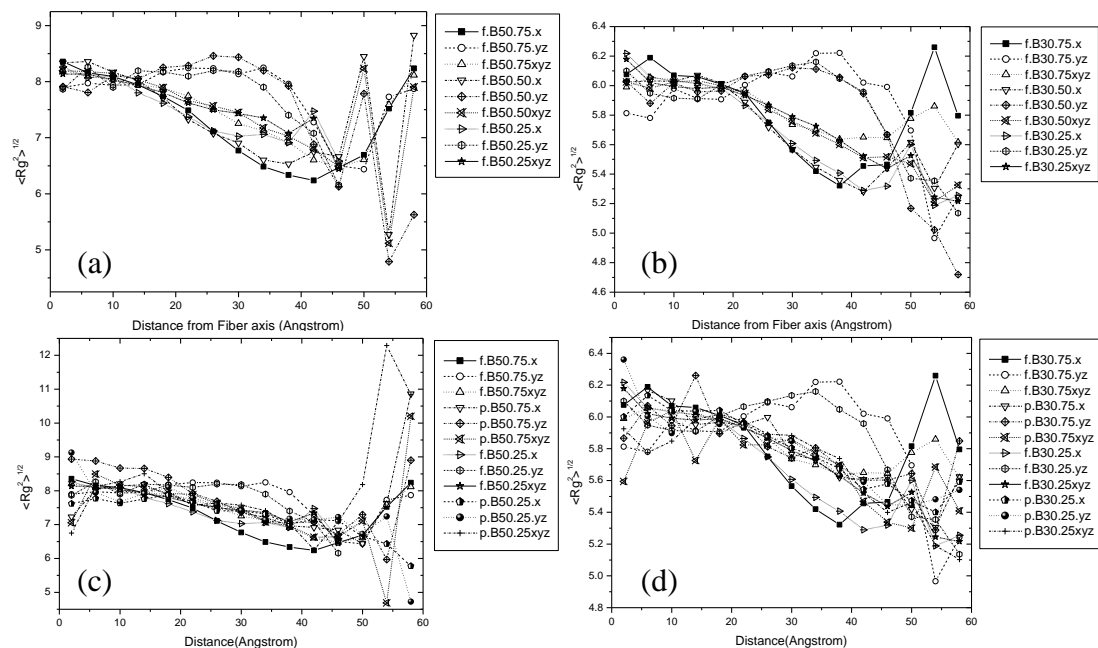
Figure 4.33 The change in R_g component in B50+B30 system (a) B50 PE nanofiber, (b) B30 PE nanofiber, (c) B50 PE nanofiber and nanoparticle and (d) B30 PE nanofiber and nanoparticle.
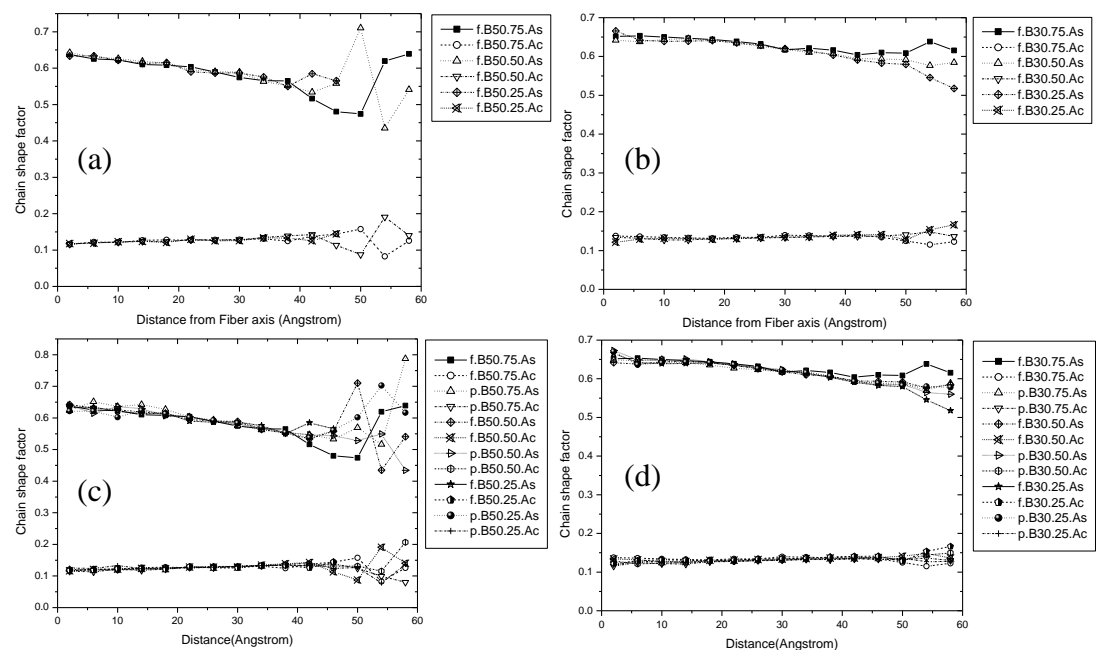
Figure 4.34 Changing in shape (asphericity and acylindricity) as a function of radial displacement of the center of mass in B50+B30 system (a) B50 nanofiber, (b) B30 nanofiber, (c) B50 nanofiber and nanoparticle and (d) B30 nanofiber and nanoparticle.
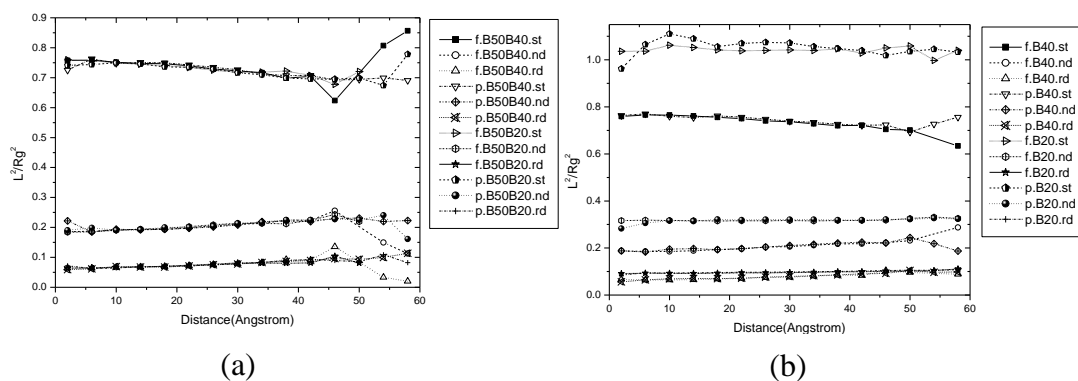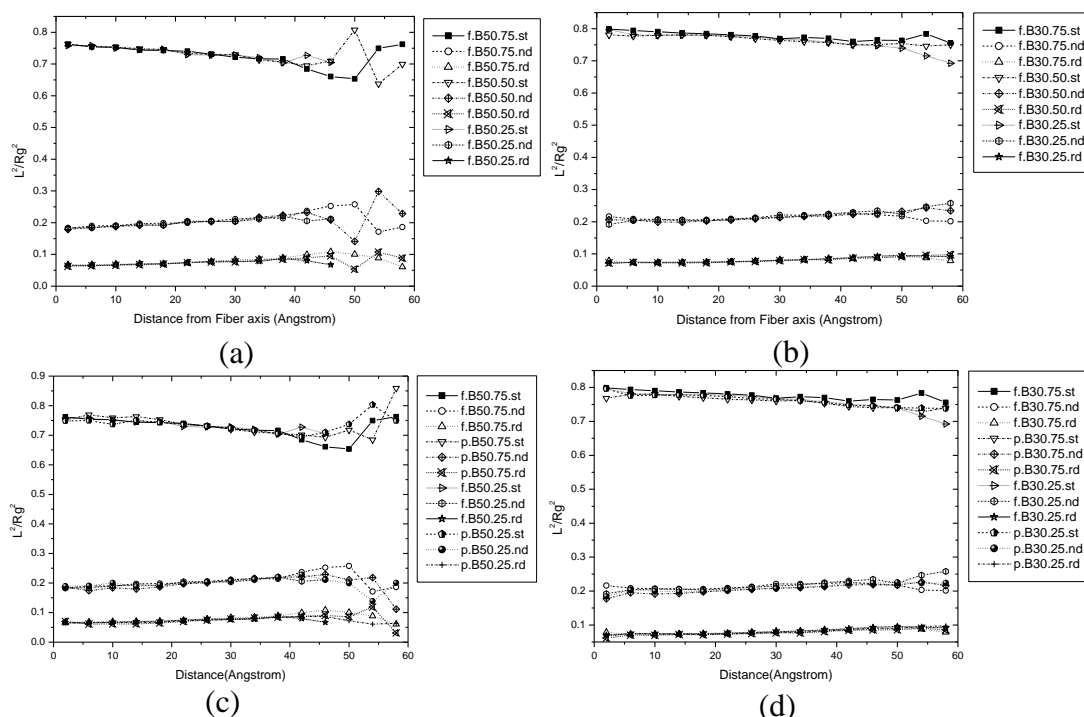
Figure 4.35 Comparison of the principal moment of chains (normalized by R_g^2) as a function of radial displacement of the center of mass in B50+B30 system (a) B50 nanofiber, (b) B30 nanofiber, (c) B50 nanofiber and nanoparticle and (d) B30 nanofiber and nanoparticle.

4.4 Crystallization

4.1.1 Density profile

Figure 4.36 shows the density profile of nanofiber after quenching from 509 K to 298 K and simulation at 298 K. The results show that the density profile both of longer and shorter chain increase while the size decrease with increasing the MCS as shown in figure 4.36. Moreover, the total density fluctuates and average value of approximately 1.20 g/cm^3 and the size of nanofiber is about 4.0 nm with constant value after 10 million MCS as shown in figure 4.37. It is confirmed that the PE crystal is formed. These behaviors can be explained that at low temperature, all

chains have more *trans* conformation and denser than high temperature. It results in increasing the density and decreasing the size of nanofiber. The densities of B20 and B15 are increasing close to interface region. It is represented that the crystallization is occurring from the surface to the center of nanofiber. At starting point of simulation, the shorter chains enrich near the surface and then they are pushed into the center of fiber. It can be explained that the longer chains has more number of beads and require more space than shorter ones when the crystal is formed.

In the case of nanoparticle, the results similar to those of nanofiber as shown in figure 3.38. But the total density and the size of nanopaticle is higher than nanofiber as shown in figure 3.40. In addition, the shorter chains prefer locate at the surface all simulation times as shown in figure 3.39 because of confinement effect and limitation of space of nanoparticle.
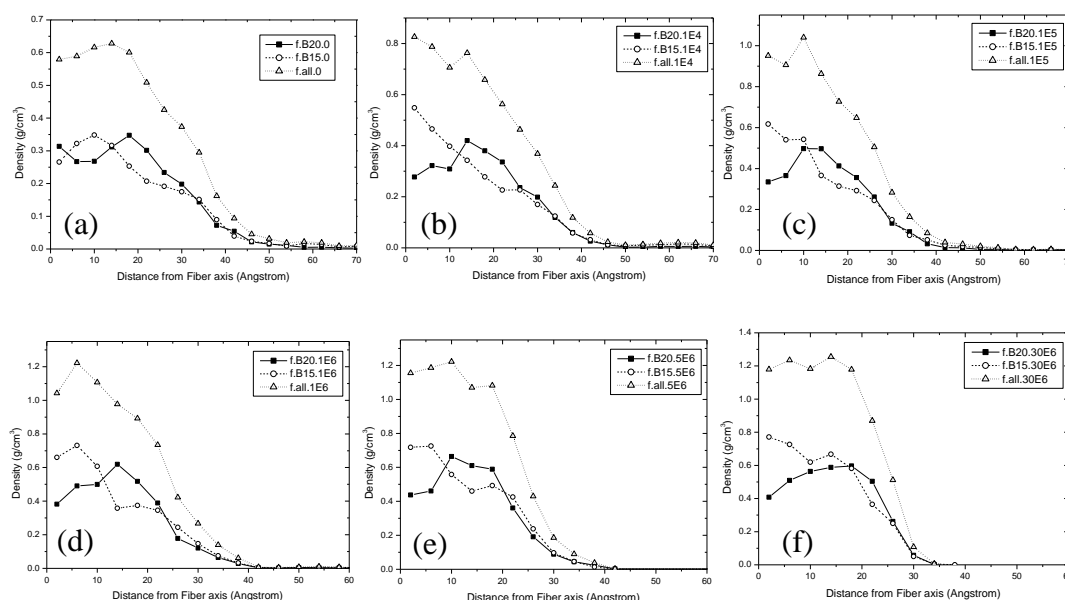
Figure 4.36 Density profile of B20 and B15 nanofiber normal to the fiber axis after quenching from 509 K to 298 K and simulation at 298 K (a) 0, (b) 1×10^{4}, (c) 1×10^{5}, (d) 1×10^{6}, (e) 5×10^{6} and (f) 3×10^{7} MCS.
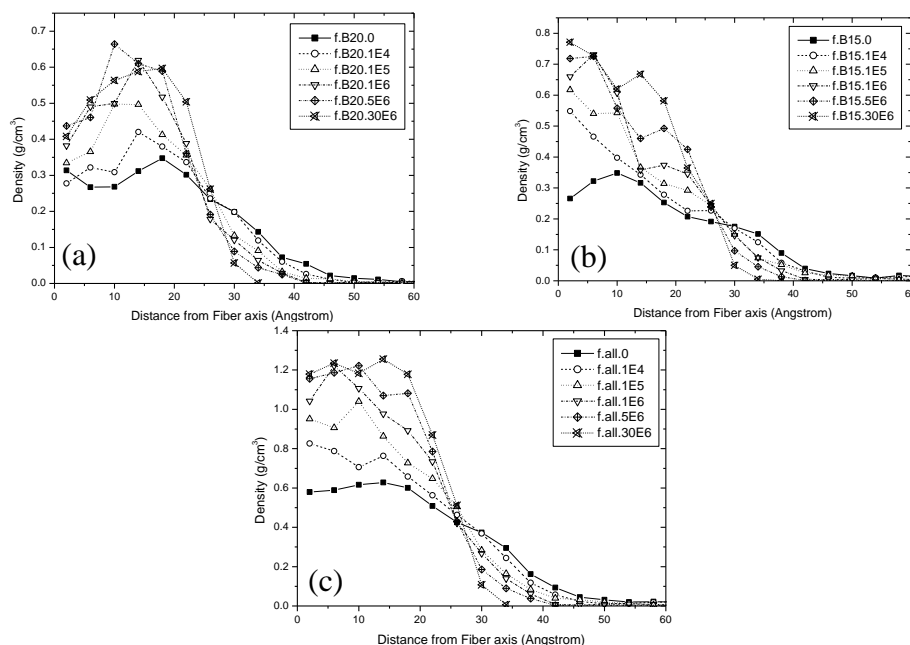
Figure 4.37 The evolution of the density profile as a function of MCS after an instantaneous cooling of the nanofiber from 509 to 298 K (a) B20, (b) B15 and (c) total density.
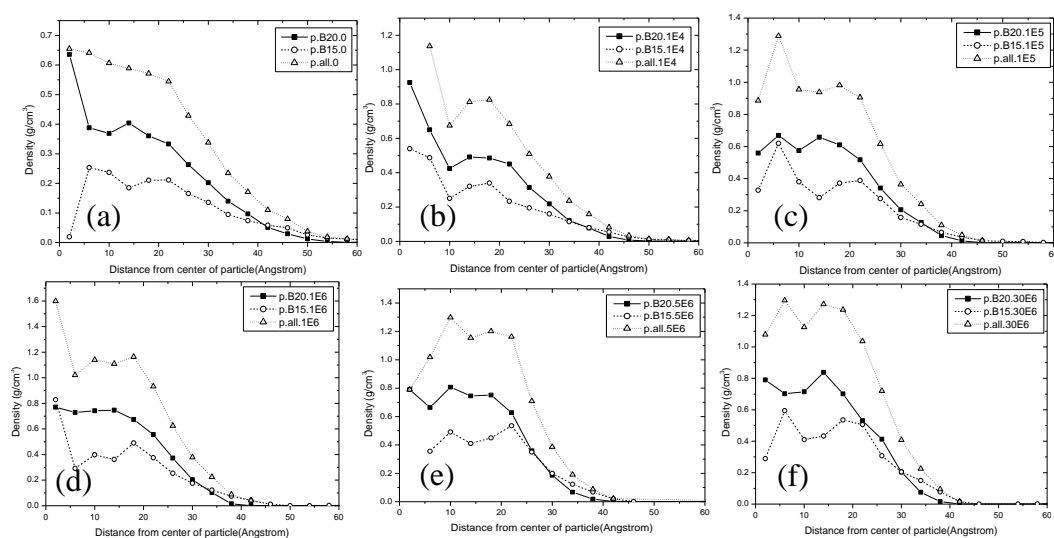
Figure 3.38 Density profile of B20 and B15 nanoparticle normal to the center of particle after quenching from 509 K to 298 K and simulation at 298 K (a) 0, (b) 1×10^4, (c) 1×10^5, (d) 1×10^6, (e) 5×10^6 and (f) 3×10^7 MCS.
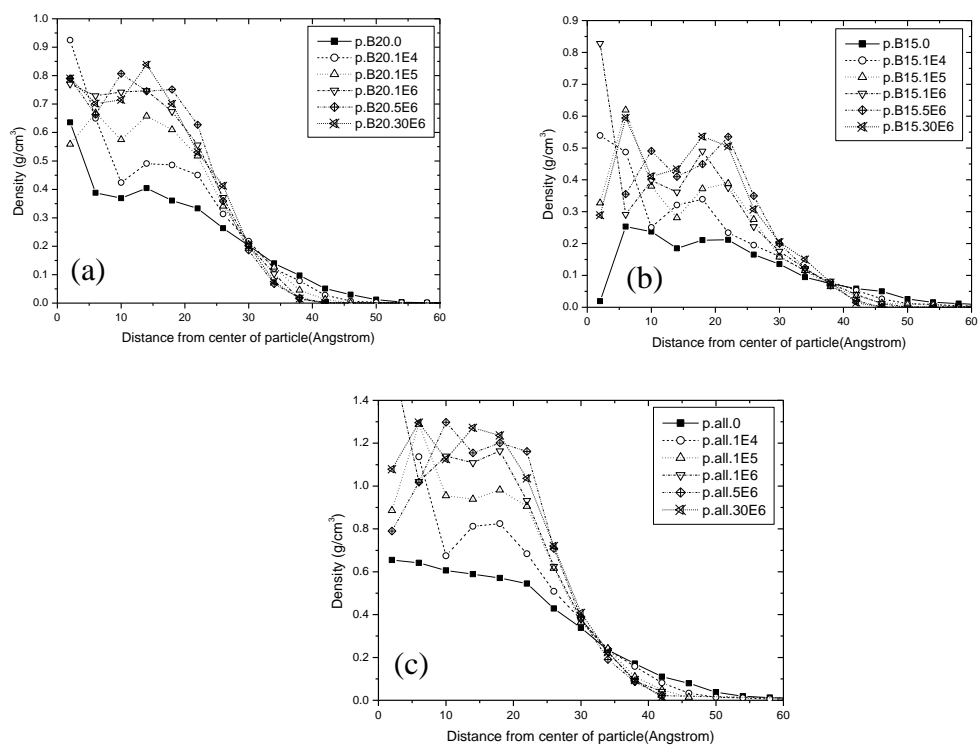
Figure 3.39 The evolution of the density profile as a function of MCS after an instantaneous cooling of the nanoparticle from 509 to 298 K (a) B20, (b) B15 and (c) total density.
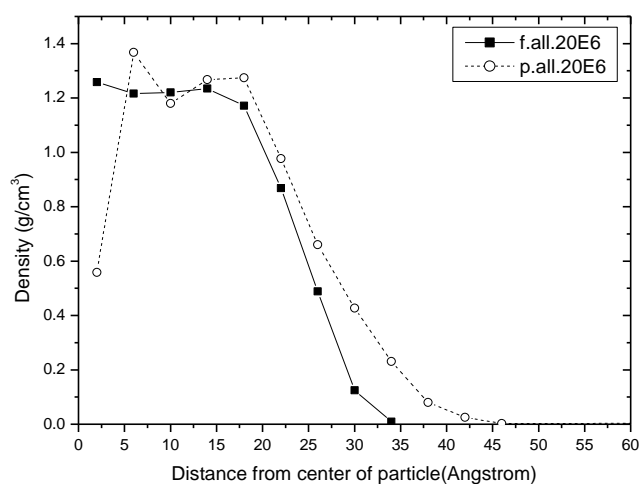
Figure 3.40 Comparison of crystal density profile between nanofiber and nanoparticle at 3×10^7 MCS.

4.4.2 Bond conformation

In order to investigate the structure formation process on the molecular level, how the conformational change takes place is examined. Figure 4.41 shows the fraction of trans conformation as a function of MCS of B20 and B15 in nanofiber and nanoparticle system. In nanofiber system the results show that after 25 million MCS, the fraction of bonds in *trans* state approaches a limiting value about 79% and 81% for B20 and B15 respectively. The shorter chain approaches to equilibrium quicker than the longer one because of the limitation of space. The shorter chain can be easily arranged the molecule to *trans* conformation. In nanoparticle system, the results are quite different. After 15 million MCS, the fraction of bonds in *trans* state approaches a limiting value about 79% both of B20 and B15 because of confinement effect. And the behavior is not difference. In addition nanoparticle approaches to equilibrium quicker than nanofiber. It can be explained by the bigger size of nanoparticle and more space than nanofiber. It can be concluded that nanoparticle is easier crystallized than nanofiber. Figure 4.42 shows the final structure after 30 million MCS of nanofiber and nanoparticle.

4.4.3 Chain ordering

When the crystallization is occurred, a PE chain has zigzag trans conformation (torsion angle 180° at internal C-C bonds). In a perfect crystalline domain, bonds have high correlation even at long distance. In order to investigate the growth process of an intermolecular orientational order, we calculate the global orientation correlation function, SG, which is defined by equation 4.2.

$$S_G = \frac{1}{2}\left[3\left\langle \cos^2 \psi \right\rangle - 1\right] \tag{4.2}$$

Here, ψ denotes the angle between the main axes of two chains, and the value of S_G is averaged for all pairs of chains in a given snapshot. The main axis of a chain is the longest principal axis of the radius of gyration tensor. This parameter, S_G, has a value of 1.0 when all chains are parallel and that of 0.0 when all chains are randomly oriented. Figure 4.43 depicts the global orientation order parameter, S_G, as a function of MCS. S_G increases steadily at the beginning of the crystallization followed by an almost constant value in the late stage. The chains finally achieve S_G ~0.15 and ~0.08 for nanofiber and nanoparticle respectively. It can be concluded that chains in nanoparticle are less ordered compared to nanofiber. The results can be explained by less fraction of *trans* or multi domain form. In addition, shorter chain is more easily crystallizing than longer chain and can be clearly observed in nanofiber system.
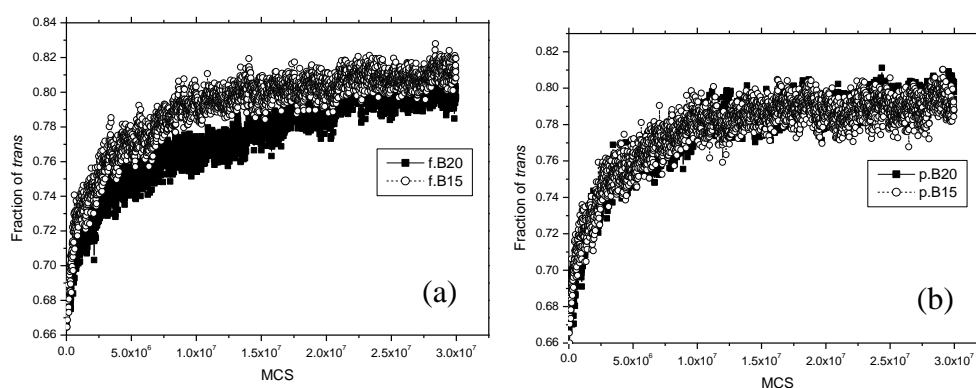
Figure 4.41 The fraction of C-C bonds that are in the *trans* state as a function of MCS after quenching from 509 to 298 K (a) nanofiber and (b) nanoparticle.
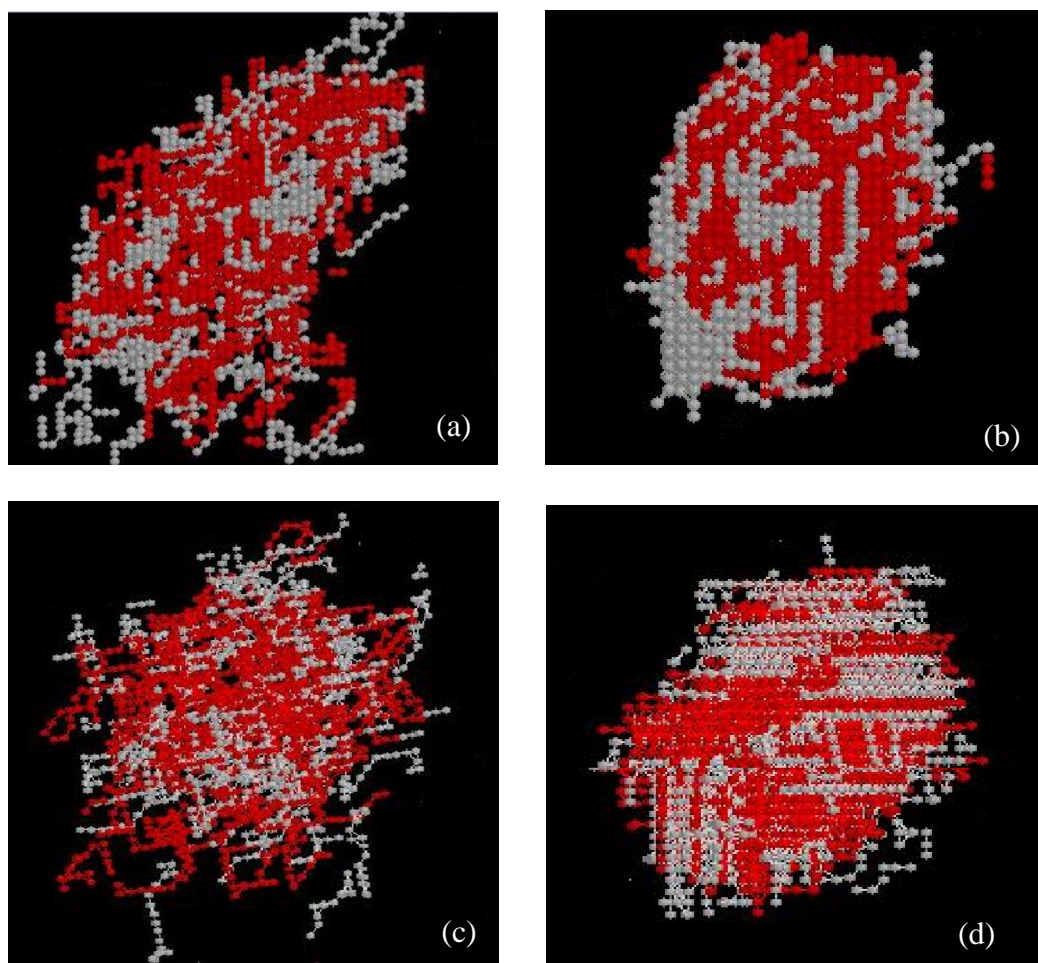
Figure 4.42 The structure of (a) nanofiber (0 MCS), (b) nanofiber (30 MCS), (c) nanoparticle (0 MCS) and (d) nanoparticle (30 MCS) (red = B20, gray = B15).
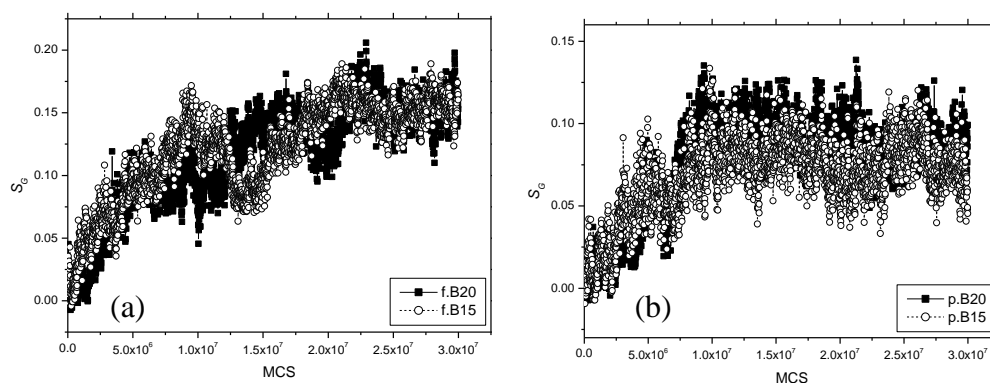
Figure 4.43 The global orientation order parameter, S_G, as a function of MCS after quenching from 509 to 298 K (a) nanofiber and (b) nanoparticle.

CHAPTER V

SUMMARY

In this thesis, MC simulation on 2nnd lattice was applied to investigate the effect of bidispersity on the structure and crystallization of PE nanofiber and nanoparticle. MC simulations, in-house software initially developed by Visit Vaosoongnern (Chemistry, Suranaree University of Technology) from the past collaboration with the Department of Polymer Science, University of Akron, USA during 2000-2004 was used.

Firstly, various chain length of PE monodisperse was used to investigate for comparing the properties with bidisperse systems. The results show that the density profiles of nanoparticle are higher than those of nanofiber and they decrease with decreasing chain length. This is due to stronger confinement effect in nanoparticle system. At the surface, end beads are more enrich than the middle beads. Both monodisperse nanofiber and nanoparticle systems, end bond tends to orient perpendicular to the surface while middle tends to orient parallel to the surface in the interfacial region. In addition, all bonds of nanofiber systems tend to orient parallel to the surface. But nanoparticle system, they tend to randomly orient. Chains and largest principal axis tend to orient perpendicular to the surface which is predominant with increasing the chain length. Moreover, the molecular orientation of nanofiber is more normal to the surface than nanoparticle. Molecular sizes are decrease with decreasing

chain length toward the surface. There is an oscillatory behavior in the distribution of the chain center of mass. In addition, this property is clearly observed in nanofiber system. Molecular shapes are changing from ellipsoid to spherical shape toward the surface.

For the effect of chain length on bidisperse nanofiber and nanoparticle, the results show that all behaviors of long chain (B50) and mixed chains (B40, B30 and B20) are similar to monodisperse systems. The density profiles of nanoparticle are higher than those of nanofiber and they decrease with decreasing chain length for mixed chain system. At the surface, the shorter chains are more abundant than longer one. The longer chain behaviors are almost similar to those of monodisperse systems and it processes similar properties in the same particle shape system. In contrast, shorter chain properties are affected due to the present of longer chain and highly difference with decreasing chain length. Moreover, these properties are not affected by the composition difference.

For crystallization study, the density profiles both of nanofiber and nanoparticle are similar to those of melt bidisperse nanofiber and nanoparticle system. For nannofiber, the shorter chains are forced into center of fiber. But in nanoparticle, it enriches near the surface. The crystallization process is easier occurring than in nanoparticle system and occurs from the surface to inner region. The shorter chain is more easily crystallizing than longer chain and can be clearly observed in nanofiber system. The chain ordering in nanofiber is higher than that in nanoparticle.

REFERENCES

REFERENCES

Abe, A., Jernigan, R. L., and Flory, P. J. (1966). Conformational Energies of n-Alkanes and the Random Configuration of Higher Homologs Including Polymethylene. **Journal of the American Chemical Society** 88(4): 631-639.

Axelbaum, R. L. (1997). Developments in sodium/halide flame technology for the synthesis of unagglomerated non-oxide nanoparticles. **The Joint NSF-NIST Conference on Nanoparticles : Synthesis, Processing into Functional Nanostructures and Characterization**.

Barnes, M. D., Ng, K. C., Fukui, K., Sumpter, B. G., and Noid, D. W. (1999). Probing Phase-Separation Behavior in Polymer-Blend Microparticles : Effects of Particle Size and Polymer Mobility. **Macromolecules** 32(21): 7183-7189.

Baschnagel, J., and Binder, K. (1995). On the influence of hard walls on structural properties in polymer glass simulation. **Macromolecules** 28(20): 6808-6818.

Baschnagel, J., Binder, K., Doruker, P., Gusev, A., Hahn, O., Kremer, K., Mattice, W., Müller-Plathe, F., Murat, M., Paul, W., Santos, S., Suter, U., and Tries, V. (2000). Bridging the Gap Between Atomistic and Coarse-Grained Models of Polymers: Status and Perspectives. **Viscoelasticity, Atomistic Models, Statistical Chemistry**, Springer Berlin / Heidelberg. 152: 41-156.

Baschnagel, J., Paul, W., Tries, V., and Binder, K. (1998). Statics and Dynamics of Bidisperse Polymer Melts: A Monte Carlo Study of the Bond-Fluctuation Model. **Macromolecules** 31(12): 3856-3867.

Becker, M. F., Brock, J. R., Cai, H., Chaudhary, N., Henneke, D., Hilsz, L., Keto, J. W., Lee, J., Nichols, W. T., and Glicksman, H. D. (1997). Nanoparticles generated by laser ablation. **The Joint NSF-NIST Conference on Nanoparticles**, Arlington, VA.

Berndt, C. C., Karthikeyan, J., Chraska, T., and King, A. H. (1997). Plasma spray synthesis of nanozirconia powder. **The Joint NSF-NIST Conference on Nanoparticles**, Arlington, VA.

Brezinsky, K. (1996). Gas-phase combustion synthesis of materials. **Symposium (International) on Combustion** 26(2): 1805-1816.

Brown, D., and Clarke, J. H. R. (1991). Molecular dynamics simulation of an amorphous polymer under tension. 1. Phenomenology. **Macromolecules** 24(8): 2075-2082.

Chen, H. L., Hsiao, S. C., Lin, T. L., Yamauchi, K., Hasegawa, H., and Hashimoto, T. (2001). Microdomain-Tailored Crystallization Kinetics of Block Copolymers. **Macromolecules** 34(4): 671-674.

Cho, J., and Mattice, W. L. (1997). Estimation of Long-Range Interaction in Coarse-Grained Rotational Isomeric State PE Chains on a High Coordination Lattice. **Macromolecules 30**(3): 637-644.

Curgul, S., Van Vliet, K. J., and Rutledge, G. C. (2007). Molecular Dynamics Simulation of Size-Dependent Structural and Thermal Properties of Polymer Nanofibers. **Macromolecules** 40(23): 8483-8489.

de la Mora, J. F., Loscertales, I. G., Rosell-Llompart, J., Serageldin, K., and Brown, S. (1994). Electrospray atomizers and ultrafine particles. **The joint NSF-NIST Conference on UltraFine Particle Engineering**, Arlington, VA.

Deutsch, H. P., and Binder, K. (1991). Interdiffusion and self-diffusion in polymer mixtures: A Monte Carlo study. **The Journal of Chemical Physics** 94(3): 2294-2304.

Dong Lu, S. (2003). **Functional Thin Films and Functional Materials**. Beijing, China. Tsinghua University Press.

Doruker, P. (2002). Simulation of polyethylene thin films composed of various chain lengths. **Polymer** 43(2): 425-430.

Doruker, P., and Mattice, W. L. (1997). Reverse Mapping of Coarse-Grained Polyethylene Chains from the Second Nearest Neighbor Diamond Lattice to an Atomistic Model in Continuous Space. **Macromolecules** 30(18): 5520-5526.

Doruker, P., and Mattice, W. L. (1998). Mobility of the Surface and Interior of Thin Films Composed of Amorphous Polyethylene. **Macromolecules** 32(1): 194-198.

Doruker, P., and Mattice, W. L. (1998). Simulation of Polyethylene Thin Films on a High Coordination Lattice. **Macromolecules** 31(4): 1418-1426.

Doruker, P., Rapold, R. F., and Mattice, W. L. (1996). Rotational isomeric state models for polyoxyethylene and polythiaethylene on a high coordination lattice. **The Journal of Chemical Physics** 104(21): 8742-8749.

Evans, C. C., Bates, F. S., and Ward, M. D. (1999). Control of Hierarchical Order in Crystalline Composites of Diblock Copolymers and a Molecular Chromophore. **Chemistry of Materials** 12(1): 236-249.

Fried, H., and Binder, K. (1991). The microphase separation transition in symmetric diblock copolymer melts: A Monte Carlo study. **The Journal of Chemical Physics** 94(12): 8349-8366.

Friedlander, S. K. (1998). **Synthesis of nanoparticles and their agglomerates : Aerosol reactors**, In R&D status and trends.

Fukui, K., Sumpter, B. G., Barnes, M. D., and Noid, D. W. (1999(a)). Molecular dynamics studies of the structure and properties of polymer nano-particles. **Computational and Theoretical Polymer Science** 9(3-4): 245-254.

Fukui, K., Sumpter, B. G., Barnes, M. D., Noid, D. W., and Otaigbe, J. U. (1999(b)). Molecular dynamics simulation of the thermal properties of nano-scale polymer particles. **Macromolecular Theory and Simulations** 8(1): 38-45.

Fukui, K., Sumpter, B. G., Barnes, M. D., and Noid, D. W. (2000). Atomistic Dynamics of Nanoscale Polymer Particles. **Macromolecules** 33(16): 5982-5987.

Fukui, K., Sumpter, B. G., Noid, D. W., Yang, C., and Tuzun, R. E. (2001). Analysis of eigenvalues and eigenvectors of polymer particles: random normal modes. **Computational and Theoretical Polymer Science** 11(3): 191-196.

Gleiter, H. (1989). Nanocrystalline materials. **Progress in Materials Science** 33(4): 223-315.

Hamley, I. W. (1988). **The Physics of Block Copolymers**. NexYork, Oxford University Press.

Harris, J. G. (1992). Liquid-vapor interfaces of alkane oligomers: structure and thermodynamics from molecular dynamics simulations of chemically realistic models. **The Journal of Physical Chemistry** 96(12): 5077-5086.

He, D., Reneker, D. H., and Mattice, W. L. (1997). Fully atomistic models of the surface of amorphous polyethylene. **Computational and Theoretical Polymer Science 7**(1): 19-24.

Ito, M., Matsumoto, M., and Doi, M. (1998). Molecular dynamics simulation of polymer film. **Fluid Phase Equilibria** 144(1-2): 395-401.

Kear, B. H., Sadangi, R. K., and Liao, S. C. (1997). Synthesis of WC/Co/diamond nanocomposites. **The Joint NSF-NIST Conference on Nanoparticles**, Arlington, VA.

Kim, W. K., and Mattice, W. L. (1998). Molecular Modeling of a Thin Film of Polybenzoxazine. **Langmuir** 14(22): 6588-6593.

Kumar, S. K., Russell, T. P., and Hariharan, A. (1994). Monte Carlo simulations of the free surface of polymer melts. **Chemical Engineering Science** 49(17): 2899-2906.

Kumar, S. K., Vacatello, M., and Yoon, D. Y. (1988). **The Journal of Chemical Physics** 89: 5206.

Kung, H. H., and Ko, E. I. (1996). Preparation of oxide catalysts and catalyst supports : a review of recent advances. **The Chemical Engineering Journal and the Biochemical Engineering Journal** 64(2): 203-214.

Lawrence Livermore National Laboratory, (2005). **Novel materials from sogel chemistry**. [On-line]. Available : https://www.llnl.gov/str/May05/Satcher .html.

Madden, W. G. (1987). Monte Carlo studies of the melt : vacuum interface of a lattice polymer. **The Journal of Chemical Physics** 87(2): 1405-1422.

Mansfield, K. F., and Theodorou, D. N. (1989). Interfacial structure and dynamics of macromolecular liquids: a Monte Carlo simulation approach. **Macromolecules** 22(7): 3143-3152.

Mansfield, K. F., and Theodorou, D. N. (1990). Atomistic simulation of a glassy polymer surface. **Macromolecules** 23(20): 4430-4445.

Mansfield, K. F., and Theodorou, D. N. (1991). Molecular dynamics simulation of a glassy polymer surface. **Macromolecules** 24(23): 6283-6294.

Mattice, W. L., and Suter, U. W. (1994). **Conformational theory of large molecules: The rotational isomeric state model in macromolecular systems**, New York: Wiley.

Messing, G. L., Zhang, S., Selvaraj, U., Santoro, R. J., and Ni, T. (1994). Synthesis of composite particles by spray pyrolysis. **The Joint NSF-NIST Conference on Ultrafine Particle Engineering**, Arlington, VA.

Metropolis, N., Rosenbluth, A. W., Rosenbluth, M. N., Teller, A. H., and Teller, E. (1953). Equation of State Calculations by Fast Computing Machines. **The Journal of Chemical Physics** 21(6): 1087-1092.

Misra, S., Fleming, P. D., and Mattice, W. L. (1995). Structure and energy of thin films of poly-(1,4-cis-butadiene) : A new atomistic approach. **Journal of Computer-Aided Materials Design** 2(2): 101-112.

Muller, M., and MacDowell, L. G. (2000). Interface and Surface Properties of Short Polymers in Solution: Monte Carlo Simulations and Self-Consistent Field Theory. **Macromolecules** 33(10): 3902-3923.

Murray, C. B., Norris, D. J., and Bawendi, M. G. (1993). Synthesis and characterization of nearly monodisperse CdE (E = sulfur, selenium, tellurium)

semiconductor nanocrystallites. **Journal of the American Chemical Society** 115(19): 8706-8715.

Natarajan, U., Misra, S., and Mattice, W. L. (1998). Atomistic simulation of a polymer-polymer interface: interfacial energy and work of adhesion. **Computational and Theoretical Polymer Science** 8(3-4): 323-329.

Nützenadel, C., Züttel, A., Chartouni, D., Schmid, G., and Schlapbach, L. (2000). Critical size and surface effect of the hydrogen interaction of palladium clusters. **The European Physical Journal D** 8(2): 245-250.

Olaj, O. F., Petrik, T., and Zifferer, G. (1995). Monte Carlo simulations of polymer surfaces in a cubic lattice, two variations of energy parameter and chain-length. **Journal of the Chemical Society, Faraday Transactions** 91(16): 2551-2558.

Ozisik, R., Doruker, P., Mattice, W. L., and von Meerwall, E. D. (2000). Translational diffusion in Monte Carlo simulations of polymer melts: center of mass displacement vs. integrated velocity autocorrelation function. **Computational and Theoretical Polymer Science** 10(5): 411-418.

Pant, P. V. K., and Theodorou, D. N. (1995). Variable Connectivity Method for the Atomistic Monte Carlo Simulation of Polydisperse Polymer Melts. **Macromolecules** 28(21): 7224-7234.

Paul, W., Binder, K., Kremer, K., and Heermann, D. W. (1991). Structure-property correlation of polymers, a Monte Carlo approach. **Macromolecules** 24(23): 6332-6334.

Piringer, O., and Baner, A. (2008). **Plastic packaging: interactions with food and pharmaceuticals**, Wiley-VCH.

Pratsinis, S. E. (1997). Precision synthesis of nanostructured particles. **The Joint NSF-NIST Conference on Nanoparticles**, Arlington, VA.

Rao, N. P., Tymiak, N., Blum, J., Neuman, A., Lee, H. J., Girshick, S. L., McMurry, P.H., and Heberlein, J. (1997). Nanostructured materials production by hypersonic plasma particle deposition. **The Joint NSF-NIST Conference on Nanoparticles**, Arlington, VA.

Rapold, R. F., and Mattice, W. L. (1995). New high-coordination lattice model for rotational isomeric state polymer chains. **Journal of the Chemical Society, Faraday Transactions** 91(16): 2435-2441.

Rapold, R. F., and Mattice, W. L. (1996). Introduction of Short and Long Range Energies To Simulate Real Chains on the 2nnd Lattice. **Macromolecules** 29(7): 2457-2466.

Roco, W. S. Ed. (2001). **Social Implications of Nanoscience and Nanotechnology**. Arlington, Virginia, Foundation.

SanchezI, C., and Lacombe, R. H. (1976). **The Journal of Chemical Physics** 80(8): 2352.

Siegel, R. W. (1991). Cluster-Assembled Nanophase Materials. **Annual Review of Materials Science** 21(1): 559-578.

Siegel, R. W. (1994). **Physics of New Materials**. Springer, Netherlands

ten Brinke, G., Ausserre, D., and Hadziioannou, G. (1988). Interaction between plates in a polymer melt. **The Journal of Chemical Physics** 89(7): 4374-4380.

Theodorou, D. N. (1988). Lattice models for bulk polymers at interfaces. **Macromolecules** 21(5): 1391-1400.

Theodorou, D. N. (1989(a)). Variable-density model of polymer melt surfaces: structure and surface tension. **Macromolecules** 22(12): 4578-4589.

Theodorou, D. N. (1989(b)). Variable-density model of polymer melt/solid interfaces: structure, adhesion tension, and surface forces. **Macromolecules** 22(12): 4589-4597.

Theodorou, D. N., and Suter, U. W. (1985). Detailed molecular structure of a vinyl polymer glass. **Macromolecules** 18(7): 1467-1478.

Uyeda, R. (1991). Studies of ultrafine particles in Japan: Crystallography. Methods of preparation and technological applications. **Progress in Materials Science** 35(1): 1-96.

Van Workum, K., and de Pablo, J. J. (2003). Computer Simulation of the Mechanical Properties of Amorphous Polymer Nanostructures. **Nano Letters 3**(10): 1405-1410.

Vao-soongnern, V., Doruker, P., and Mattice, W. L. (2000). Simulation of an amorphous polyethylene nanofiber on a high coordination lattice. **Macromolecular Theory and Simulations** 9(1): 1-13.

Vao-soongnern, V., Ozisik, R., and Mattice, W. L. (2001). Monte Carlo Simulation of the Structures and Dynamics of Amorphous Polyethylene Nanoparticles. **Macromolecular Theory and Simulations** 10(5): 553-563.

Verdier, P. H., and Stockmayer, W. H. (1962). Monte Carlo Calculations on the Dynamics of Polymers in Dilute Solution. **The Journal of Chemical Physics** 36(1): 227-235.

Wikimedia commons (2009). **Electrospinning**. [On-line]. Available : http://commons.wikimedia.org/wiki/File:Electrospinning_setup.png.

Wikipedia (2011(a)). **Nanotechnology**. [On-line]. Available : http://en.wikipedia.org/ wiki/Nanotechnology.

Wikipedia (2011(b)). **Lennard-Jones potential**. [On-line].Available : http://en. wikipedia.org/wiki/Lennard-Jones_potential.

Xu, G., and Mattice, W. L. (2001). Study on structure formation of short polyethylene chains via dynamic Monte Carlo simulation. **Computational and Theoretical Polymer Science** 11(6): 405-413.

Xu, G., and Mattice, W. L. (2002(a)). Monte Carlo simulation of the crystallization and annealing of a freestanding thin film of n-tetracontane. **The Journal of Chemical Physics** 116(5): 2277-2283.

Xu, G., and Mattice, W. L. (2002(b)). Monte Carlo simulation on separation and co-crystallization of a mixture of short polyethylene chains in a thin film. **The Journal of Chemical Physics** 117(7): 3440-3447.

Yethiraj, A., and Hall, C. K. (1989). Monte Carlo simulation of hard chain--hard sphere mixtures in slitlike pores. **The Journal of Chemical Physics** 91(8): 4827-4837.

Zachariah, M. R. (1994). In-Situ Characterization, and Atomistic Modeling of Nanoparticles in the Reacting Flows Group at NIST. **The NSF Confrence on Ultrafine Particle Engineering**, Arlington, VA.

APPENDICES

MONTE CARLO SIMULATION OF BIDISPERSE POLYETHYLENE NANOFIBERS AND NANOPARTICLES

Harnchana Gatemala, Visit Vao-soongnern[*]
Laboratory of Computational and Applied Polymer Science,
School of Chemistry, Institute of Science, Suranaree University of Technology,
Nakhon Ratchasima, 30000, Thailand
E-Mail : harnchana_gate@yahoo.com, visit@sut.ac.th

Abstract

Monte Carlo simulation of bidisperse polyethylene (PE) nanofibers and nanoparticles have been performed on the second nearest neighbor diamond (2nnd) lattice. An atomistic PE chain is mapped onto a coarse-grained model which each bead represents series of linked vector connecting the CH_2CH_2 was constructed. Both short-range interactions based on the modified rotational isomeric state model and long-range interactions from a discretized form of the Lennard-Jones (LJ) potential energy function are included. LJ parameters σ and ε/k_B of 4.2 Å and 205 K, respectively, are estimated for the coarse-grained model. Then, conformational and structural properties of bidisperse PE melts (50 %wt of B40, B30 and B20 mixed with B50 where B is number of CH_2CH_2 beads) were studied at 509 K. The results show: (i) the overall density profiles of bidisperse PE nanofibers are smaller than those of nanoparticles and decrease with decreasing chain length (ii) at the surface, the shorter chain is more abundant than longer one and end beads are more enrich than middle beads (iii) longer chains are more anisotropic arrangement than the shorter ones (iv) PE chains and their largest principal axis tend to orient perpendicular to the surface .

Keywords : nanofiber, nanoparticle, Monte Carlo simulation, 2nnd lattice, bidisperse PE

การจำลองมอนติคาร์โลเส้นใยนาโนและอนุภาคนาโนสำหรับพอลิเอทิลีนที่มีน้ำหนักโมเลกุลสองค่าผสมกัน

<u>หาญชนะ เกตมาลา</u> วิสิษฐ์ แววสูงเนิน[*]

ห้องปฏิบัติการเคมีคำนวณและพอลิเมอร์ประยุกต์ สาขาวิชาเคมี สำนักวิชาวิทยาศาสตร์

มหาวิทยาลัยเทคโนโลยีสุรนารี จังหวัดนครราชสีมา

E-Mail : harnchana_gate@yahoo.com, visit@sut.ac.th

บทคัดย่อ

การจำลองมอนติคาร์โลเส้นใยนาโนและอนุภาคนาโนสำหรับพอลิเอทิลีนที่มีน้ำหนักโมเลกุลสองค่าผสมกันนี้ ได้จำลองแบบโครงสร้างของหน่วยเอทิลีนบนผลึกของเพชร แรงกระทำระยะใกล้สามารถคำนวณโดยใช้ rotational isomeric state model และแรงกระทำระยะไกลคำนวณโดยใช้ฟังก์ชันศักย์ของ Lennard-Jones (LJ) ซึ่งมีค่าตัวแปร σ และ ε/k_B เท่ากับ 4.2 Å และ 205 K ตามลำดับ ระบบที่ทำการศึกษาคือ การผสมกันร้อยละ 50 โดยน้ำหนักของพอลิเอทิลีนที่มีค่าน้ำหนักโมเลกุลสองค่าผสมกัน (B50 ผสมกับ B40 B30 และ B20 ตามลำดับ) ซึ่งทำการจำลองที่อุณหภูมิ 509 เคลวิน ผลการจำลองพบว่า 1.) ความหนาแน่นของเส้นใยนาโนมีค่าน้อยกว่าอนุภาคนาโนในทุกระบบที่ได้ศึกษา และความหนาแน่นจะมีค่าลดลงเมื่อความยาวของสายโซ่ของพอลิเอทิลีนที่นำมาผสมสั้นลง 2.) พอลิเอทิลีนที่มีสายโซ่สั้นกว่าจะมีปริมาณมากกว่าสายโซ่ยาว และหน่วยของเอทิลีนที่อยู่ปลายจะมีปริมาณมากกว่าเอทิลีนที่อยู่ตรงกลาง บริเวณพื้นผิวของเส้นใยนาโนและอนุภาคนาโน 3.) การจัดเรียงตัวของโมเลกุลพอลิเอทิลีนที่มีสายโซ่ยาวจะมีการเปลี่ยนแปลงมากกว่าสายโซ่สั้น 4.) โมเลกุลพอลิเอทิลีนที่มีสายโซ่ยาวและสั้น มีการจัดเรียงตัวของโมเลกุลให้ตั้งฉากกับพื้นผิวของเส้นใยนาโนและอนุภาคนาโน โดยให้แกนเอกตั้งฉากกับพื้นผิว

คำสำคัญ : เส้นใยนาโน อนุภาคนาโน การจำลองมอนติคาร์โล พอลิเอทิลีนที่มีน้ำหนักโมเลกุลสองค่าผสมกัน

1. Introduction

Nanostructural materials have gained considerable attention recently owing to their unique properties and intriguing applications in many areas. Confined macromolecules at nanometer scale exhibit a fascinating and unexpected dynamic behavior and provide many unique properties due to the size reduction to the point where critical length scales of physical phenomena become comparable to or larger than the size of the structure. Various experimental techniques have been applied to polymer surfaces and interfaces. Individual polymeric nanofibers as well as nanoparticles are challenging to characterize experimentally due to their small size. Various simulation techniques have been applied to investigate the confinement of polymeric systems in one or two dimensions. The simulations use a variety of approaches, for examples to represent the system in discretized (lattice) (1–5) or continuous (5–10) space, adoption of coarse-grained (4, 5, 9) or atomistically detailed (6–8,10) models, and focus on either static (1–6,9,10) or dynamic (7,8,11) aspects of the surface. For large scale simulations, Fukui *et al*. used Molecular Dynamic (MD) simulation which very high efficiency for studying the atomistic details of nanometer-scale polyethylene particles with up to 120,000 atoms. (12-17)

Rapold and Mattice developed a Monte Carlo simulation method on a high-coordination lattice which constructed from diamond lattice (18). The short-range intramolecular interactions treated by Rotational Isomeric State model (19,20) can be incorporated in the simulation, forcing the coarse-grained chains on the high coordination lattice to retain the short-range conformational characteristics of the real chain of interest (21). The long-range interaction is derived from Lennard-Jones potential energy function. The interaction is mapped onto the discrete space of the 2nnd lattice to describe the long-range interaction of pair beads (22). The coarse-grained system can be 'reverse mapped' to the fully atomistic model in continuous space (23). The reverse mapping recovers excellent local intrachain (population of torsion angles) and interchain (pair correlation functions) properties (23). The simulation also produces excellent longer range properties, such as cohesive energy density in the bulk (22,23) and surface energies of thin films (24), both when in the coarse-grained representation on the 2nnd lattice, and also after reverse mapping back to the fully atomistic structure in continuous space.

In general, polymers in the real system contain various chain lengths which affect the properties of the materials. In this work, a coarse-grained molecular model will be used to study the effect of bidispersity on the structures of polyethylene (PE) nanofiber and nanoparticle. It is expected that both surface geometries and nanoscale confinement should influent on the behavior of PE molecules in different way for shorter and longer chain component.

2. Simulation Methodology

2.1 Model

Monte Carlo (MC) technique would be applied to investigate the effect of mixed molecular weight (short- and long-chain bi-mixtures) on structures of PE nanofiber and nanoparticle. The simulations are performed on a high coordination lattice using the coarse-grained PE chains which the number of site (n) in shell i^{th} is given by

$$n = 10i^2 + 2 \qquad (1)$$

The lattice can be constructed by eliminating every second carbon atoms of the diamond lattice. So it is called the second nearest neighbor diamond (2nnd) lattice. The step length of this lattice is 0.25 nm. This lattice is similar to the distorted cubic lattice with the same box angle in all three dimensions ($\alpha = \beta = \gamma = 60°$). The coordination number increase from 4 for the normal cubic lattice to 12 which is identical to the closest packing of uniform hard sphere. Each occupied site contains either C_2H_4 or C_2H_5 unit. The shortest distance, zero, is disallowed by invoking self-avoidance. The four different non-zero distance between methyl groups of pentane on 2nnd lattice site are shown in Table 1 which correspond to the fully atomistic representation.

2.2 Energy

The Hamiltonian has two parts. The first part is short-range intramolecular interactions which treated by the modified Rotational Isomeric State (RIS) model (22, 23). This model is re-cast in a statistical weight matrix which contains two usual statistical weights (σ and ω) for the step length of 0.25 nm on the 2nnd lattice. The 9 x 9 statistical weight matrix can be reduce to the 3 x 3 extended statistical weight matrix which contains three coarse-grained statistical weight matrix, a, b and c.

Table 1 Length of vectors connecting beads i and $i +2$ for coarse-grained PE model.

Category	Length (nm)	Detailed conformation
A	0.500	tt
B	0.433	tg^+, tg^-, g^+t, g^-t
C	0.353	g^+g^+, g^-g^-
D	0.250	g^+g^-, g^-g^+

Long-range intermolecular interactions are calculated with an isotropic Lennard-Jones (LJ) potential. The LJ potential for PE is changed to accommodate the 2nnd lattice where every bead represents an ethylene unit rather than a methylene unit. The calculation of the average interaction energies between lattice sites is performed through the second virial coefficient expression. The LJ parameters (σ and ω) and interaction energies between first (u_1), second (u_2) and third (u_3) neighboring shells are given in Table 2.

Table 2 Non-bonded energy parameters for coarse-grained PE model on 2nnd lattice simulation**.**

2nnd parameter	value
ε/k_b	185
σ (nm)	0.44
u_1 (kJ/mol)	16.214
u_2 (kJ/mol)	0.731
u_3 (kJ/mol)	-0.623

$$U_{PE} = \begin{bmatrix} 1 & \sigma & \sigma \\ 1 & \sigma & \sigma\omega \\ 1 & \sigma\omega & \sigma \end{bmatrix} \longrightarrow U_{2nnd} = \begin{bmatrix} 1 & 4\sigma & 2\sigma\sigma & 2\sigma\sigma\omega \\ 1 & 4a & 2\sigma b & 2\sigma\omega b \\ 1 & 4b & 2c & 2c\omega \\ 1 & 4b & 2c & 2c\omega \end{bmatrix} \longrightarrow U_{2nnd} = \begin{bmatrix} 1 & 4\sigma & 2\sigma\sigma(1+\omega) \\ 1 & 4a & 2b\sigma(1+\omega) \\ 1 & 4b & 2c(1+\omega) \end{bmatrix}$$

where $\sigma = \sigma_0\exp(-E_\sigma/kT)$, $\omega = \omega_0\exp(-E_\omega/kT)$, $a = \sigma\omega^{1/8}$, $b = \sigma\omega^{1/4}$ and $c = \sigma^2\omega^{1/2}$

2.3 Moves

Local bead moves on the 2nnd lattice are accepted according to the Metropolis Monte Carlo algorithm which the probability of bead moving within a chain is given by

$$P_{move} = \min(1, P_{LR}P_{new}/P_{old}) \tag{6}$$

where, $P_{LR} = \exp(-\Delta E_{LR}/RT)$ is the probability from the change in the long-range interaction energy (ΔE_{LR}), and P_{new}/P_{old} is the ratio of the probabilities for the new and old local conformations according to the short-range interaction. In this simulation, one Monte Carlo step (MCS) is defined as a series of single bead move, in which all the beads in the system are randomly attempted once on average. A moving on lattice corresponds to a displacement of two or three backbone atoms on the real PE chain.

2.4 System constructions
2.4.1 Bulk system

A random configuration of PE chains is generated by mapping PE beads on 2nnd lattice with an application of periodic boundary conditions in all three directions. For an initial step, only self-avoiding random walks with excluded volume

condition is employed and the next step, intramolecular and intermolecular interactions are introduced. Then the initial structure is relaxed by minimizing the potential energy of the system by Dynamics Monte Carlo technique.

2.4.2 Nano thinfilm, nanofiber and nanoparticle formation

Thin film can be obtained by extending the *x* axis of the periodic box of the bulk system about 3-4 times. This new box size is large enough to ensure that there is no interaction between the parent chains and their images. Then the system is equilibrated and employed as an initial structure of fiber.   The nanofiber can be obtained by extending the *y* axis of the latest conformation of thin film about 3-4 times to prevent any interaction between the parent chains and their images with other chains. Then the system is carried out in the same way as the thin film system. Eventually the equilibrated nanofiber is obtained. Finally, polymer nanoparticle can be obtained in a similar way to nanofiber by extending the *z* axis of the latest conformation of the fiber about 3-4 times. After equilibration step, nanoparticle is obtained. All structural generation can be described by the following scheme:
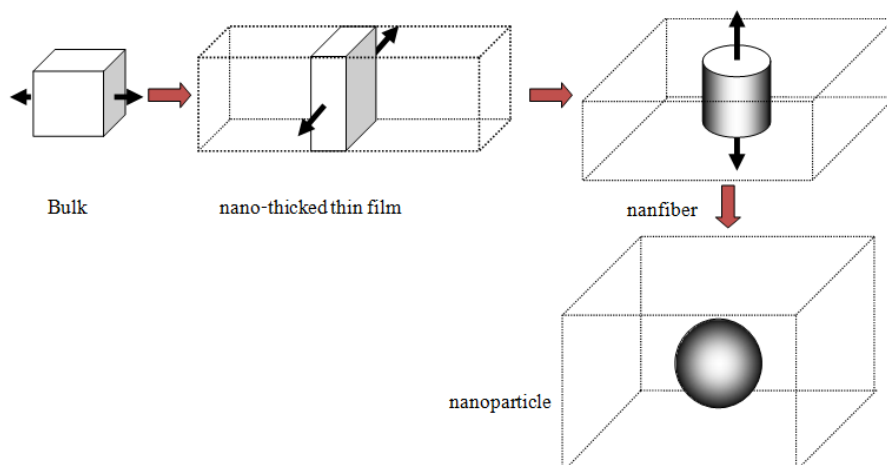
Figure 1 The method to generate a new cohesive polymer structure from bulk (3D) → nano-thicked thin film (2D) → nanofiber (1D) → nanoparticle(0D).

2.4.3 Bidisperse system generation

For the bidisperse systems, the total number of chains in nanofiber and nanoparticle is initially constructed with only the longer chains. Afterward, the long chains from the latest conformation of the equilibrated systems are cut down to shorter ones according to the length needed in each simulation. Then the systems are equilibrated at least 10 million Monte Carlo steps (MCS) and are employed as new initial structures. The latest conformations of nanofiber and nanoparticle are run for an additional 10 million MCS for subsequent data analysis.

2.5 System

The systems of bidisperse PE nanofibers and nanoparticles are shown in Table 3 which the number behind B are the number of beads (one bead represent the

CH_2-CH_2 unit). All systems have the same total number of beads. The mixed systems are varied in chain lengths but the composition of B50 is fixed.

Table 3 Number of chains in bidisperse PE nanofibers and nanoparticles system which the composition of B50 is 50 %wt (B50+B40, B50+B30, and B50+B20).

System	Number of B50	Number of mixed chain
B50+B40	28	36
B50+B30	28	48
B50+B20	28	71

3. Results and discussions
3.1 Density profile
Radial density profile

Figure 2 shows the density profile of all systems with each component composition. The total densities are in the range of 0.6 – 0.7 g/cm^3. The densities of shorter chain component are decreased nearer to the fiber principal axis than those of the longer chain. In addition, the diameter and the interfacial width of shorter chains were slightly larger than those in longer chains, when the interfacial width defined as the distance over which the density decreases from 90% to 10% of its bulk value. Because the shorter chain component has more number of end beads, they need more room to move than the longer chains. The overall densities are then decreased for short chain system. The shorter chains are also more predominant at the surface region compared to the bulk region. For the mixed system, there is a small difference in overall density. The shorter chains disperse near the surface than longer ones.
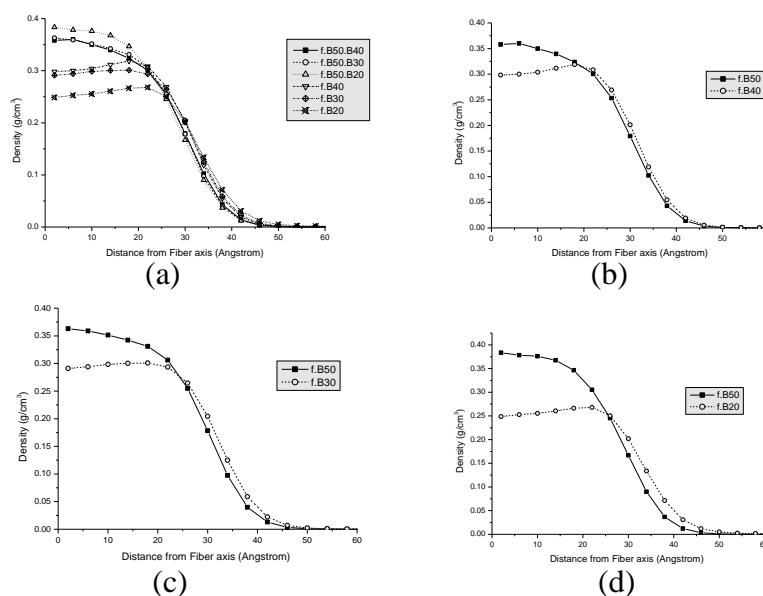

Figure 2 The density profiles of bidisperse PE nanofiber (a) total density, (b) component in B50+B40, (c) B50+B30 and (d) B50+B20 systems.

(a) (b) (c)
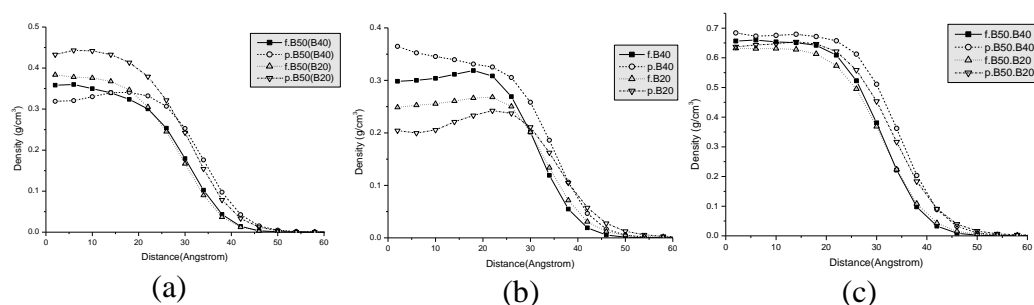
Figure 3 Comparison of the density profiles of bidisperse PE nanofibers and nanoparticle (a) B50, (b) B40, B30, B20 and (c) total density.

In nanoparticle systems, the characteristics of density profiles of shorter and longer chain are similar to those of nanofiber system but the total densities are slightly higher. The diameters of nanoparticle are smaller than that of nanofiber with the same number of beads as shown in Fig. 3. This behavior should be related to the stronger confinement effect in nanoparticle which is more dominant than nanofiber. Therefore, the chains in nanoparticle should pack denser and its density is more increased. The nanoparticle diameter is therefore smaller than that of nanofiber with the same number of PE beads.

Beads distribution and segregation of chain ends

The end beads of both short and long chain are enriching near the surface. Compared between shorter and longer chains, the density of end beads for short chain is higher than that of the longer ones. In addition, the bead densities are increasing with decreasing chain length for mixed system. The change is found at the distance after a bulk region which is described by greater number of shorter chain end beads. Figure 4 shows a comparison of bead distributions between nanofibers and nanoparticles. Both of bead distributions of longer chain (B50) in nanofiber and nanoparticle system are not different but the distribution in the mixed system is quite different. The bead distributions of mixed chains in nanofiber are higher than those of nanoparticle with the same number of beads. Because nanofiber has lower surface area than nanoparticle, the distribution of end bead near the surface of nanofiber is higher than that seen in nanoparticle.

(a) (b)
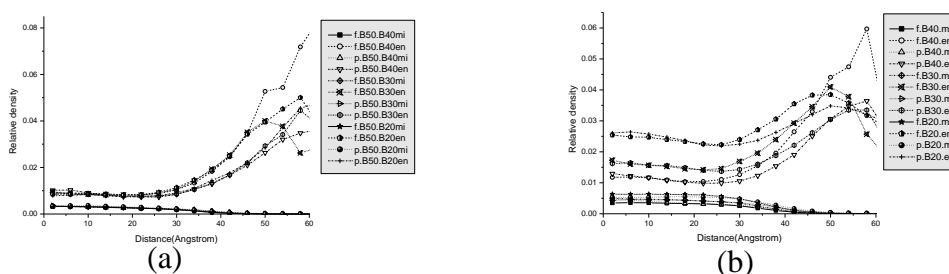
Figure 4 The relative density of middle bead and end bead of bidisperse polyethylene nanofibers and nanoparticle with the composition of B50 = 50% (a) B50 and (b) B40, B30, B20.

3.2 Orientation

Bond orientation

Local orientational tendency of chord vector (from carbon atom *i* to carbon atom *i + 2*) across the fiber are examined. The definition of chord order parameter is

$$S = \frac{1}{2}\left\langle 3\left(\cos^2\theta\right) - 1\right\rangle \qquad (4.1)$$

where θ is the angle formed between a 2nnd bond and the fiber axis. $\langle\ \rangle$ is indicative of an ensemble average within the cylindrical bin. The *S* value –0.5, 0.0 or 1.0 means perfectly perpendicular, random, and parallel orientation with respect to the fiber axis respectively.

Figure 5 shows the orientation of all chain of nanofibers and nanoparticles. Most bond orientation of nanofiber is perpendicular while it is relatively random in nanoparticle system. The orientation of end and middle bond of nanofibers and nanoparticles is generally similar. The end bond is perpendicular while the middle bond is parallel to the surface. The orientation change of all bonds for both longer chain and mixed chains is not significant difference for the particle with the same shape. As well as other properties, these changes are observed after the bulk region.
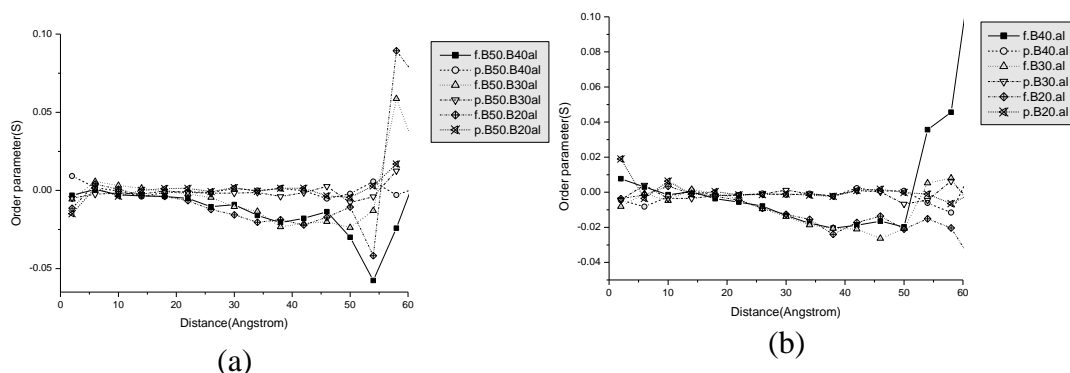

Figure 5 Comparison of the orientation of chords (all) of nanofibers and nanoparticles (a) B50 and (b) B40, B30, B20.

Particle orientation

To define the shape and orientation of the chains more clearly, it is appropriate to approximate a coil by an equivalent ellipsoid, which is defined by the principal components *L1 < L2 < L3* of the radius of gyration tensor for individual configurations taken along the principal axes system. The largest eigenvectors are perpendicular but the smallest eigenvectors are parallel in nanofiber systems. These behaviors can be described by the molecular size. In the limitation of space, the longer chains would adjust their molecular orientation to perpendicular direction which is more confined than shorter chains. In opposite, for nanoparticle, they are in perpendicular direction. The results can be described similar to nanofiber systems because the chains in nanoparticle are more confined than those in nanofiber. The longer chains have to adjust their molecular orientation more parallel to the surface than shorter chains. Furthermore, mixing with shorter chains does not affect the longer chain behavior. The tendency of orientational change in the mixed system has higher magnitude when the chain length difference increases as shown in Figure 6.

3.3 Chain properties

The profiles of the center of mass distribution are shown in Figure 7(a). For longer chains, the highest densities for the center of mass are insignificant different in all systems. For mixed system; however, the highest density increases with decreasing chain length. This behavior is related to higher number of chains for shorter chain system. For nanoparticle, the results are similar to nanofiber systems. A comparison between longer chain and mixed system is shown in Figure 7(b) and 7(c) respectively, for nanofiber and nanoparticle. The distance which has the highest center of mass densities of nanoparticle is closer to the surface than nanofiber whereas their distribution of nanoparticle is broader than nanofiber.

(a)   (b)
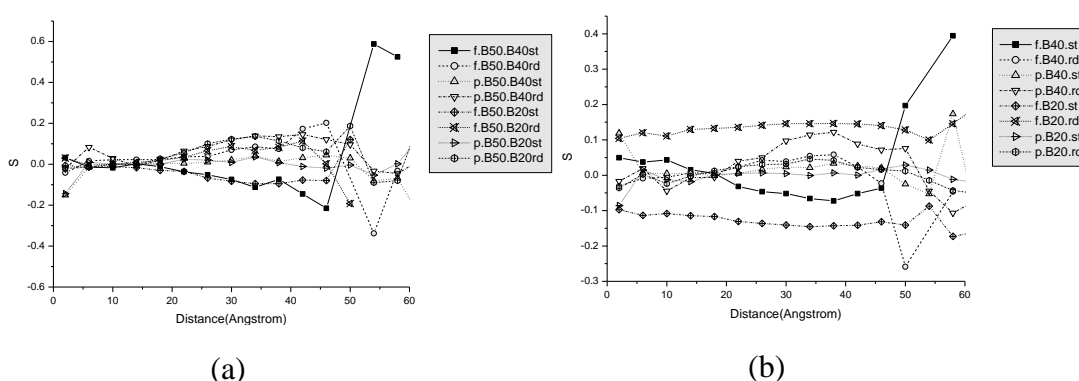
Figure 6 Comparison of the orientation of the largest and smallest principal moment to axis after equilibration of nanofibers and nanoparticles (a) B50 and (b) B40 and B20.

(a)   (b)   (c)
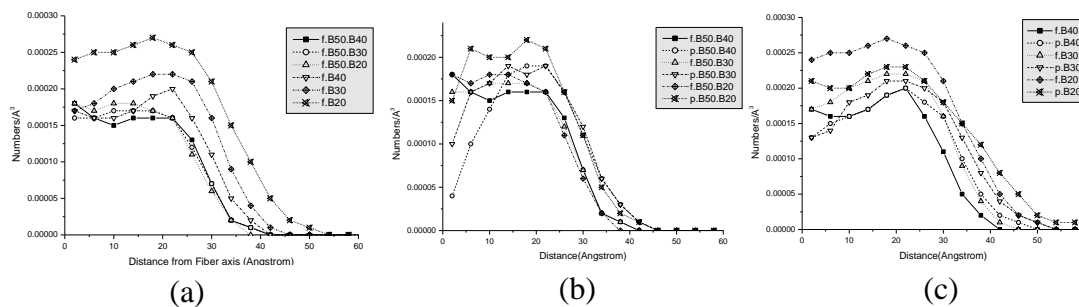
Figure 7 The center of mass distribution as a function of radial (a) nanofiber (b) the longer chain (B50) nanofiber and nanoparticle (c) the mixed chain nanofiber and nanoparticle.

The size of longer chains is larger than the shorter chains due to larger number of beads. The change in R_g components of longer chains is higher than that of shorter chains because of the entropic effect of end beads. The longer chain has more number of middle beads which are less entropy than the shorter chain. So, the longer chains are highly packed and there is much change in larger size. The R_g in X component becomes smaller as chains approach the surface region from the bulk side. In accord with X component, the Y-Z component increases, while the total R_g remains relatively decrease. These results are simply a manifestation of the flattening of chains

into pancake like objects as their centers of mass are forced to lie near an impenetrable surface. Mixing of the shorter chain does not affect the longer chain behavior. Comparing the change in R_g components of mixed system, the change in overall R_g and its component is depended on their chain length that increase with increasing chain length as shown in Figure 8.
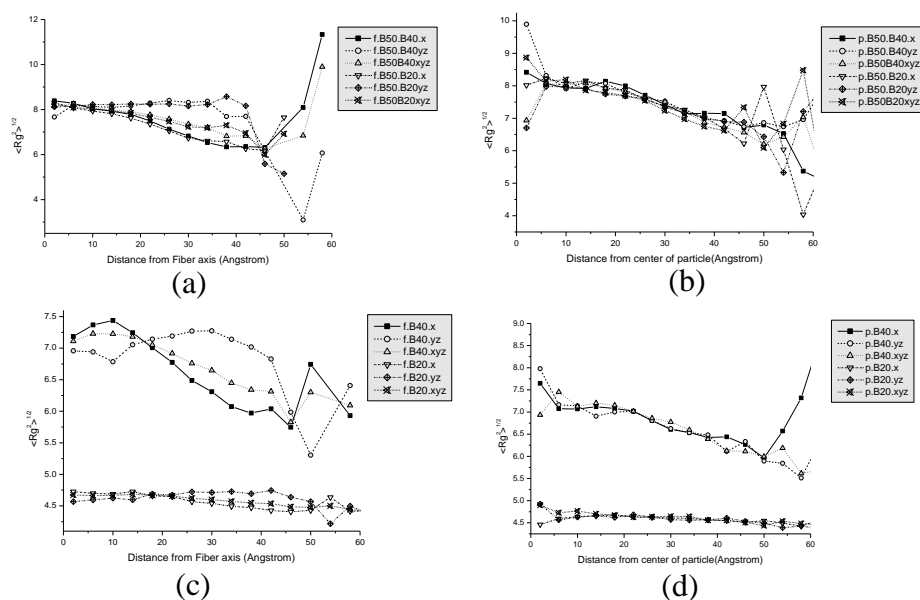
Figure 8 Comparison of the change in R_g components to the center of mass of nanofibers and nanoparticles (a) B50 nanofiber (b) B50 nanoparticle (c) B40 and B20 nanofiber and (d) B40 and B20 nanoparticle.
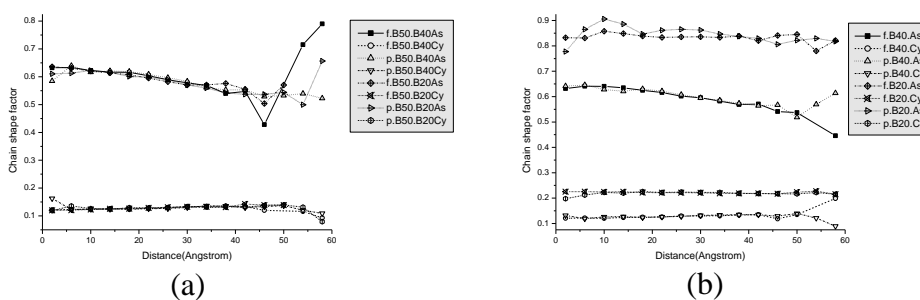
Figure 9 Comparison of the change in molecular shape (asphericity and acylindricity) as a function of radial displacement of the center of mass (a) B50 nanofiber and nanoparticle (b) B40 and B20 nanofiber and nanoparticle.

The chain shapes can be investigated by acylindricity and asphericity values, which are defined as $c = L_2^2 - L_3^2$ and $b = L_1^2 - \frac{1}{2}(L_2^2 - L_3^2)$, respectively. These values were divided by the squared radius of gyration to determine the extent of deviation from cylindrical and spherical shape in the range of 0 to 1. From Figure 9, it is observed that chain shape changes as a function of the radial displacement from the center. The asphericity decreases toward the surface whereas the acylindricity slightly

increase, most of which is occurring close to the vacuum side. The longer chains (B50) are not affected by shorter chains in the mixed system. In the case of mixed chains, the change in asphericity and acylindricity of longer chain is higher degree than that of shorter chain which can be described by the same reason of the change in R_g. For nanoparticle systems, the results are similar to nanofiber systems as shown in Figure 9.

Figure 10 shows the comparison of three eigenvalues (principal moments) of the chains normalized by their square radius of gyration as a function of radial displacement from the center of mass. There is slightly change in the eigenvalues at the surface region for both longer chain (B50) and mixed chains in all systems. This property is not affected by mixing of shorter chain. The change in these eigenvalues for longer chain is higher degree than that of shorter chain for both systems. For the mixed system, this change is decreasing with decreasing chain length. This can be explained in a similar way to the change in R_g component.

(a)   (b)
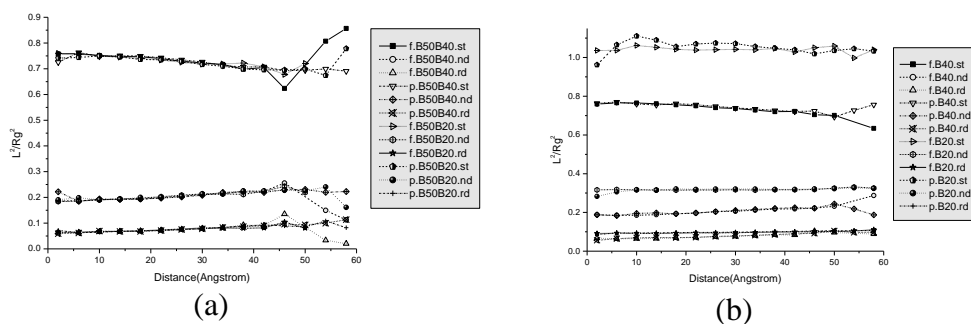
Figure 10 Comparison of the principal moment of chains (normalized by R_g^2) as a function of radial displacement of the center of mass (a) B50 nanofiber and nanoparticle (b) B40 and B20 nanofiber and nanoparticle.

4. Conclusion

The density profiles of nanoparticle are higher than those of nanofiber and they decrease with decreasing chain length for mixed chain system. This is due to stronger confinement effect in nanoparticle system. At the surface, the shorter chains are more abundant than longer one and the end beads are more enrich than the middle beads. For nanofiber systems, bonds tend to orient parallel to the surface in the interfacial region, whereas this behavior diminishes toward the vacuum side due to the end beads, which tend to orient normal to the surface. In opposite, for nanoparticle system, bonds tend to randomly orient. There is an oscillatory behavior in the distribution of the chain center of mass. Chains and their largest principal axis tend to orient perpendicular to the surface. The longer chain processes similar properties in the same particle shape system. In contrast, shorter chain properties are affected due to the present of longer chain.

References

(1) Madden, W. G., 1987, J. Chem. Phys. 87, p.1405.

(2) Theodorou, D. N., 1988, Macromolecules. 21, p.1391.

(3) Olaj, O. F., Petrik T., Zifferer, G., 1995, J. Chem. Soc., Faraday Trans. 91, p.2551.

(4) Doruker, P., Mattice, W. L., 1998, Macromolecules. 31, p.1418.

(5) Müller, M., MacDowell, L., 2000, Macromolecules. 33, p.3902.

(6) Mansfield, K. F., Theodorou, D. N., 1990, Macromolecules. 23, p.4430.

(7) Mansfield, K. F. and Theodorou, D. N., 1991, Macromolecules. 24, p.6283.

(8) Harris, J. G., 1992, J. Phys. Chem. 96, 5077.

(9) Kumar, S. K., Russell, T. P., Hariharan, A., 1994, Chem. Eng. Sci. 49, p.2899.

(10) Misra, S., Fleming III, P. D., Mattice, W. L., 1995, J. Comput.-Aided Mater. Des. 2, p.101.

(11) Doruker, P., Mattice, W. L., 1999, Macromolecule.s 32, p.194.

(12) Fukui, F., Sumpter, B. G., Barnes, M. D., Noid, D. W., 1999, Polym. J. 31, p.664.

(13) Fukui, F., Sumpter, B. G., Barnes, M. D., Noid, D. W., Comput. 1999, Theor. Polym. Sci. 9, p.245.

(14) Fukui, K., Sumpter, B. G., Barnes, M. D., Noid, D. W., Otaigbe, J. U., 1999, Macromol. Theor. Simul 8, p.38.

(15) Fukui, K., Sumpter, B. G., Barnes, M. D., Noid, D. W., 2000, Macromolecules. 33, p.5982.

(16) Fukui, K., Sumpter, B. G., Noid, D. W., Yang, C., Tuzun, R. E., Comput. 2001, Theor. Polym. Sci.11, p.191.

(17) Otaigbe, J., Barnes, M., Fukui, K., Sumpter, B. G., Noid, D. W., 2001, Adv. Polym. Sci. 1, p.154.

(18) Rapold, R.F., Mattice, W. L.. 1995, J. Chem. Soc., Faraday Trans. 21,p.2435.

(19) Flory, P.J., 1969, Statistical mechanics of chain molecules. Wiley, New York.

(20) Mattice, W. L., Suter, U.W., 1994, Conformational theory of large molecules. The rotational isomeric state model in macromolecular systems. Wiley, New York.

(21) R.F., Rapold, Mattice, W., 1996, Macromolecules. 29, p.2457.

(22) Cho, J., Mattice, W. L., 1997, Macromolecules. 30, p.637.

(23) Doruker, P., Mattice, W. L., 1997, Macromolecules. 30, p.5520.

(24) Doruker, P., Mattice, W. L., 1998, Macromolecules. 31, p.1418.

EFFECT OF POLYDISPERSITY ON STRUCTURES AND DYNAMICS OF POLYMER NANOFIBERS

Harnchana Gatemala[1-2], Visit Vao-soongnern* [1-2]

[1] Laboratory of Computational and Applied Polymer Science,
[2] School of Chemistry, Suranaree University of Technology, Nakhon Ratchasima, Thailand

ABSTRACT : Electrospinning of polymeric nanofibers is a promising approach for development and commercialization of onedimensional (1D) nanomaterials. The small fiber diameter (50- 500 nm) and large surface area (10-100 m^2/g) of such polymeric nanofibers offer a new class of materials that can be used in diverse applications including filters, composites, fuel cells, catalyst supports, drug delivery devices, and tissue Scaffolds. This work presents a recently developed strategy that has used a method where an atomistic chain is mapped onto a coarse-grained model. Polyethylene (PE) model which each bead represents series of linked vector connecting the CH_2CH_2 was constructed. Both short-range interactions based on the rotational isomeric state model and long-range interactions from a discretized form of the Lennard-Jones (LJ) potential energy function are included. LJ parameters σ and ε/k_B of 4.2 Å and 205 K, respectively, are estimated for the coarse-grained model. Then, the static and dynamic properties of mono- and bidisperse PE melts (C_{408}, C_{204} and C_{102}) were studied at 509 K. The results show: (i) the overal density profiles of bidisperse PE nanofibers are similar to the monodisperse system with the same number of beads (ii) the shorter chains prefer locate at the outer surface and the center of nanofibers (iii) longer chains are more anisotropic arrangement than the shorter ones (iv) diffusivity and chain relaxation of PE molecules in nanofiber are higher than those in the bulk PE.

INTRODUCTION

One-dimensional (1D) nanostructural materials have gained considerable attention recently owing to their unique properties and intriguing applications in many areas. Various experimental techniques have been applied to polymer surfaces and interfaces. Individual polymeric nanofibers are challenging to characterize experimentally due to their small size. This is due in large part to the requirement that a single nanofiber be isolated and manipulated without introducing defects prior to physical or mechanical analysis. Atomistic computer simulations can be helpful in determining and predicting the properties of individual nanofibers, especially as a function of length scales that are comparable to molecular dimensions.

Various simulation techniques have been applied to investigate the confinement of polymeric systems in one or two dimensions. First, lattice Monte Carlo (MC) simulations of a melt-vacuum interface were performed by Madden using a film adsorbed on a solid surface. The film was shown to have a central region with bulklike characteristics, sandwiched between two interfacial regions. The structural features at the interface were found not to scale with molecular weight.

A coarse-grained molecular model of an amorphous polyethylene nanofiber was recently formed on a high coordination lattice, and the static properties of the equilibrated fibers were determined. Major findings of this study were (i) fibers of different sizes, i.e., consisting of different numbers of parent chains, exhibit almost

identical hyperbolic density profiles at the surfaces, (ii) the end beads are predominant and the middle beads are depleted at the free surfaces, (iii) there is anisotropy in the orientation of bonds and chains at the surface, and (iv) the center of mass distribution of the chains exhibits oscillatory behavior across the fibers. These static proper properties are qualitatively similar to the properties deduced from the simulation, by the same technique, of a freestanding thin film, where there is no curvature at the surface. In this work we report effect of polydispersity of polymer on the dynamics and structures of the nanofiber using two local properties (acceptance rate and randomization of chord vectors) and two chain properties (diffusion of the center of mass and randomization of the end-to-end vector). The results are compared to the dynamics in the bulk and in thin films.

OBJECTIVE

To investigate the effect of polydispersity on structures and dynamics of nanofibers.

METHOD

The bulk simulations of linear PE are performed on a high coordination lattice with the use of an on-lattice coarse-graining method and Monte Carlo (MC) algorithm that was first proposed by Rapold and Mattice in 1995. The lattice was named the second nearest neighbor diamond lattice (2nnd). The 2nnd lattice is derived from the diamond lattice by eliminating every other lattice site. The coarse-graining procedure maps the CH_2CH_2 units of PE monomers onto one bead. Both short-range interactions based on the rotational isomeric state model and long-range interactions from a discretized form of the Lennard-Jones (LJ) potential energy function are included. LJ parameters σ and ε/kB of 4.2 Å and 205 K, respectively, are estimated for the coarse-grained model. Then, the static and dynamic properties of mono- and bidisperse PE melts (C_{408}, C_{204} and C_{102}) were studied at 509 K.

Simulations of the polymer fiber consist mainly of two part (i) generation of the polymer fiber structure (ii) relaxation of the initial structure to thermodynamics equilibrium.

Table 1 Simulation systems.

| Fiber	Chain 1	Chain 2
f102	120 C_{102}	-
f204	60 C_{204}	-
f408	30 C_{408}	-
f102-f204	60 C_{102}	60 C_{204}
f102-f408	60 C_{102}	15 C_{408}
f204-f408	30 C_{204}	15 C_{408}

Table 2 Length of vector connecting beads *i* and *i+2*.

Category conformatiom	Length in nm	Details
A	0.500	*tt*
B	0.433	tg^+, tg^-, g^+t, g^-t
C	0.353	g^+g^+, g^-g^-
D	0.250	g^+g^-, g^-g^+

Table 3 Energy parameters for PE on 2nnd lattice simulation.

2nnd parameter	value
ε/k_b in K	205
σ in nm	0.42
u_1 in kJ/mol	14.122
u_2 in kJ/mol	0.526
u_3 in kJ/mol	-0.627
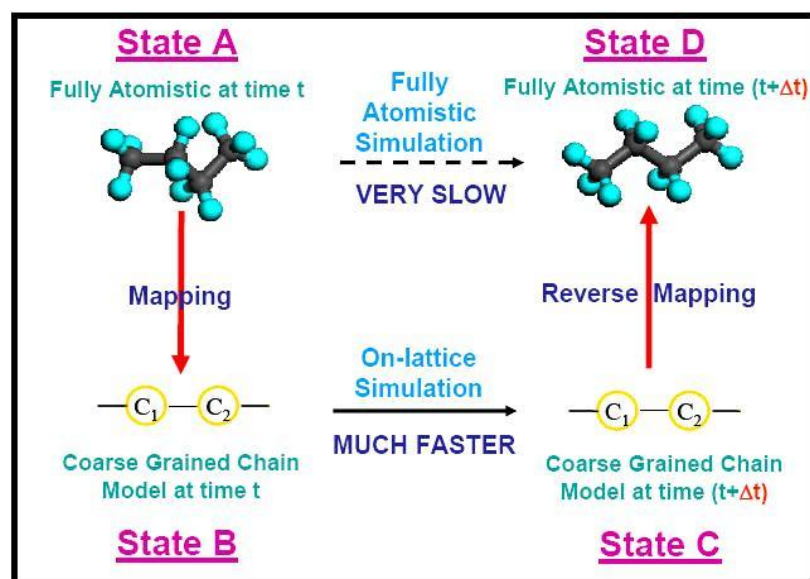
Figure 1 Schematic representation of the comparison between two alternative pathways: fully atomistic off-lattice and coarse-grained on lattice simulations.
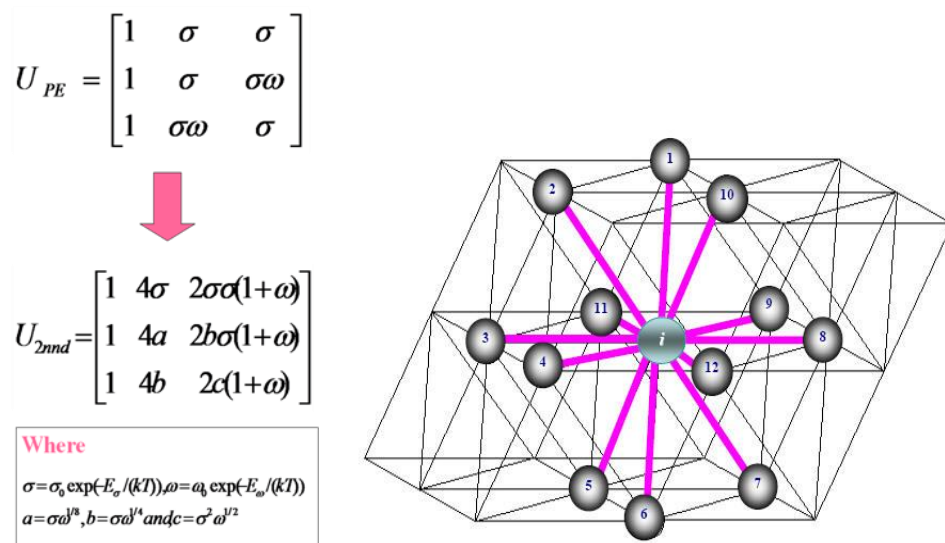
$$U_{PE} = \begin{bmatrix} 1 & \sigma & \sigma \\ 1 & \sigma & \sigma\omega \\ 1 & \sigma\omega & \sigma \end{bmatrix}$$

$$U_{2nnd} = \begin{bmatrix} 1 & 4\sigma & 2\sigma\sigma(1+\omega) \\ 1 & 4a & 2b\sigma(1+\omega) \\ 1 & 4b & 2c(1+\omega) \end{bmatrix}$$

Where

$\sigma = \sigma_0 \exp(-E_\sigma/(kT)), \omega = \omega_0 \exp(-E_\omega/(kT))$
$a = \sigma\omega^{1/8}, b = \sigma\omega^{1/4}$ and $c = \sigma^2\omega^{1/2}$

Figure 2 Schematic representation of the first shell contacts on the 2nnd lattice.

Bulk (3D)   **Thin film (2D)**   **Fiber (1D)**
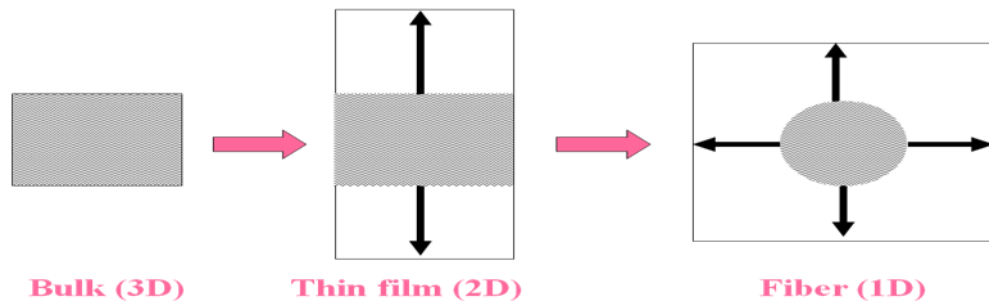
Figure 3 Elongation method to generate a new cohesive polymer structure from bulk (3D) $\rightarrow$ Thin film (2D) $\rightarrow$ Fiber (1D). The views of the film and fiber are in the plane of the film and along the axis of the fiber.
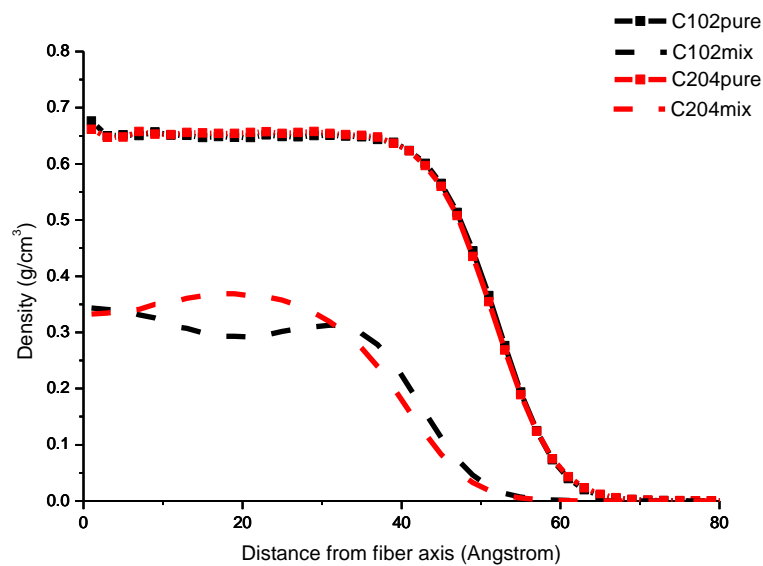
RESULTS AND DISCUSSION

Figure 4 Concentration profiles of mono- and bidisperse PE nanofiber.
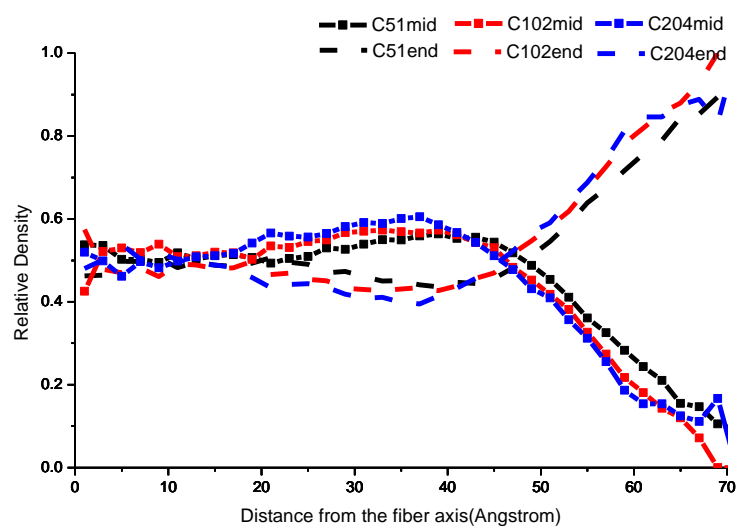

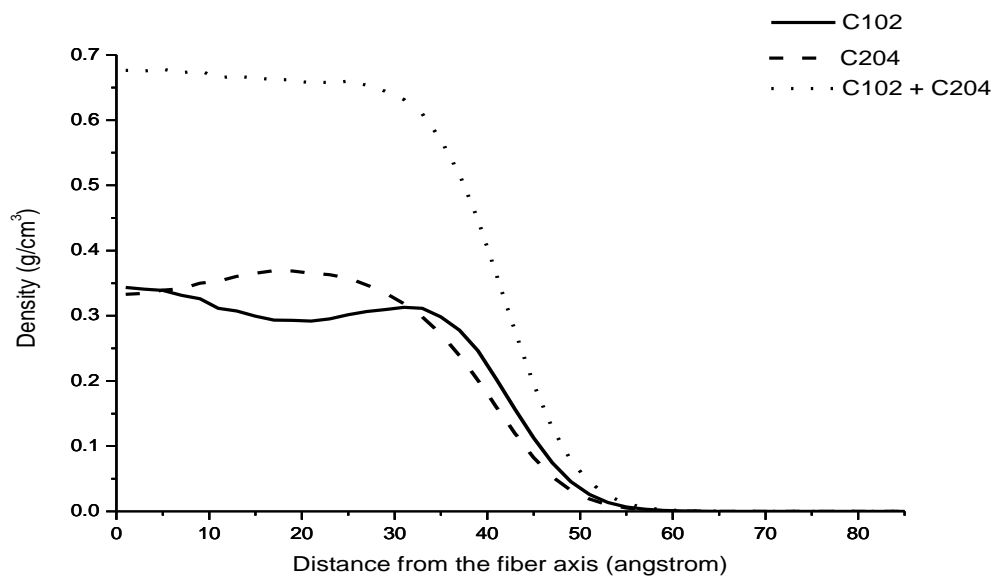**Figure 5** Radial density profiles for mid/end beads of monodisperse PE.

Figure 6 Concentration profiles of polydisperse PE nanofiber.
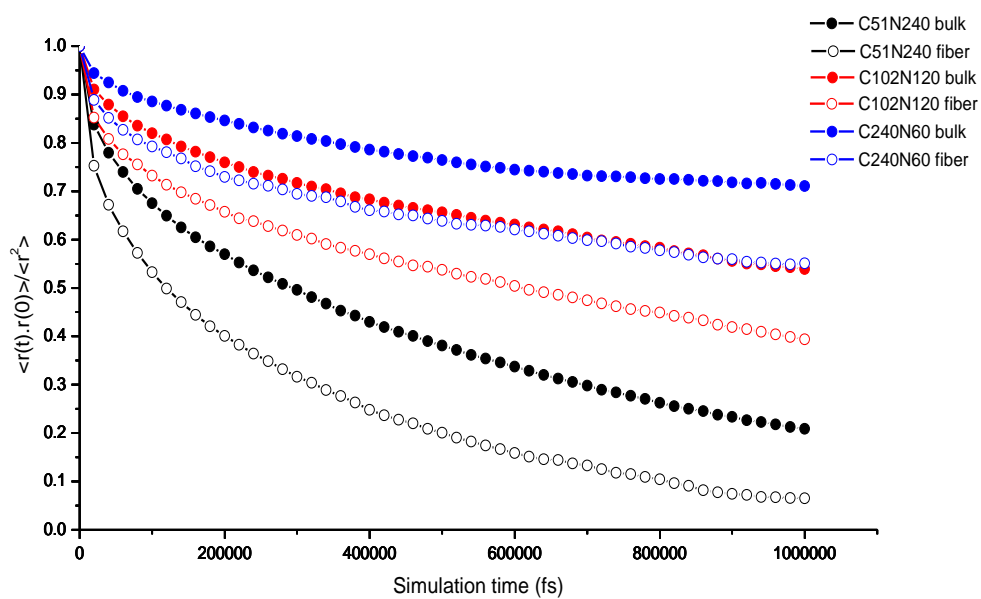
Figure 7 Decorrelation function of the end-to-end vector of PE molecules as function of simulation time.

CONCLUDING REMARKS

The density profile are hyperbolic tangent. Because of stronger confinement, the thinner finer has a slightly higher density in the bulk region as well as small thickness. The end beads dominate (as compared to their bulk density) at the surface, where as the middle beads are depleted. The shorter chains prefer locate at the outer surface and the center of nanofibers. The longer chains are more anisotropic arrangement than the shorter ones . Diffusivity and chain relaxation of PE molecules in nanofiber are higher than those in the bulk PE.

การจำลองพลวัติเชิงโมเลกุลเกลือโพแทสเซียมไอโอไดด์ในเอทิลีนคาร์บอเนต โพรพิลีนคาร์บอเนต คาร์บอเนต และไดเมทิคาร์บอเนต

Molecular Dynamics Simulation of Potassium Iodide Salt in Ethylene Carbonate, Propylene Carbonate, and Dimethyl Carbonate

หาญชนะ เกตมาลา [1,2], วิสิษฐ์ แววสูงเนิน [1,2]

Harnchana Gatemala [1,2] and Visit Vao-soongnern [1,2]

[1] Laboratory of Computational and Applied Polymer Science (LCAPS). [2] School of Chemistry, Institute of Science, Suranaree University of Technology, Nakhon Ratchasima, 30000 Thailand.

E-mail: visit@sut.ac.th

บทคัดย่อ   :   ได้ใช้เทคนิคการจำลองพลวัติเชิงโมเลกุลเพื่อศึกษาโครงสร้างและสมบัติของสาร อิเล็กโตรไลท์ที่ใช้ในแบตเตอร์รี่ที่อัดประจุใหม่ได้สำหรับระบบสารละลายเกลือโพแทสเซียมไอโอ ไดด์ในเอทิลีนคาร์บอเนต โพรพิลีนคาร์บอเนตและไดเมทิคาร์บอเนตที่ความเข้มข้นเจือจาง โดยได้ วิเคราะห์สมบัติเชิงโครงสร้าง สมบัติเทอร์โมไดนามิกส์ และสมบัติเชิงพลวัต ที่อุณหภูมิ 323, 348 และ 500 เคลวิน สำหรับเอทิลีนคาร์บอเนต และ 298, 323 และ 500 เคลวิน สำหรับโพรพิลีน คาร์บอเนตคาร์บอเนต และไดเมทิคาร์บอเนต ผลการศึกษาพบว่าค่าสัมประสิทธิ์การแพร่ และ ฟังก์ชันการกระจายเชิงรัศมีของโพแทสเซียมไอออนที่ทำนายได้สอดคล้องกับค่าที่ได้จากการ ทดลอง

Abstract : Molecular dynamics simulations of KI in liquid ethylene carbonate, propylene carbonate, and dimethyl carbonate at low concentration which used as electrolytes in rechargeable batteries are reported. Structural, thermodynamic, and dynamical properties have been obtained at 323, 348 and 500 K in ethylene carbonate, 298, 323 and 500 K in propylene carbonate and dimethyl carbonate respectively. The diffusion coefficient and g(r) of the potassium cation predicted by simulations were consistent with experimental values.

Introduction : Cyclic carbonates such as ethylene carbonate (EC) and propylene carbonate (PC) are dipolar aprotic solvents which find a broad range of applications as both solubilizing and reactional environments. These solvents are notable for their physical properties including high dielectric constants, high boiling points and high dipole moments. EC is mostly used in mixtures with other liquids because of its high freezing point. Since it has high miscibility with water as well as with a large variety of non-aqueous solvents , solutions melting below room temperature and having a wide range of dielectric constants may be obtained. PC is a versatile solvent, as it has an extensive liquid range and dissolves a large variety of organic and inorganic substances. Solutions of lithium salts and these cyclic carbonates associated with other organic solvents have been the electrolytes of choice for lithium batteries.

Recently, the use of PC in the degreasing, paint stripping and cosmetic industries has increased significantly due to its biodegrability and low toxicity.

Solutions of lithium salts in liquid propylene carbonate (PC), ethylene carbonate (EC), and dimethyl carbonate (DMC) or their mixtures have considerable industrial interest due to their use as electrolytes in rechargeable lithium batteries.Such solvents and their mixtures have proved to be among the most efficient in terms of battery cyclability, and the analysis of the electrolyte physical properties is a necessary step in the understanding of the differences between the electrolytes.

Potassium secondary cells can be used as well as lithium batteries, providing high-voltages with high energy density, which is strongly needed for new technologies. Interestingly, the potential of potassium anode and lithium anode are approximately the same with only a 0.12V difference. Indeed, among alkali metals, the potential of potassium anode is the closest one to that of lithium anode. Even for the sodium anode, this difference is 0.32V. Therefore, potassium batteries has no disadvantage related to the cell voltage in comparison with available lithium batteries.

The potassium battery designed had some valuable advantages in comparison with similar lithium batteries.So, this work want to study structure at atomistic level of alkyl carbonate and alkyl carbonate-KI by Molecular simulation methods

Methodology : Amorphous cells of pure EC, PC, DMC (214 molecules) and EC, PC, DMC (214 molecules) with KI (1 ion pair) were generated and simulated using Materials Studio 4.1 with COMPASS force field, licensed from NANOTEC, Thailand. All MD simulations were performed under NVT conditions with the working temperature T 323, 348 and 500 K for ethylene carbonate, 298, 323and 500 K for propylene carbonate and dimethyl carbonate respectively. A time step = 1 fs for the integration of the atomic motion equations was used. The van der Waals and Coulombic nonbonding interactions were calculated by the atom based and cell multipole method, respectively. The structure of both systems were first minimized with respect to all the internal coordinates by a conjugate gradient method until the maximum derivative was smaller than 0.1 kcal/(Å mol). Then, the system was submitted to an equilibration process consisting on a 200 ps long MD run. The data collecting stage consisted on MD runs of 1 ns. In both cases, the trajectories were saved each 1000 fs for subsequent analysis.

Results, Discussion and Conclusion :
    A. Structure and Thermodynamics. The simulation results found that the total potential energy is given as well as the interaction energy of each ion with the solvent. For each solution, the ion-solvent energy is mainly electrostatic and close to -1000 kJ/mol in each solvent for K^+ and -450 kJ/mol for I^-.

The cumulative coordination number $n_{\alpha\beta}(R)$ of one atom R is obtained from the relation From some appropriate atom-atom RDFs, eq 1 reveals that there are four solvent molecules in the first solvation shell of the lithium ion and 6 or 7 molecules in the case of I^- for the systems studied. This observation is in agreement with the experimental results.

$$ n_{\alpha\beta} = 4\pi\rho_\beta \int g_{\alpha\beta}(r)r^2 dr \qquad \text{……eq(1)} $$

B. Diffusion. The ion diffusion coefficients are computed from mean square displacement (MSD),

$$D^{MSD} = \lim_{t \to \infty} \frac{< |\vec{r}(t) - \vec{r}(0)|^2 >}{6t} \qquad \ldots\ldots eq(2)$$

The diffusion coefficient of the potassium cation is found to be similar in the three solvents with a moderate temperature dependence, and increasing in the order EC < PC < DMC. All temperature, diffusion coefficients of I⁻ was greater than K⁺ and this observation is in agreement with the experimental results.

References:
1. Soetens et al. *J. Phys. Chem. A*, Vol. 102, No. 7, 1998
2. Borodin and Smith. *J. Phys. Chem. B*, Vol. 110, No. 10, 2006
3. A. Eftekhari, *Journal of Power Sources* 126 (2004) 221–228

Keywords : Ethylene Carbonate, Propylene Carbonate, Dimethyl Carbonate, molecular simulation, Diffusion

CURRICULUM VITAE

Name : Mr. Harnchana Gatemala

Contact Address: School of Chemistry, Institute of Science, Suranaree University

of Technology (SUT), Nakhon Ratchasima, 30000, Thailand

Phone 087-2277187 E-mail: harnchana.gate@gmail.com

Personal : September 16, 1984, Mahasarakham, Thailand

Presentation:

1. Oral presentation , **MOLECULAR DYNAMICS SIMULATION OF POTASSIUM IODIDE SALT IN ETHYLENE CARBONATE, PROPYLENE CARBONATE, AND DIMETHYL CARBONATE**, 34th Congress on Science and Technology of Thailand (STT34), 31 October - 2 November 2008, Queen Sirikit National Convention Center, Bangkok, Thailand.

2. Poster presentation, **EFFECT OF POLYDISPERSITY ON STRUCTURES AND DYNAMICS OF POLYMER NANOFIBERS** , The Fourth International Workshop for Far East Asian Young Rheologist, 21 -23 January 2008, SUT, Thailand.

3. Oral presentation , **MONTE CARLO SIMULATION OF BIDISPERSE POLYETHYLENE NANOFIBERS AND NANOPARTICLES**, SUT Graduate Academic Seminar 3rd, 2010, SUT, Thailand.